RSC Advances

ROYAL SOCIETY OF CHEMISTRY

www.rsc.org/advances

Review on modified N-TiO_2 for green energy applications under UV/visible light: Selected results and reaction mechanisms

L. Gomathi Devi* and R. Kavitha

Department of Post Graduate Studies in Chemistry, Central College City Campus, Dr. Ambedkar Street, Bangalore University, Bangalore-560001, INDIA

e-mail: gomatidevi_naik@yahoo.co.in

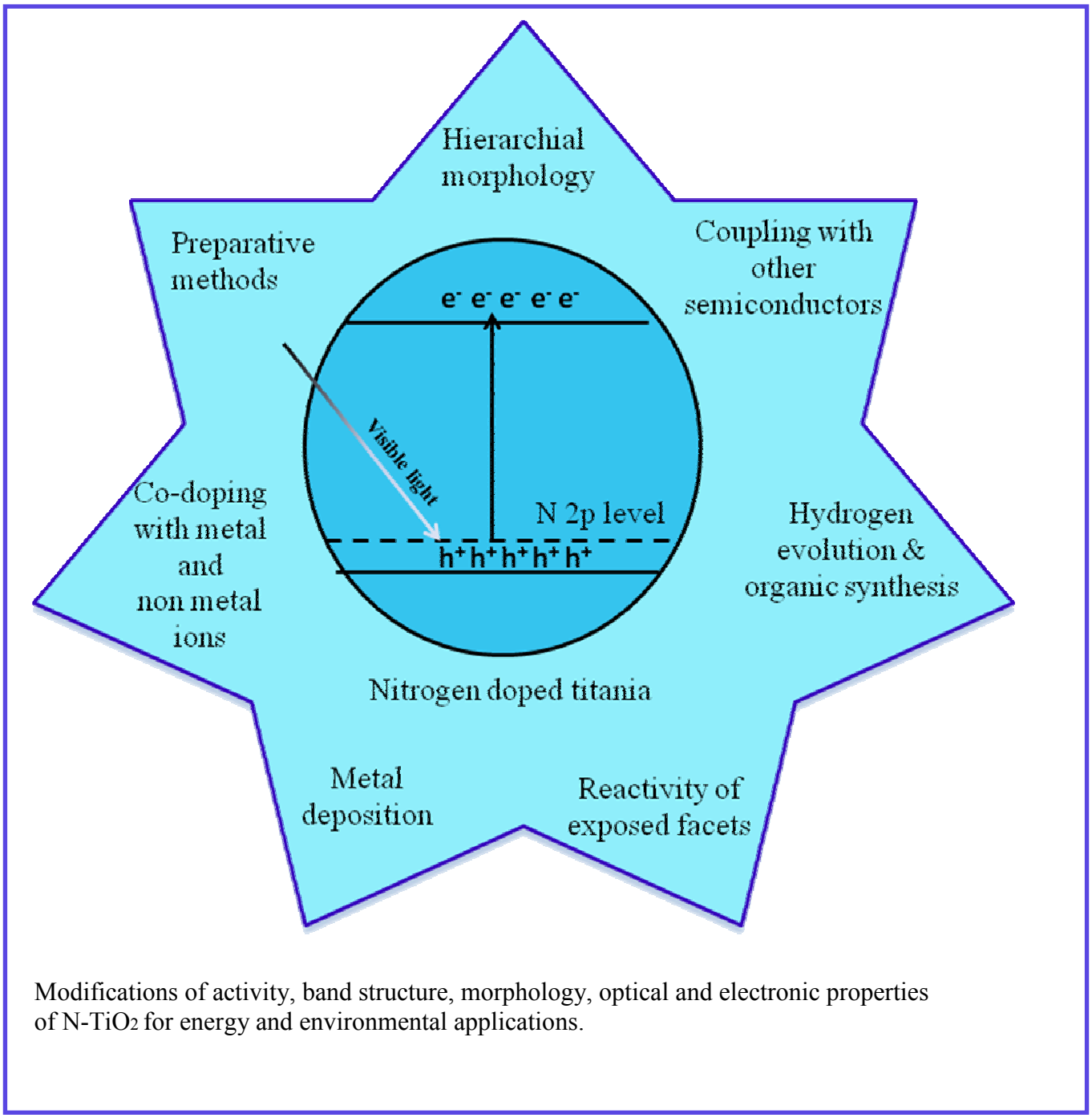

Modifications of activity, band structure, morphology, optical and electronic properties of N-TiO_2 for energy and environmental applications.

Review on modified N-TiO_2 for green energy applications under UV/visible light: Selected results and reaction mechanisms

L. Gomathi Devi* and R. Kavitha

Department of Post Graduate Studies in Chemistry, Central College City Campus, Dr. Ambedkar Street, Bangalore University, Bangalore-560001, INDIA

Phone: 080-22961336(O), e-mail: gomatidevi_naik@yahoo.co.in

Abstract

Titanium dioxide photocatalyst has witnessed an explosion of interest in water and air cleanup, owing to its fascinating properties like non-toxicity, ease of preparation, favorable band edge positions, water insolubility, multifaceted electronic properties, surface acid-base properties, super hydrophilicity and so on. In spite of being blessed with much functionality, large bandgap and massive charge carrier recombination step back its wide utility under natural solar light. The intensified efforts to overcome these drawbacks were considerably achieved through nitrogen doping into titania matrix (N-TiO_2), that alters surface-bulk structure for visible light absorption with high quantum efficiency. In this review, we highlight the recent progress of N-TiO_2 towards pollutant degradation, hydrogen evolution and its use in organic synthesis under ambient conditions. The preparation of N-TiO_2 via different methods (physical and chemical methods) with diverse morphologies, nature of chemical dopants, induced defects and fundamental reaction parameters governing efficient photoinduced reactions are explored in this review. Further improvement in the photoefficeincy of N-TiO_2 was achieved through co-doping with foreign ions, heterostructuring with other semiconductors, metal deposition and tuning the N-TiO_2 with reactive exposed facets. The insight for high activity in each modification is discussed in the light of charge carrier generation-separation-transfer-recombination dynamics together with pollutant adsorption and their reactions with reactive oxygenated species in liquid or

gaseous regime. This review attempts to give an overview of research highlights concerned with N-TiO_2. Though it is impossible to cover all the research articles, several milestones in the pathway of N-TiO_2 are explored. It is hopeful that this review article would trigger deep research interest in synthesizing N-TiO_2 with multifunctional features to enhance its capacity for many green energy applications.

1.0 Introduction

Titania has witnessed great promise in several green applications like wastewater purification, as a catalyst in organic compound synthesis, as gas sensors, in photovoltaics and also in hydrogen generation, ascribed to its suitable electronic band structure, biochemical compatibility, strong oxidizing power, non-toxicity and long-term stability against photochemical corrosion.[1-10] However, TiO_2 exhibits low photochemical quantum yield due to its relatively high recombination rate of photogenerated electron hole pairs. In addition, large bandgap of TiO_2 absorbs only UV light which accounts for merely ~5% of solar photons resulting in very low quantum yield in light to energy conversion. The above mentioned challenges serve as impetus to engineer an environmentally benign and adsorptive-solar photocatalytic functional material via modifying the surface-electronic structure of TiO_2, while retaining its advantageous catalytic properties. [11-13] Numerous efforts including crystal shape engineering, doping, co-doping with foreign ions, noble metal surface deposition and sensitization by inorganic complexes or with organic dyes, hydrogen plasma reduction of TiO_2, surface complexation, defect creation and multi component heterostructuring are frequently reported to display very high photocatalytic efficiency.[14-30] Among the various approaches, non metal doping is one of the promising techniques especially nitrogen incorporation (N-TiO_2) with different chemical entities into the

titania lattice or on its surface is accepted to be beneficial for the improvement of photoefficiency of titania under UV/visible light.

The previously published review articles dealt with several fundamental aspects like synthesis, physical/chemical properties, role of nitrogen dopant, wavelength dependent photoactivity and synergism of electronically modified N-TiO_2 with other materials aimed at enhancing TiO_2 applications.[11,13] Recently, our research group reported a comprehensive overview on non metal doped TiO_2 which emphasized several factors like surface modification by noble metal deposition, co-doping with other foreign ions, organic dye sensitization and heterostructuring with other semiconductors besides highlighting the correlations with photocatalytic reaction mechanism.[11] Till to date, review solely dedicated to N-TiO_2 are rare in the literature. To fill this vacuum, we have discussed selected results of N-TiO_2 mainly concerned with the preparation, structural modifications, morphology and synergistic effects of co-doping with other elements for the enhancement of photocatalytic activity to trigger research in this field.

2.0 Influence of preparative methods on photocatalytic activity of N-TiO_2

$TiOHN_x$ (x = 10 min N_2 plasma discharge time in min) obtained by reduction-nitridation method via non thermal plasma treatment was more favorable for Methylene Blue (MB) degradation under visible light compared to the samples prepared in other conditions like in the absence of N_2 (TiOH) and H_2 plasma treatment ($TiON_x$).[31] The above experimental condition promoted N_s doping in $TiOHN_x$, which narrowed the bandgap efficiently when compared to simple nitridation treatment. Under visible light, electron excites from N_s to conduction band (CB) which initiates superoxide radical production. The induced oxygen vacancies created by nitrogen dopant serve as trap sites for electrons at lower concentration, while it facilitates recombination of electrons

with holes in N_s at high concentration.[32-33] The TiOHNx was found to be more stable in the photocatalytic reactions compared to the $TiON_{10}$ for three consecutive runs as the oxygen vacancies created by H_2 plasma leads to the incorporation of nitrogen doping deep into TiO_2 lattice (Table 1). When the lattice nitrogen on surface layer is oxidized by holes in the first use,[34] a protective passivation layer is formed. This inhibits further oxidation of nitrogen in TiO_2 present in deep layers leading to stable lattice nitrogen content in subsequent cycles. In case of $TiON_{10,}$ nitrogen is doped only into surface layer which is oxidized easily by holes.[31] The $TiO_{2-x}N_x$ prepared by annealing TiO_2 under NH_3 flow decomposed gaseous 2-propanol at a faster rate under even under UV light compared to visible light. UV light excites electrons from both valence band (VB) and dopant energy level, while visible light excites electrons only from dopant level.[35] The quantum yield for degradation reaction decreased as nitrogen content is increased in N-TiO_2 (Fig. 1). During the process of annealing, oxygen sites were partially replaced with nitrogen atoms enhancing the Ti^{3+} states and also oxygen vacancies below CB edge (0.75-1.18 eV) at higher dopant concentration which promote the recombination process.[36] The N-TiO_2 (N/Ti = 0.025 atomic ratio) prepared by sol-gel reverse micelle method with Disodium ethylenediaminetetraacetate (Na_2EDTA) as nitrogen source showed remarkable activity for Methyl Orange (MO) degradation under visible light, attributed to the synergistic effects of nitrogen content, high crystallinity and large surface area.[37] These properties enable the extent of adsorption of oxygen/molecular water to react with photogenerated charge carriers to form oxygenated free radicals (hydroxyl/hydroperoxy/superoxide).[37] The N-TiO_2 calcined in air atmosphere (200-250˚ C, 0.5 h) displayed superior activity for MB decomposition under visible light compared to sample sintered in N_2 ambience (Fig. 2).[38] In the former case, number of active sites increases with removal of organic residues on the surface, while in the later case the number

of such active sites will be lower as the organic residues cannot be oxidised. The zeta potential of N-TiO_2 was higher than TiO_2 implying that nitrogen doping and sintering induced more charges on nanoparticles surface. The computational and ATIR results indicated that nitrogen doping occurs as a complexation between the titanium central metal ion and nitrogen atom.[38] The preparation of N-TiO_2 via precipitation of $[(TiO(C_2O_4)_2)^{2-}]$ in aqueous ammonia under alkaline conditions at low temperature followed by calcination at 400˚ C exhibited better MO degradation under UV/visible light.[39] This was attributed to Bronsted acid sites created from covalently bonded dicarboxyl groups which enhanced the capacity of N-TiO_2 for MO adsorption (Fig. 3). The adsorption process in the dark conditions revealed that N-TiO_2 releases H^+ ions when mixed with MO solution reducing the solution pH and altering the catalyst surface more acidic.[39] The N-TiO_2 obtained by wet method using $TiCl_4$ and NH_4Cl as nitrogen source showed high performance for 4-nitrophenol degradation under UV/visible light compared to N-TiO_2 catalyst prepared by using $TiOSO_4$ (NaOH) via wet and hydrothermal methods.[40] The high photoactivity was due to optimum anatase/rutile ratio, [41-44] which allowed vectorial transfer of charge carriers and retarded their recombination. Further, bandgap narrowing,[45-46] formation of oxygen vacancies and color centers also contribute to the activity in visible light.[47] Contrarily, the presence of rutile phase was detrimental towards the degradation of MB and 4-Cholorphenol (4-CP) using N-TiO_2 prepared by solgel method using 1, 3 diaminopropane as nitrogen source calcined at > 500˚ C.[48] The VB of nitrogen doped rutile TiO_2 is lowered by 0.4 eV on the insertion of N2p levels which are lower in energy than pure rutile VB (0.05eV). In this study, interstitial nitrogen served as mid bandgap states to render visible light response and also promoted anatase to rutile phase transition (ART).[49] This suggests that titanium and nitrogen

source along with the preparative methods plays a vital role in altering the electronic properties of N-TiO_2.

The N-TiO_2 thin films prepared by laser ablation method under 200 Pa N_2 gas atmospheres showed activity for MB degradation under UV/visible light. The reaction rate decreased for samples prepared >200 Pa N_2 gas pressure due to ART under low N_2 gas pressure.[50] The XRD and XPS explained a plausible mechanism for N-TiO_2 by laser ablation. It is found that crystal structure transition from rutile to anatase occurs in the pressure range of 27 to 67 Pa. It is observed that the nitrogen incorporation is easier near critical transition point due to crystal instability. The molecular nitrogen becomes monoatomic and splits more easily under low N_2 pressure compared to higher ones. [51] In addition, film turned yellow for the substrate temperature >500˚C suggesting that thermal energy originating from higher substrate temperatures is required for nitrogen doping, which otherwise does not occur in gas phase between target and substrate.[50] The nitrogen doping in the form of O_x-Ti-N_y and -(NO) obtained under O_2/Ar plasma was active for isopropyl alcohol decomposition under UV/visible light, while nitrogen substitution in the form of -(NO_2) under N_2/O_2/Ar plasma was less active compared to bare TiO_2.[52] The N_i-TiO_2 thin films synthesized by combinatorial atmospheric pressure chemical vapour deposition showed better MB and stearic acid degradation under UV and white light respectively than N_s-TiO_2 due to instantaneous charge carrier recombination processes in N_s-TiO_2.[53] The N-TiO_2 films fabricated by annealing TiO_2 films in gaseous NH_3 showed lower quantum yields for gaseous propanol decomposition and high decomposition rates for aqueous ethylamine ions ($CH_3CH_2NH_3^+$) as N-TiO_2 surface was negatively charged and positively charged cationic ethylamine ions were efficiently adsorbed on its surface.[54] The zeta potential evaluation of N-TiO_2 revealed that surface is negatively charged with increase in the

concentration of nitrogen dopant (Fig. 4). However, quantum yield values under visible illumination were much lower compared to studies under UV illumination although numbers of absorbed photons were identical in both the excitation sources. This suggests that holes produced by visible light are localized at isolated levels between VB and CB which were unable to diffuse to the upper edge of VB due to inefficient mixing of N 2p levels with O 2p orbital.[54]

The N-TiO_2 prepared by heat treatment of nanotubic titanic acid (NTA) in ammonia solution and along with gaseous ammonia flow possessed better activity for organic degradation under visible light.[55-56] This was attributed to single electron trapped oxygen vacancy (SETOV), electron trapping sites, interstitial nitrogen doping (N_s) and also to the formation $V^{\cdot}_O$-NO-Ti hot centers as shown in the following mechanism.[57]

$$V^{\cdot}_O + e^- \rightarrow V^{\cdot\cdot}_O \qquad (1)$$

$$V^{\cdot\cdot}_O + N \rightarrow N^{\cdot} + V^{\cdot}_O \qquad (2)$$

$$N^{\cdot} + O_2 \rightarrow O_2^- + N \qquad (3)$$

On illumination, electrons transfer takes place from VB to CB and later will be trapped by SETOV, which prevents instant recombination. Meanwhile, nitrogen atoms in Ti-O-N occupied in the interstitial site transfers the electron cloud towards oxygen atom and gains high chemical valence by entrapping another electron from SETOV. This interstitial nitrogen atom with an excess electron is unstable and immediately detraps the electron to oxygen (Fig. 5).[58] However, undoped TiO_2 did not show visible light photocatalytic activity despite SETOV formation due to the absence of nitrogen dopant.[56]

The N-TiO_2 obtained by mixing TiO_2 with 0.5M guanidine carbonate as nitrogen source exhibited better activity for 2-propanol decomposition in visible light than the N-TiO_2 samples

prepared using urea and guanidine hydrochloride.[59] The N-TiO_2 synthesized at 160˚ C by hydrothermal treatment showed superior MO degradation under visible light compared to N-TiO_2 samples prepared at 120˚ C by the same method.[60] The visible light activity of N-TiO_2 increases with decrease in pH (3-10) value in the preparative process as the nitrogen concentration strongly depends on pH of the reaction medium.[60] The electron spin resonance spectra (ESR) revealed that anatase N-TiO_2 with N_b˙ centers was active for formic acid degradation, while rutile N-TiO_2 with paramagnetic Ti^{3+} centers had very low performance.[61-62]

3.0 N-TiO_2 with hierarchical morphologies

To resolve the problem of low quantum efficiency, bulk diffusion and effective surface charge transfer are the important key factors along with maximum light harvestation. It is believed that complex hierarchical morphologies would offer new opportunities in integrating the fascinating properties like increased surface area, high porosity, low bulk density, enhanced photonic efficiency and dispersity in reaction solution together with structural and catalytic stability with high extent of charge carrier separation.[63-64] These properties originate from geometrical structure, good mechanical strength, multiple scattering, and better access of reactants to the catalyst together with high light harvesting efficiencies.[65]

The amorphous N-TiO_2 nanotubes exhibited activity for Rhodamine B (RhB) and MB degradation under visible light than crystalline N-TiO_2 and DP25 indicating that high nitrogen content, high surface area and large pore volume played a crucial role for promoting the activity.[66-67] The loss of nitrogen content,[67] destruction of tubular structure, reduced specific surface area and oxygen vacancy formation became detrimental after calcining the catalyst >350˚ C.[66] The CO_2 was reduced to HCOOH, HCHO and CH_3OH effectively on N-TiO_2 nanotube under visible light compared to unmodified TiO_2 nanotube.[68] The energy state of substituted

nitrogen (N_s) was found on VB edge, while the energy state of N_i appeared in the forbidden TiO_2 bandgap altering its electronic structure.[69-70] In addition, increased surface area favored more CO_2 adsorption on the catalyst surface.[68] Oxidation of CO fails with N-TiO_2 nanotube, but promotes reduction of resazuring to resofurin under visible light which was kinetically favored reaction.[71] The high degree of recombination induced by N 2p state hampered the activity under UV light, as oxygen reduction is a four electron reaction with tedious kinetics and requires high over potential.[71] The N-TiO_2 nanotubes synthesized via solvothermal treatment method heated at 120˚ C for 5h using protonated titanate nanotube in an NH_4Cl/ethanol/water solution followed by calcination at 450˚C shows better performance for MB degradation under visible light compared to protonated titanate nanotube.[72] The presence of chloride ion in the synthesis route played a key role in transition from titanate to TiO_2 at low temperature. This fact is revealed by the presence of only titanate phase with other various nitrogen sources like aqueous NH_3, $(NH_4)_2CO_3$, NH_2CONH_2 and NH_4NO_3 where conversion was not efficient.[72] The N-TiO_2 mesosponge fabricated by transformation of TiO_2 nanotube arrays in ethanolic NH_3 exhibited high photocurrent densities and MO degradation under UV light, which was attributed to the excellent degree of crystallinity and efficient utilization of UV light by N-TiO_2 as a result of localized N 2p level above TiO_2 VB which narrowed the bandgap and efficiently promoted charge carrier separation.[73] The stable and reusable N-TiO_2 nanotube array films fabricated by electrochemical anodization followed by wet immersion in aqueous NH_3 and followed by calcination at 450˚ C for 2h decomposed MO efficiently under UV/visible light.[74] The XRD patterns revealed that bare TiO_2 was composed of anatase and rutile phases, while nitrogen doping via O-Ti-N surface state suppressed ART process owing to strong crystal distortion force.[75-76] In addition, presence of porous nanotube structure and nitrogen dopant inhibited the

migration and rearrangement of titanium and oxygen atoms to form rutile phase during calcination process.[77-78] The electrochemical impedance spectroscopy (EIS) spectra showed smaller impedance arc radius for N-TiO_2 under UV illumination demonstrating that N-TiO_2 displayed greater charge carrier separation efficiency and fast charge transfer than pure TiO_2 at solid liquid interface.[74]

The N-TiO_2 hollow sphere was more active for bisphenol-A (BPA) degradation and mineralization under blue, green and yellow light illumination compared to undoped TiO_2 hollow spheres and Hombikat UV100 (Table 2).[79] The degradation rate monotonically increased with increase in pH and rate was highest even at pH ~ 9.6 (pka of BPA ~1) and this activity is attributed to increased hydroxyl radical concentration. The high surface area, high porosity and low bulk density enhanced the photonic efficiency and dispersity in reaction solution.[79] In another study, activity of N-TiO_2 hollow spheres synthesized by co-precipitation and template elimination method and spherical N-TiO_2 showed similar performance for di-chlorophenol (DCP) degradation, indicating that photocatalytic reaction does not occur in the inner surface of hollow sphere but occurs only on the outer surface of the hollow sphere as sufficient light cannot reach the inner surface.[80] The photoanode consisting of multilayer films of $Ti_{0.91}O_{2-x}N_x$ nanosheets shows an increase in photocurrent compared to undoped nanosheets under visible light irradiation which was mainly attributed to photoexcitation of oxygen vacancy related states induced by nitrogen doping.[81] These nanosheets were prepared by solid state proton exchange of $Cs_{0.68}Ti_{1.83}O_4$ with $H_{0.68}Ti_{1.83}O_4$ and followed by subsequent exfoliation process.[82] The nitrogen doping was carried out using solid state reaction step with gaseous NH_3. The interlayer galleries of layered $Cs_{0.68}Ti_{1.83}O_4$ precursor provided excellent channels for nitrogen diffusion over whole layered titanate particles.[83] The N-TiO_2 was obtained from these titanates via ion exchange

process in HCl solution (1 mol dm^{-3}) and followed by a subsequent exfoliation process in tetrabutylammonium (TBAH) solution (Fig. 6).[81] The mesoporous N-TiO_2 prepared by exfoliation- reassembling strategy with ethylamine as nitrogen source and also a delaminating agent for layered titanate showed exceptional activity for MO and 4-aminobenzoic acid degradation under visible light compared with P25, pristine protonic titanate and N-TiO_2 fabricated from template-free route.[84] This high activity is ascribed to high porosity; enhanced visible light absorption, increased surface area and efficient charge carrier separation. The mesopore size of 5 nm was large enough for easy access of organic molecules at the catalyst surface. Due to structural similarity, both TiO_6 octahedra and titanate nanosheets were modified by nitrogen species[85-86] which introduced localized states in both TiO_2 and titanate nanosheets enabling visible light absorption and bandgap narrowing.[87-88] The charge carrier transfer was improved due to the presence of straddling gap in energy potentials between TiO_2 and titanate nanosheets. The MO degradation was hardly suppressed with addition of tertiary butanol and was completely inhibited in presence of ethylenediaminetetraacetate (EDTA) suggesting the dominant role of holes and negligent contribution from sensitization process. The X-ray diffraction (XRD) and transmission electron microscope (TEM) images revealed that random reassembling between titanate nanosheets and TiO_2 gave rise to its porous structure.[84] The fibrous hierarchical meso-macroporous N-TiO_2 enhanced the hydrogen evolution under visible light irradiation with 10 vol% methanol attributed to porous network with uniform nitrogen dispersion throughout the catalyst.[89] The hierarchical and fibrous structure allows channelization of electron for effective surface charge transfer process (Fig. 7). The presence of macroporous channel within the catalyst enhances the efficiency of photoabsorption and improves the mass transfer process within the macro-mesoporous frame. The macrochannel act as light transferring

path which introduces incident photon flux into the inner surface and this light activated surface area increases as the process absorption, reflection and scattering takes place within the material.[90] With increase in calcination temperature > 400˚C, destruction of mesoporosity and loss of nitrogen content occurs leading to poor activity.[89] The N-TiO_2 with various morphologies like nanooctohedra, nanoparticles and nanospherical shape were successfully synthesized through nitrification of TiO_2 in presence of NH_3 (700˚ C, 30 min) as depicted below;[91]

$$TiO_2 + NH_3 \rightarrow \text{N-}TiO_2 \qquad (4)$$

The N-TiO_2 nanooctahedra exhibited best activity for MO degradation compared to other N-TiO_2 structures under UV/visible light irradiation attributed to impurity state above the VB by nitrogen dopant which also improved TiO_2 conductivity and inhibited recombination rates. In addition, well exposed {101} facet on crystallized surface serves as possible reservoirs of electrons to facilitate production of superoxide radicals.[91] The N-TiO_2 having rice grains like structure prepared by electrospinning method followed by annealing at 450˚C for 1h showed superior MB degradation and hydrogen evolution compared to TiO_2 rice grains attributed to nitrogen dopant with rice grain nanostructure.[92] The rutile N-TiO_2 with V shaped nanorods synthesized by hydrothermal method using HCl and TiN showed enhanced visible light absorption and red shift in bandgap absorption.[93] The separation of nitrogen ions from TiN provided a route for self doping in the formation of nanorods with HCl. The chemical reactions involved in the transformation from TiN to TiO_2 are represented as;[94]

$$TiN \rightarrow Ti^{3+} + N^{3-} \qquad (5)$$

$$Ti^{3+} + H_2O \rightarrow Ti(OH)_2 + H^+ \qquad (6)$$

$$Ti(OH)_2 + O_2 \rightarrow Ti(IV)\text{oxo species} \qquad (7)$$

$$\mathrm{Ti(IV)\,oxo\ species + N\ species} \rightarrow \mathrm{N\text{-}TiO_2} \quad (8)$$

The Ti (IV) oxo species is an intermediate between TiO^{2+} and TiO_2, consisting of partly dehydrated polymeric Ti(IV) hydroxide.[95-96] The $Ti(OH)_2$ was derived from the precursor solution ($Ti^{3+}N^{3-}$) and O_2 from autoclave or from the reaction solution. There were two types of V-shaped nanorods at inner angles of 114.4˚ and 134.9˚ with same coherent boundary of the {101} plane. The Oriented attachment (OA) and Ostwald ripening (OR) leads to the formation of straight and V-shaped N-TiO_2 nanorods (Fig. 8). The small V-shaped nanocrystal formed via OA mechanism by attaching two similar grains, in which two {101} high energy planes join together and are eliminated, and finally follows OR coarsening process. The formation of V-shaped nanocrystal is essentially a facet-mediated aggregation and there is sequential elimination of high energy surfaces, owing to significant contribution of surface energy to the total free energy in a nanoscale system.[93] The V-shaped structures are of particular interest because the sudden break down in lattice periodicity at the junction offers a good lateral confinement and thus can enhance the excitonic optical response.[97] The dual structure of rutile N-TiO_2 nanoflower film aggregates sitting on top of the anatase layer showed superior activity for RhB degradation under visible light compared to the activity of titania nanorod film and titania derived from P25 slurry.[98] The activity was ascribed to its unique morphology of top layer which possessed high specific surface area of 77.8 m^2/g.[98] These N-TiO_2 nanoflower films were fabricated by oxidizing metallic Ti plates with H_2O_2 containing hexamethylene tetra amine (HMT) and concentrated nitric acid at 353 K for 72h. The low-temperature growth of top flower-like rutile TiO_2 occurred only after 60 h of reaction when the reaction solution contained almost no hydrogen peroxide or Ti(IV) ions.[98] In thermodynamics, two factors were believed to contribute to low-temperature growth of rutile nanoflower i.e., additives like HMT, nitric acid and porous hydrated titania layer formed before

60 h of reaction. At this stage, a porous hydrated amphorous titania layer was deposited onto the titanium substrates on which a top layer of rutile nanoflower precipitated due to supersaturated Ti(IV) solution. With prolonged reaction time of up to 72 h, tiny rutile nanorods precipitated from the solution which aligned to form bundle and eventually fused through an OA mechanism to achieve a larger nanorod. The large nanorods were self assembled to flower like morphology with the assistance of structure directing agents like NH_3 and NO_3^- produced by the decomposition of HMT;[99-100]

$$(C_6H_2)_6N_4 + 6H_2O + H^+ \rightarrow 6HCHO^- + 4NH_4^+ \quad (9)$$

These ions also helped in synchronal incorporation of nitrogen into titania matrix, but however red shift for the light response of the titania nanoflower film was not observed.[98]

4.0 Codoping

There exist unfavorable factors such as oxygen vacancy and Ti^{3+} defects due to charge imbalance induced by nitrogen, which may serve as recombination center. However, codoping maintains charge balance through charge compensation, creates new electronic level, delays recombination of charge carriers and further shifts the absorption edge to visible region. The probability of charge carriers to reach catalyst surface before recombination is higher for codoped TiO_2 compared to single ion doped and undoped counterparts. The activity of codoped titania is largely determined by dopants chemical nature and the bonds between them.[101-104]

4.1 Incorporation of nitrogen into TiO_2 with other non metal dopants

Nitrogen and boron codoped TiO_2 (N-B-TiO_2) with 10 mol % dopant exhibited high activity for 4-CP degradation under UV/visible light compared to single doped titania.[105] The X-ray photoelectron spectroscopy (XPS) and XRD gave evidence for the coexistence of interstitial nitrogen, [NOB] species in bulk and NO_x species, B_2O_3 on TiO_2 surface at high boron content.

The interstitial B^{3+} ion was sp^2 hybridized with lattice oxygen forming a planar structure and lattice oxygen atoms links with one boron and two titanium atoms to form Ti-O-B-O-Ti structure,[106-109] which shifted the bandgap absorption to visible region. Although, [NOB]$^{\cdot}$ species do not directly contribute for visible light response, CB electrons will be trapped generating [NOB^-] diamagnetic center which inhibits the recombination reaction pathways.[110] Under UV light, electrons are excited either from both TiO_2 VB and [NOB]$^{\cdot}$ species to TiO_2 CB which in turn are transferred to B_2O_5 CB.[111-112] The simultaneous hole transfer from VB to surface state energy level of NO_x species leads to direct oxidization of surface adsorbed 4-CP.[113] On the other hand the electron could transfer from dopant induced electronic states to CB under visible light illumination. The electrons residing at B_2O_3 CB are trapped by adsorbed oxygen to generate superoxide radical.[114] The N-B-TiO_2 (red anatase TiO_2) prepared by heating anatase TiO_2 microspheres (with an predoped interstitial boron shell) between 580 and 620˚ C in a gaseous NH_3 atmosphere with a flux of 50 mL min^{-1} for 60 min exhibited high photoelectrochemical water splitting activity under visible light.[115] The UV visible absorption spectra of red anatase TiO_2 shows an extended absorption edge up to 700 nm covering full visible light spectrum due to bandgap gradient produced which varies from 1.94 eV on the surface to 3.22 eV in the core by gradually elevating VB maximum (Fig. 9). The Raman studies showed an additional active mode in the range of 450 to 500 cm^{-1} for red TiO_2 which is attributed to substitutional nitrogen dopant in the TiO_2 bulk breaking down the Raman selection rules to generate a new active mode by lowering the geometric symmetries of TiO_2.[116] This new doping approach by using a predoped interstitial boron gradient improved the solubility of substitutional nitrogen in TiO_2 bulk without introducing Ti^{3+} impurity level. The interstitial boron dopant effectively weakened surrounding Ti-O bonds facilitating easier nitrogen substitution and it also increased the chemical stability of

codoped TiO_2. Meanwhile the extra electrons from boron dopant compensated the charge difference between the lattice O^{2-} and substitutional N^{3-} ion to maintain charge neutrality.[116]

The nitrogen and carbon codoped TiO_2 (N-C-TiO_2) showed high activity for MB decomposition under visible light due to synergistic effect between carbon and nitrogen codoping.[117] The degradation process followed two pathways: (i) reactive CB electrons reduced surface adsorbed oxygen to its radical anion which transforms to H_2O_2 and hydroxyl radical; (ii) reactive holes oxidize MB to its radical cation through hydroxyl radical produced by oxidation of water. During the course of interfacial electron transfer, adsorbed carbonaceous species gets excited and injects electrons to TiO_2 CB thereby increasing the kinetics of dioxygen reduction. The nitrogen dopant creates intra bandgap state close to VB and also shifts the position of flat band potential to higher level than undoped TiO_2 increasing the interfacial electron transfer kinetics. The ion dipole interaction between TBA^+ (carbon source) and water molecules hinders the TBA diffusion into the TiO_2 bulk inferring that carbon atoms are difficult to weave into TiO_2. This leads to TBA segregation on the TiO_2 surface inhibiting the crystal growth. The adsorption experiments indicated that surface carbonaceous species degraded more number of MB molecules and transferred them to residual vacancies through surface diffusion which is faster than free diffusion in solution enhancing its degradation rate.[117] The hydrothermal synthesis of N-C-TiO_2 nanotubes exhibited 2.3 times higher sonocatalytic activity for RhB degradation ascribed to various factors like codoping, high surface area, lower bandgap energy and creation of surface vacancies as a result of Ti^{3+} formation.[118] The XPS results indicated that nitrogen atoms were bonded to oxygen atoms in interstitial sites via Ti-O-N and Ti-N-O bonds and also substituted oxygen sites via N-Ti-O bond, while the carbon dopant as Ti-C and also in the form of complex carbonate species on the catalyst surface. Sonoluminescence technique produces light flash with

average photon energy of 6 eV. Under these conditions both surface adsorbed carbonaceous species and RhB serve as sonosentizers injecting electrons into TiO_2 CB[119-121] resulting in the reduction of Ti^{4+} to Ti^{3+} state which is localized at 0.75-1.18 eV below TiO_2 CB. These reactive sites facilitates oxygen adsorption on the TiO_2 surface.[118-123] In addition, water molecules are also decomposed under acoustic cavitation to release active hydroxyl and hydrogen radical species additionally contributing to overall performance.[118]

$$N\text{-}C\text{-}TiO_2 +))) \rightarrow e^- + h^+ \quad))) = \text{ultrasonic irradiation} \qquad (10)$$

$$Ti^{4+} + e^- \rightarrow \quad Ti^{3+} \qquad (11)$$

$$O_{2(ads)} + e^- \rightarrow O_2^{\bullet -} \qquad (12)$$

$$Ti^{4+} + e^- \rightarrow \quad Ti^{3+} \qquad (13)$$

$$O_{2(ads)} + e^- \rightarrow O_2^{\bullet -} \qquad (14)$$

$$H_2O + h^+ \rightarrow OH^{\bullet} + H^+ \qquad (15)$$

$$O_2^{\bullet -} + H^+ \rightarrow HOO^{\bullet} \qquad (16)$$

$$2HOO^{\bullet} + H_2O \rightarrow H_2O_2 + OH^{\bullet} \qquad (17)$$

$$H_2O_2 +))) \rightarrow 2OH^{\bullet} \qquad (18)$$

$$H_2O + N\text{-}C\text{-}TiO_2 +))) \rightarrow OH^{\bullet} + H^+ \qquad (19)$$

The N-F-TiO_2 under optimized conditions (600 mgL^{-1} catalyst dosage, ratio of Cr (VI)/Benzoic acid (BA) is 5 and pH 4) initiated the simultaneous redox reaction; reduction of Cr (VI) ions and oxidation of BA under visible light.[124] In this binary system, coupled oxidation of BA consumes holes or hydroxyl radicals, while Cr (VI) ions serves as electron acceptors. The electrons in states below N-F-TiO_2 CB have weaker reduction ability, which can preferably reduce strong

oxidizing agents like Cr (VI) enhancing the target reduction reaction without competence of other ineffective reduction reactions.[124] The mesoporous N-F-TiO_2 performed better for Acid Orange (AO7) degradation under visible light due to large surface area and surface acidity which promoted the increased adsorption of organic pollutants on catalyst surface.[125] In addition fluorine doping suppressed anatase to rutile phase transformation process and it enhanced the formation of oxygen vacancies and facilitated the generation of highly oxidative free hydroxyl radicals in solution.[126-127] The N-F-TiO_2 nanobelts prepared by a solvothermal method employing amorphous titania microspheres showed pronounced activity for MO degradation under UV/visible light ascribed to the following factors;[128] (i) enhanced visible light absorption and scattering;[129-131] (ii) transport of diffusion-free electron rapidily along the longest direction; [132-133] (iii) high degree of crystallinity with minimum grain boundaries;[129-131] (iv) smaller pore size and larger surface area. The fluorine doping leads to the formation of several new active sites and generates more number of hydroxyl radicals. The photocatalytic test measurement via new testing method using scotch tape covered N-F-TiO_2 nanobelt further enhanced its activity as more photons were captured by the nanobelts to simulate charge carrier generation compared to conventional methods. The BET results revealed larger amount of wormhole like mesopores prison and the “Prison Break” is not easy for the photons to escape leading to collision of photons with nanobelts for the exchange of energy.[128]

N-Si-TiO_2 hollow microspheres obtained by facile aerosol flow method showed good performance for salicylic acid degradation under visible light due to the co-operative effects of nitrogen dopant and Ti-O-Si bond.[134] The aerosol assisted flow synthesis process was initiated with homogeneous aqueous solution containing soluble precursors, when the droplets pass through tubular furnace carried by an air stream reduces the temperature of the droplets from

outer to interior layer.[109] The solvent evaporated swiftly and precursor ions assembled in the interior layer of droplets via diffusion process (Fig. 10). Simultaneous generation of NH_3 and HF from the decomposition of NH_4F played a vital role in the formation of hollow structured particles. Further treatment with HF solution led to formation of microspheres with macroscopic porous which increased the specific surface area of the catalyst.[134] The N-P-TiO_2 (0.05 P to Ti ratio) showed remarkable visible light activity for MB and RhB decomposition rather than N-TiO_2 and N-S-TiO_2.[135] The nitrogen doping resulted in formation of O-Ti-N linkage, while the dopant phosphorous existed either in pentavalent oxidation state (P^{5+}) or as PO_4^{3-} group coordinated to TiO_2. The oxygen vacancies formed due to this coordination promoted electron and hole transfer to surface reducing the charge recombination.[136,56]

The cooperative effects of visible light response and high charge carrier lifetime contributed to excellent performance of mesoporous N-S-TiO_2 (B) nanobelts (thiourea to Ti molar ratio [R]=3) for potassium ethyl xanthate degradation under visible light.[137] With further increasing the R value to 4 the activity decreased as the dopants sites acted as recombination centers.[137] The mixed phase (62% anatase + 38% rutile) N-S-TiO_2 modified by thiourea exhibited superior activity for MB degradation under visible light. [138] The fourier transform infra red spectroscopy (FTIR) and XPS studies showed the formation of a Ti^{4+}-thiourea complex, S^{6+} doping and the existence of nitrogen as lattice (N-Ti-N) and interstitial (Ti-N-O) species in the heterojunction. The isolated S3p, N 2p and π^* N-O states between VB and CB narrowed the bandgap thereby rendering visible light response.[139-140] The increased surface acidity of TiO_2 due to electron withdrawing inductive effect of sulphate ions and effective charge transfer in biphasic anatase-rutile coupled system increased the performance.[141,49] In another study N-S-TiO_2-montmorillonite was synthesized by impregnating doped titania sol into the interlayers of

montmorillonite and followed by calcination at 350˚C showed better performance for acid red decomposition under UV light than undoped TiO_2-montmorillonite which is attributed to its large surface area, pore volume, crystallinity and to the high number of hydroxyl radical species on the surface.[142] Furthermore, electron deficient nitrogen atom in O-Ti-N states traps the CB electron and prevents the charge carrier recombination.[143] The N-I-TiO_2 having 1:5 Ti:N/I molar ratio showed simultaneous reduction of Cr (Vl) and BA oxidation under visible light irradiation similar to N-F-TiO_2 as reported earlier.[144] The electron paramagnetic resonance (EPR) data suggests that $N_b^{\bullet}$ species narrows the bandgap and facilitates the formation of Ti^{3+} surface ion which plays a key role in capturing gaseous oxygen and simultaneous reduction-oxidation process. The light absorption ability of co-doped titania was proportional to the concentration of $N_b^{\bullet}$ species insertion and it was found deeper in TiO_2 lattice with lower E_g values. The doping of I^{5+} promotes formation of photoinduced surface Ti^{3+} electrons which reacts with adsorbed Cr(VI) and O_2 to form radicals such as $O_2^{\bullet -}$, $HO_2^{\bullet -}$ and $OH^{\bullet}$. In addition, EPR experiments showed the stabilization of oxygen trapped holes TiO^{4+}-$O^{\bullet -}$. This was created by the reaction of anatase holes with lattice oxygen O^{2-} and its concentration is inversely correlated with the oxidation rates. [144] The hierarchical macro-/mesoporous N-TiO_2, N-S-TiO_2 and N-F-TiO_2 prepared by using hydrothermal method without calcination did not show any visible light activity for RhB degradation, since the non metal ions existed as surface impurities before calcinations. This thermally calcined N-TiO_2, N-S-TiO_2 and N-F-TiO_2 was active for RhB degradation under the same experimental conditions.[145] The thermal calcination effectively increases the nitrogen implantation into TiO_2 lattice and causes red shift in optical absorption. But sulphur and fluoride ions resided mainly on the surface. The activity was enhanced when the catalyst was stored for six months in desiccators or by stirring it in water for 1h, which facilitates the electrostatic

adsorption of water molecules with surface hydroxyl groups on catalyst surface. But water treated N-TiO_2 and N-S-TiO_2 were not active than TiO_2 calcined at 400˚ C due to the presence of nitrogen and sulphur residues on the surface which disturbed bonding of water and subsequent water mediated adsorption switching process. Interestingly water treated N-F-TiO_2 showed high activity in spite of presence of nitrogen and fluoride species on the surface which can induce the formation of electrostatic adsorption with RhB.[146-147]

4.2 Incorporation of nitrogen along with other metal dopants into titania lattice

The codoping of nitrogen with other metals ions improves the photoactivity of titania, wherein metal ions with changing valence serve as carrier reactive trapping sites and passivates the defect bands produced by monodoping.[148-150] In general, metal ion dopants form energy level below CB edge and anionic dopants of non metals generate energy levels just above the TiO_2 VB effectively, narrowing the bandgap which enables to utilize large fraction of solar spectrum.[150]

4.2.1 Incorporation of nitrogen along with 3 d block metal ions into titania lattice

The codoping of nitrogen and vanadium in TiO_2 lattice (N-V-TiO_2) showed activity for RhB degradation under visible light and the activity is attributed to optimal dopant concentration with enhanced light absorption ability and efficient charge carrier separation.[151] In addition, N-V-TiO_2 with small crystallite size with good degree of dispersion provided high surface to volume ratio thereby increasing the contact area between active sites and reactants. Due to strong V-N covalent bond, V 3d states lowers N 2p energy levels bringing them closer to VB and thereby enhancing the mixing of N 2p and O 2p states which produces favorable condition for trapping holes.[152] On the contrary, position of V 3d states are shifted to low energy regions and diminish any possible overlapping between V 3d and Ti 3d due to bonding interaction between V 3d and N 2p orbital. The presence of V^{5+} ions in the form of V_2O_5 (E_g = 2 eV) produces a space charge

layer at the TiO_2 interface due to the difference in electrochemical potential,[153] which acts as driving force for CB electron to be instantaneously injected into V^{5+} species.[154] The co-doping of Mn and nitrogen (Mn-N-TiO_2) stabilized anatase phase and also performed better RhB degradation under visible light,[155] while doping only with Mn is reported to promote rutile formation even at moderate temperature.[156-162] In case of Fe-N-TiO_2 the synergy of higher degree of crystallization and pronounced mesoporosity with narrow pore size distribution resulted in phenol and MO degradation under visible light.[163-164] The high degree of crystallization and small crystallite size facilitated rapid electron transfer from bulk to surface effectively inhibiting carrier recombination,[32] while ordered mesoporous channels facilitated the diffusion and adsorption of reactant molecules for efficient degradation process.[164-165] The ferrum atoms distributed on TiO_2 surface in the form of Fe_2O_3 suppressed the recombination and it also increased the quantum efficiency.[166] The N-Zn-TiO_2 (1 atom % Zn) displayed excellent activity for MB degradation under visible light due to the oxygen vacancies induced by zinc doping and formation of N 2p states above VB edge.[167] The codoping of zinc into N-TiO_2 shifted the bandgap absorption to lower wavelength region due to the formation of oxygen vacancies and also to the Ti^{3+} state in TiO_2.[168-169] The PL spectra indicated that zinc doping suppressed the free exciton recombination emission due to electron trapping by oxygen vacancies and these trapped electrons further recombine with holes increasing the low energy PL intensity. However, nitrogen dopant can hold back the recombination of trapped electron in oxygen vacancy in TiO_2 with holes by N 2p states above VB maximum. It has been stated that the surface oxygen vacancy interacts strongly with exoteric oxygen molecules to form O_2^- (efficient electron scavenger) which traps electrons to form O^- which is crucial for oxidation process.[169-171]

4.2.2 Incorporation of nitrogen along with 4 d block metal ions into titania lattice

The photoactivity of N-Y-TiO_2 towards MB degradation in visible light was ascribed to charge trapping and photocatalytic active centers induced by yttrium doping.[172] However, high content of yttrium dopant served as recombination centers reducing the activity. The ionic radius of Y^{3+} (0.089nm) is higher than Ti^{4+} (0.068nm) which expand the TiO_2 lattice on Y^{3+} substitution. [172] The N-Zr-TiO_2 synthesized via modified sol gel route using supercritical CO_2 decomposed MB under visible light, which was ascribed to several factors like;[173] (i) high surface area with mesoporous structure favoring adsorption of reactant molecules; (ii) reduction in crystallite size which provided higher interfacial area and access to active sites; (iii) defects induced by nitrogen dopant capture more electrons and reduce the recombination.[174-177] The nitrogen doped $Ti_{1-x}Zr_xO_x$ solid solutions obtained through hydrothermal method exhibited much higher activity for acid red 88 and benzene degradation under visible light irradiation compared to N-TiO_2 attributed to synergistic effect of nitrogen and zirconium dual modification.[178] The XPS and DRS studies revealed that nitrogen was mainly doped in the surface layer of catalyst and induced surface state close to VB. On the other hand, lattice Ti^{4+} ions were substituted by Zr^{4+} ions resulting in the elevation of CB facilitating electron transfer and separation of charge carriers.[178] In N-TiO_2 solid solutions, electrons are excited from surface state to CB and subsequently transferred to adsorbed surface species. In comparison with N-TiO_2, the elevation of CB in N-$Ti_{1-x}Zr_xO_2$ would not efficiently utilize the visible light however it had strong potential to reduce oxygen leading to formation of active oxygen radicals (Fig. 11).[178] The N-Nb-TiO_2 (25 mol % Nb) prepared by sol gel process followed by nitridation under flowing ammonia exhibited 6 fold increase in MB degradation under visible light compared to the other Nb doped samples (< 25 mol%).[179] The N 2p levels are close in energy to the hydroxyl radical potential [$E(H_2O/^{\bullet}OH)$ = 2.37 eV], such that the photoinduced holes can react with surface hydroxyl species to form

hydroxyl radicals.[180-182] However, the O 2p levels are low enough in energy for the photoinduced holes to oxidize either H_2O or surface OH^- to $^{\bullet}OH$. The XPS results revealed that mole percentage of substituted nitrogen in the TiO_2 was a linear function of mole percentage of niobium. The incorporation of Nb^{5+} in the sol-gel reaction leads to the charge compensation as depicted below;[183]

$$Nb_2O_5 \rightarrow 2Nb_{Ti}^{\bullet} + 2e^- + 4O_o^x + \frac{1}{2}O_2 \quad (20)$$

$$2e^- + 2Ti_{Ti}^x \rightarrow 2Ti_{Ti}^{'} \quad (21)$$

The free electrons formed facilitated the reduction of Ti^{4+} to Ti^{3+} ions which act as recombination centers. At low mole percentages (1-5 %), a stronger Ti^{3+} EPR signal and less substitutional nitrogen was found, while opposite trend was observed at high mole percentages of niobium (10-30%).[179] The N-Nb-TiO_2 nanotube arrays showed enhanced photoelectrochemical activity for water splitting under UV/visible light.[184] The XPS results suggested that nitrogen content increased because of niobium predoping, which reduced the formation energy of codoped systems compared to monodoped TiO_2.[185-186] The ratio between β-N and niobium was 0.46 suggesting that the positive charge induced by niobium was partially compensated by nitrogen at the surface. In addition, Nb reduced charge recombination by the presence of continuum like hybridized states from N 2p to Nb 4d orbital above the VB instead of localized states as observed in N-TiO_2.[185]

The narrow bandgap of N-Mo-TiO_2 was effective in RhB degradation under visible light.[187] The electronic structure and optical properties calculated using polarized density functional theory revealed that continuum states of hybridized N 2p and O 2p states at VB edge and Ti 3d and Mo 4d states at CB lower energy edge. Meanwhile, localized states vanish

completely from the forbidden bandgap which prolonged the lifetimes of charge carriers.[188-189] The N-Mo-TiO_2 synthesized through hydrolysis precipitation method combined with sonication post treatment was positive for phenol degradation under visible light attributed to small crystallite size, intense visible light absorption and narrow bandgap.[190] On codoping with Mo^{6+} and N^-, the electrons migrate from N 2p level to CB and Mo^{6+} dopant level leading to generation of more charge carrier density for participation in photocatalytic reactions. The XPS results revealed that anionic N^- substitutes oxygen atoms and coexisted as β-N and γ-N, while Mo^{6+} substitutes Ti^{4+} lattice sites.[190] The N-Cd-TiO_2 was better for MO degradation under visible light attributed to modification of TiO_2 structure as doping leads to crystal structure distortion, crystallinity reduction and increased specific surface area that promoted the effective adsorption of organics on the catalyst surface.[191] The crystal surface defects could inhibit the electron-hole recombination on catalyst surface. The cadmium was present as $CdCO_3$ due to gradual expulsion from Ti-O framework to titania surface and hindered the crystal growth during thermal treatment. The first principle calculations indicated that the energy gap of N-Cd-TiO_2 became narrow and local internal fields induced by codoping enabled photoexcited electron hole pair separation more efficiently.[191]

4.2.3 Incorporation of nitrogen along with poor metal ions into titania lattice

The photoactivity of various catalysts for 4-CP degradation under UV/visible light showed the sequence: N-Sn-TiO_2> N-TiO_2> Sn-TiO_2> TiO_2, attributed to enhanced visible light absorption and inhibition of charge carrier recombination.[192] The XRD studies revealed no unit cell expansion for N-Sn-TiO_2 despite the large ionic radius of nitrogen compared to oxygen, suggesting that nitrogen was distributed on titania surface rather than doping into the bulk. The Sn^{4+} substitutes Ti^{4+} lattice sites forming energy level below CB edge, while nitrogen on the

surface generates energy states that are situated above VB edge. During photocatalysis, electrons are excited from VB to Sn^{4+} energy level and from surface states energy level to CB. Meanwhile, CB electrons get trapped at Sn^{4+} energy level located at 0.4 eV below the CB.[193] Since the energy level of O_2/O_2^- is lower than Sn^{4+} and CB level, the excited electron are directly captured by surface adsorbed O_2 molecules to form reactive oxygen species. Contrarily, holes in the VB and surface states oxidize hydroxyl groups to hydroxyl radical or can directly oxidize 4-CP molecules.[192] Similarly, N-Bi-TiO_2 was active for Acid Orange (AO7) degradation under UV/visible light.[194] On visible light irradiation, electrons are excited from VB or nitrogen impurity states to titania CB which are later captured by Bi^{4+}/Bi^{3+} state. The density of oxygen vacancies induced by nitrogen dopant was decreased upon bismuth doping thus passivating the recombination centers and increasing the photocatalytic activity.[195] The N-In-TiO_2 (In = 7%) exhibited high activity for 4-CP degradation under visible light irradiation than N-TiO_2 and TiO_2.[196] The XPS and diffused reflectance spectroscopy (DRS) results revealed unique chemical species such as N-O and O-In-Cl_x (x =1 or 2) on the surface whose surface state energy levels were located close to VB and CB respectively. The electrons are excited from both the energy levels of N-O species to TiO_2 CB and from VB to O-In-Cl_x (x =1 or 2) on the surface leading to enhanced visible light absorption and charge carrier separation. Meantime, CB electrons may fall into O-In-Cl_x energy levels and the VB holes migrate to energy levels of N-O species. The 4-CP molecules adsorbed in the surface active sites is immediately oxidized by holes resulting in complete decomposition.[196]

4.2.4 Incorporation of nitrogen along with 5d metal ions into titania lattice

Mesoporous N-W-TiO_2 (W=1.5%) showed high tendency for RhB degradation under visible light due to synergism in nitrogen and tungsten codoping.[197] Upon illumination, electrons

are promoted from VB to tungsten impurity level which is captured by adsorbed oxygen giving rise to superoxide radical, while holes react with surface adsorbed water to give hydroxyl radical. Finally, these active oxygen species attack dye radical cations and decompose them.[197] The N-W-TiO_2 synthesized by micro emulsion method followed by a NH_3 treatment (400˚ C) shows selective oxidation of toluene and styrene under sunlight illumination and the activity was attributed to lack of tungsten rich patches/zones on the surface, decrease in bandgap and also to the favorable surface properties for hydroxyl radical formation.[198] The chemical entity of nitrogen species in N-W-TiO_2 existed as $(CN)^{n-}$ species in bulk and as $(NH_x)^{n+}$ on surface. The increase in calcination temperature > 450˚ C results in detrimental effect since tungsten was excluded from TiO_2 lattice resulting in large heterogeneity of nitrogen species.[199] The superior activity of N-W-TiO_2 (1% W) with twist like helix structure for phenol degradation under UV/visible was ascribed to following reasons;[200] (i) high specific surface area which allows efficient diffusion of electrons, vacancies and adsorbed molecules to catalyst surface leading to photoreactions;[201] (ii) stable mesoporous architecture and 3D connected pore system improved molecular transport of reactants and products; (iii) W^{6+} trapped the CB electron to prevent recombination centers; (iv) existence of Ti^{3+} and tungsten dopant creates a new band below CB, that serves as reactive electron trapping sites; (v) highly crystalline anatase phase facilitated the transfer of vacancies from bulk to surface. The twist like helix structure was formed due to the use of acetic acid in the synthesis, where the bidentate acetate ligand replaces chloride ion and gets bounded to metal ions in $TiCl_4$ precursor modifying the polymeric structure at molecular level promoting the emergence of 3D type polymeric structure, which are later transferred to helix like structure with regular ventages by the decomposition of acetate ligands in the gel. The acetic acid inhibits the hydrolysis condensation process which prolongs the gelation time and

prevents formation of irregular TiO_2 particles.[202] The N-W-TiO_2 (3 wt% W) nanoparticles fabricated by combining sol-gel and mechanical alloying method showed activity for MB degradation, while increasing tungsten content to 10 wt% favored sulfosalicyclic acid degradation under visible light.[203] The 'F' center induced by oxygen vacancies and donor-acceptor level induced by codopants serves as carrier traps that contributed to high photocatalytic activity. The XRD results showed the presence of anatase, rutile, srilankite and brookite phases, where srilankite phase was formed only in the ball milling process. During the mechanical activation, the powders were repeatedly welded, fractured and rewelded. The mechanical alloying increases the contact area between reactant powder particles as a result of reduced particle size and allows fresh surfaces to come into contact repeatedly. As a consequence, phase transformations that normally require high temperature proceeds preferably at low temperature. A large number of defects such as vacancies and dislocations could be induced into TiO_2 which can accelerate the atom diffusion process greatly inducing nitrogen incorporation.

$$2(NH_2)_2CO \rightarrow NH_3 + NH_2CONHCONH_2 \quad (22)$$

$$3(NH_2)_2CO \rightarrow 3NH_3 + C_3H_3N_3O_3 \quad (23)$$

The NH_3 adsorbed on surface and interface released active [N] and [H] under high pressure which diffuses faster through defects created by mechanical alloying. The [H] reacts with lattice oxygen to produce new oxygen vacancy, while active [N] occupies the oxygen vacancy position or serve as interstitial atom via O-Ti-N bond.[203] The N-W-TiO_2 showed exceptional potential for partial oxidation of styrene under visible light due to combined effect of codoping. The theoretical calculations revealed that titanium cation vacant sites (V_{Ti}) and surface wolframyl (W=O) species compensated the extra charge of the W^{6+} and N anions in N-W-TiO_2.[204] The incorporation of nitrogen at substitutional positions with the concomitant presence of W=O

species introduces localized states within the bandgap. The nitrogen impurity prefers the first coordination sphere of tungsten cation by ~0.43 eV with respect to equivalent positions of the first coordination sphere of the titanium cation. The stability diagrams for nitrogen incorporation in an undoped and tungsten doped anatase {101} surface show that implantation energy of substitutional nitrogen decreases with increasing tungsten content. On the contrary, interstitial nitrogen is destabilized by the presence of tungsten impurity (Fig. 12). The nitrogen doping allows absorption of visible light as electrons in VB is excited into these mid gap states and later to CB. The placement of W=O π levels above VB and partial overlap with N 2p levels, facilitates the electrons to excite from this midgap state. As result weaker W−O and highly specific reactive surface oxygen radical was formed. The W=O entity was regenerated at the surface by the presence of oxidative atmosphere which is thermodynamically favorable process with ΔE = 1.3eV.[204] The visible light activity of N-W-TiO_2 electrode sensitized with Fe-chlorophyllin (Fe^{3+}-Por) towards MO and phenol degradation was found to be dependent on the concentration of sensitizer.[205] The activity was maximum at 2mM Fe^{3+}-Por and decreased at higher concentration since the electrons are inclined to be consumed on TiO_2 surface. Adsorption of Fe^{3+}-Por at high concentration hinders the surface activity and light absorption capacity of TiO_2 resulting in lower photoelectrocatalytic (PEC) activity (Fig. 13).[206] In addition, 3d orbital of tungsten lowered the CB level and 2p orbital of nitrogen shifted the VB upwards.

$$TiO_2 + hv \rightarrow TiO_2(e^-_{CB}\ h^+) \quad (24)$$

$$Fe^{3+}\text{-Por} + e^-_{CB} \rightarrow Fe^{2+}\text{-Por} \quad (25)$$

$$TiO_2\text{-Por} + h\nu \rightarrow TiO_2\ (e^-)\text{-Por}^+ \quad (26)$$

$$TiO_2\ (e^-)\text{-Por}^+ + O_2 \rightarrow [TiO_2\text{-Por}^+] + O_2^{-\bullet} \quad (27)$$

$O_2^{-\bullet}$ + organic → degradation products (28)

Ti-OH + h^+ → Ti-OH^+ (29)

Ti-$OH^{\bullet-}$ + organic → degradation products (30)

4.2.5 Incorporation of nitrogen along with f block metal ions into titania lattice

The advantages of the lanthanides (Ln) as doping agent for TiO_2 can be outlined as follows; (i) complexing ability of Ln provides an effective mode for adsorption of organic pollutants on TiO_2 surface; (ii) effective trapping of CB electrons by Ln when they are confined to the TiO_2 surface; (iii) the electronic structure of lanthanide ions could lead to different optical properties and to the formation of labile oxygen vacancies with relatively high mobility.[207-209] The lanthanide ions with special 4f electron configurations are known for their ability to form complexes with various Lewis bases like acids, amines, aldehydes, alcohols, thiols etc. This interaction can increase the extent of adsorption of organic pollutants on the catalyst surface and is beneficial for improving the photocatalytic activity.[210]

The N-Ce-TiO_2 was exceptional for MO and reactive red dye X-3B degradation under visible light illumination due to the combined effects of nitrogen and cerium dopant in the titania lattice.[211-212] The nitrogen doping narrowed the bandgap and cerium with varied valence and special 4f level served as an electron trap.[213-215]

$Ce^{4+} + e^- \rightarrow Ce^{3+}$ (31)

$Ce^{3+} + O_2 \rightarrow O_2^{-\cdot} + Ce^{4+}$ (32)

$h^+ + H_2O \rightarrow {}^{\cdot}OH + H^+$ (33)

$O_2^{-\cdot} + 2H^+ \rightarrow 2{}^{\cdot}OH$ (34)

The existence of Ce^{4+}/ Ce^{3+} pairs created charge imbalance resulting in adsorption of more number of hydroxide ions on the surface, producing large numbers of hydroxyl radicals.[216] In addition, cerium doping also increased TiO_2 surface area by decreasing crystallite size. The XRD and thermogravitmetric differential scanning calorimetry (TG-DSC) analysis showed that cerium dopant inhibited the phase transformation to rutile as Ce^{4+} ion with larger ionic radius cannot substitute Ti^{4+} ion and therefore it surrounds the anatase crystalline forming Ti-O-Ce bonds at CeO_2-TiO_2 interface.[217] At this interface, Ti^{4+} is expected to substitute for Ce^{4+} in CeO_2 lattice to form octahedral Ti sites. This interaction between tetrahedral Ti and octahedral Ti inhibited anatase to rutile phase transformation.[218-219] Similar results were also found for N-Pr-TiO_2 towards BPA decomposition under visible light.[220-221] In contrast, N-Nd-TiO_2 showed poor photocatalytic activity for Malachite green degradation compared to undoped and individually doped TiO_2.[222]

The Sm-N-TiO_2 with 1.5 mol % samarium calcined at 400˚ C exhibited high activity for salicylic acid decomposition under visible light owing to its appropriate crystallite size, high surface area, good adsorptive capacity due to the formation of Lewis acid base complexes between Sm-N-TiO_2 and salicylic acid (Fig. 14).[223] In addition the recombination process was effectively inhibited by samarium dopant. The optimal dopant concentration of samarium was found to be 1.5 mol % as the charge carriers are efficiently separated only when thickness of space charge region is equal to light penetration depth.[224-225] The dopant inside the matrix can suppress or enhance the recombination depending on its concentration and its energy level position. The charge carrier trapping at low dopant concentration may not be obvious and at high concentration they may serve as recombination centers. Thus, optimal dopant concentration is necessary to

prolong the lifetime of charge carriers. Beyond the optimum dopant concentration, the rate of recombination starts dominating the reaction in accordance with the following equation:[226-227]

$$K_{RR} \alpha \exp(-2R/a_0) \quad (35)$$

where K_{RR} is the rate of recombination, R is the distance separating the electron and hole pairs, and a_0 is the hydrogenic radius of the wave function for the charge carrier.[228-229] As a consequence, the rate of recombination increases exponentially with the dopant concentration. This is because the average distance between the trap sites decreases with increasing the number of dopant atoms. On the other hand, the thickness of space charge layer is influenced by the dopant concentration according to the following equation:

$$W = \left(\frac{2\varepsilon\varepsilon_0 V_s}{eN_d} \right)^{\frac{1}{2}} \quad (36)$$

where 'W' is the thickness of space charge layer, ε and ε_0 are the static dielectric constants of the semiconductor and vacuum respectively, V_s is the surface potential, N_d is the number of dopant donor atoms and e is the electronic charge. The above equation clearly shows that W decreases as the dopant concentration increases. In addition, penetration depth (*l*) of the light into the solid is given by $l = 1/a$, where 'a' is the light absorption coefficient at a given wavelength. When the value of W approximates that of *l*, all the photons absorbed by the solid catalyst generates electron-hole pairs that are efficiently separated. Consequently, the existence of optimum value of N_d for which a space charge region exist whose potential is not less than 0.2 eV and whose thickness is more or less equal to light penetration depth can be understood by the above equations.[224-225] The charge carriers thus generated beyond the space charge region are not under the influence of electric/potential field and hence recombine rapidly. At high dopant concentrations, the dopant level itself can act as recombination sites for the charge carriers

evidently decreasing the photocatalytic activity. The N-Eu-TiO_2 particles with spheriodal shape synthesized through modified sol-gel method exhibited high photocatalytic activity for the degradation of brilliant red X-3B under visible light illumination ascribed to the high crystallinity and bandgap narrowing.[230] The Eu 4f level is shown to trap the CB electron to activate superoxide radical formation.[231-232] The N-Eu mesoporous TiO_2 microspheres with yolk-shell structure (TiO_2@void@TiO_2) obtained by facile one pot hydrothermal method at low temperature (180˚ C, 8h) showed better activity for RhB and MO degradation under visible light illumination due to synergistic effects induced by unique yolk shell structure with high specific surface area and large pore volume.[233] The scanning electron microscope (SEM) and TEM techniques revealed that formation of yolk-shell structure followed OR mechanism.[234-237] The XRD and XPS studies suggested that Eu^{3+} ions are distributed over titania surface as Eu^{3+} ion since it is difficult to incorporate into TiO_2 matrix at low temperature (180˚ C) due to its larger radius (0.112 nm) compared to Ti^{4+} (0.064 nm) ion. The abundant mesoporous structure was formed by CO_2 gas bubbles released during the hydrothermal decomposition of urea. Upon excitation, electrons located in localized nitrogen states are stimulated to CB and they are trapped quickly by Eu 4f level followed by reaction with molecular oxygen.[238-239] The photo-generated holes formed in localized nitrogen states react with hydroxyl groups and H_2O molecule to produce hydroxyl radicals which degrades the pollutant molecules.[240]

$$TiO_2\,(e^-) + Eu^{3+} \rightarrow TiO_2 + Eu^{2+} \quad (37)$$

$$Eu^{2+} + O_2 \rightarrow Eu^{3+} + O_2^{\bullet -} \quad (38)$$

$$Eu^{2+} + O_2 + H^+ \rightarrow Eu^{3+} + H_2O_2 \quad (39)$$

$$H_2O_2 + O_2^{\bullet -} \rightarrow OH^{\bullet} + OH^- + O_2 \quad (40)$$

$$TiO_2\,(h^+) + H_2O(\text{or } H_2O_2 \text{ or } O_2^{\bullet -}) \rightarrow\rightarrow \text{Products} \qquad (41)$$

N-Gd-TiO_2 prepared by hydrothermal method showed high photocatalytic activity for RhB degradation under visible light illumination.[241] The activity is attributed to the inhibition of particle growth which resulted in larger surface area and surface active sites.[242] In addition Gd^{3+} ion on the surface acts as sensitizer and absorbs light energy and transfers it to TiO_2, thereby enhancing its activity.[243]

4.3 Photocatalytic activity of Tridoped TiO_2

The tridoped C-N-S-TiO_2 hollow microspheres were prepared by fluoride-induced self transformation using L-cysteine as carbon, nitrogen and sulphur source showed superior activity for Brilliant Red X3B degradation under visible light illumination.[244] This enhancement in the activity was due to; (i) ability of photocatalyst to harvest photons from visible light; (ii) enrichment of dye adsorption on catalyst surface; (iii) effective charge carrier separation by two phases of the same semiconductor-undoped and doped TiO_2.[245-247] In another study C-N-S-tridoped TiO_2 nanorods prepared by hydrothermal method with 1:25 molar ratio of L-cysteine to $TiCl_4$ showed high removal efficiency for gaseous NO under simulated solar light irradiation.[248-251] The XRD study revealed enhancement in anatase fraction with increase in L-cysteine amount at the expense of rutile. During synthesis of undoped TiO_2, large amount of H^+ ions produced by $TiCl_4$ hydrolysis increased the solution acidity leading to production of rutile phase. In the presence of L-cysteine, -NH_2, -COOH and –SH groups coordinate with Ti atoms to bind L-cysteine to protonated neigbouring octahedrons sharing one edge. When another TiO_6 octahedra complex attacks the two octahedra sharing one edge with L-cysteine, only a spinal chain of octahedrons forms because of steric hindrance given by L-cysteine linked tightly to terminal Ti ions which inhibit rutile formation.[248] The C-N-S-TiO_2 (molar percent of cysteine to TiO_2 [R] is

4.2) was active for phenol degradation under simulated sun light illumination attributed to large number of surface hydroxyl groups and efficient charge carrier separation.[252] The XRD results showed only anatase phase for C-N-S-TiO_2 and triphasic for undoped TiO_2 (85% anatase, 10% rutile and 5% brookite) (Table 3). The XPS studies revealed that S^{6+} substituted Ti^{4+} ion, nitrogen occurs as both substitutional (N-O-Ti) and interstitial (O-Ti-N) position and carbon exist as mixed layer of carbonate on TiO_2 surface. The C-N-S-TiO_2 (R = 4.2) showed stronger Surface Photovoltage Signal (SPS) at 345 nm because of electronic transition from O^{2-} anti bonding orbital to lowest empty Ti^{4+}orbital;[253] stronger the SPS signal, higher the charge carrier separation as SPS signal arises from electron hole pair generation followed by separation under in built electric field (also called space-charge layer). With positive electric field, SPS signal increases markedly due to same direction of added outer and in built electric field and the signal became broad which was ascribed to trap-to-band transitions from surface states, while SPS response decreased for negative electric field which is characteristic of n-type semiconductors.[254] The highly transparent N-C-F-TiO_2 films prepared by a simple layer by layer dip coating method using TiO_2 sol and NH_4F methanol solution as precursors without using additional pore inducing agent showed enhanced activity for stearic acid degradation under visible light.[255] The high performance was originated from combined effects of tridoping and high surface area of the photocatalyst.[255] The doped carbon on the surface acts as sensitizers which could be excited to inject electrons into TiO_2 CB.[256] The doped nitrogen atoms improve the visible light absorption, while doped fluorine atoms facilitated formation of oxygen vacancies, which are important active species for initiating a photocatalytic reaction.[257-258] Initially, a layer of TiO_2 was coated onto the glass substrate then a second layer of NH_4F methanol solution was coated, followed by a third coating of TiO_2 sol. The first TiO_2 coating prevents the reactions of fluoride ions with

glass substrate. Subsequent coatings of NH_4F solution and TiO_2 sol prevent immediate precipitation of the reactants. The ensuing heat treatment at 500˚C results in the reaction between NH_4F and TiO_2 sol to form N- C-F-TiO_2. The gaseous byproducts (NH_3 and HF) induced high surface roughness in TiO_2 coating and generates non irradiated superhydrophilic surface. This superhydrophilicity is mainly due to the high roughness and highly accessible pores in N-C-F-TiO_2 films that reduce diffusion resistance within the film structure and subsequently allows a better penetration of water through the void. [259] The contact angle measurements of the films were 2.3-3.1˚ in the absence of illumination and they increase slowly in the dark (<1.8 in 30 days) which could be applied for fabricating self cleaning surfaces.[255] The contact angles were tested without light illumination and kept in dark for 1-30 days.

The N-S-Fe-TiO_2 synthesized through simple one step sol-gel reactions in presence of ammonium ferrous sulphate showed visible light activity for phenol degradation.[260] The dopants Fe^{3+}, S^{4+} and S^{6+} substituted Ti^{4+} ion and nitrogen coexisted as substitutional (O-Ti-N) and interstitial (Ti-O-N) forms. The mechanism of photocatalytic process is shown in the following equations.[260]

$$\text{F-N-S-TiO}_2 + h\nu \rightarrow h^+_{VB} + e^-_{CB} \quad (42)$$

$$Fe^{3+} + e^-_{CB} \rightarrow Fe^{2+} \quad (43)$$

$$Fe^{2+} + O_{2(ads)} \rightarrow Fe^{3+} + O_2^- \quad (44)$$

$$Fe^{2+} + O_{2(ads)} \rightarrow Fe^{3+} + O_2^- \quad (45)$$

$$O_2^- + 2H^+ + e^-_{CB} \rightarrow OH^\bullet + OH^- \quad (46)$$

$$h^+_{VB} + OH^- \rightarrow OH^\bullet \quad (47)$$

$$OH^\bullet + C_2H_5OH \rightarrow .... \rightarrow CO_2 + H_2O \quad (48)$$

The high SPS response of Fe-N-S-TiO_2 was due to the improvement in crystallinity which made semiconductor electronic band structure perfect, leading to decrease in surface defects promoting the charge separation and transfer process.[260]

The ellipsoidal N-F-W-TiO_2 particles around 20 nm in length and 10 nm in width showed 98 % RhB degradation and 94 % carbon removal under visible light.[261]The doping of fluorine induces the formation of Ti^{3+} ion and W^{6+} dopant forms energy level below CB that serves as electron trapping sites to reduce recombination. On the other hand, nitrogen doping creates acceptor level facilitating visible light absorption to produce more charge carriers.[262-263]

$$W^{6+} + e^{-} (TiO_2)_{CB} \rightarrow W^{5+} \quad (49)$$

$$W^{5+} + h^{+} (TiO_2)_{VB} \rightarrow W^{6+} \quad (50)$$

In another study, MO degradation on N-S-Gd-TiO_2 (Gd = 0.6 at wt %) was observed under visible light and the activity is accounted to;[264] (i) an increase in charge carrier lifetime by Gd^{3+} ions using 4f level for trapping the electron and the results are substantiated by fluorescence lifetime studies; (ii) all dopants introduced new electronic states in bandgap enhancing visible light absorption.[265-267] The PL studies revealed that PL signals were largely raised from defect level and peak maximum around 430 nm was due to the increased electron density at oxygen site as a result of nitrogen and sulphur substitution in TiO_2 lattice which are less electronegative than oxygen.[264]

The N-F-Ta-TiO_2 with 1 % molar ratio of Ta to Ti using NH_3 and TaF_5 as precursors shows efficiency for RhB and phenol degradation under visible light due to the synergistic effects such as increased crystallite surface area, increased hydroxyl radical generation and high visible light absorption.[268] The EPR and XPS studies revealed that N-Ta interaction induced charge

compensation to form fully occupied continuum like N 2p-Ta 5d hybridized states in VB edge, which promotes visible light absorption and improves charge carrier separation (Fig. 15). The fluorine dopant facilitated nitrogen incorporation promoting the formation of N 2p-Ta 5d hybridized states. The coexistence of tantalum and nitrogen narrows the bandgap by the formation of charge transfer from positively charged tantalum to negatively charged nitrogen leading to the formation of stable N-Ta chemical bond. The N_n (nitrogen atom neighbored to tantalum atom) and N_f (nitrogen atom without adjacent tantalum atom) existed in tridoped TiO_2 and the holes produced in N 2p band from N_n had high oxidation power than N 2p band of N-TiO_2.[269] The N-C-Ce-TiO_2 mesoporous membrane synthesized via a weakly alkaline sol-gel route using P123 template and calcined at 450˚C showed potential for MO degradation under visible light.[270] The cerium ion facilitates successful doping of nitrogen and carbon atoms which lowered the bandgap to 2.14 eV and improved the visible-light activity. The cerium doping strengthened the Ti-O bond and inhibited the transformation to rutile and rapid growth of the crystals, thereby preventing the collapse of assembled pores during the calcinations process. The filtration experiments of the composite membrane presented a low cut-off molecular weight of 3300 Da and pure water flux of 4.05Lm^{-2} h^{-1}per bar suggesting that such photocatalytic membranes have great implications for environmental applications like wastewater treatment, because of their ability to decompose dissolved organic contaminants while simultaneously removing pollutants.[270]

The N-Yb-P-TiO_2 with optimal 5 wt% phosphorous dopant exhibited highest photoactivity for MB degradation under UV/visible light due to cooperative effects of tripdoping.[271] The doped phosphorous inhibited crystal growth, recombination of charge carriers by serving as electron traps centers and enhanced the photon absorption efficiency.[272] In

addition, substituted P^{5+} ion induces charge imbalance which is compensated by additional surface hydroxyl group and by the decrease of oxygen vacancies. The Yb^{3+} ions act as electron scavengers and then release them to surface adsorbed O_2 to form superoxide radicals. Also, tridoping increases the surface hydroxyl groups and decreases the point of zero charge of TiO_2 from 6.58 to 3.29 contributing to higher extent of adsorption and dispersion of MB molecules on the surface. The increased mesopore sizes were beneficial to mass transfer through rapid diffusion of reactants and products. During photocatalytic reactions, apparent rate constant indicated that ytterbium and phosphorous doping enhanced the activity while N-TiO_2 lowered its activity compared to undoped TiO_2 (Table 4). On the contrary, N-P-TiO_2 shows a higher photoactivity than N-TiO_2, but a lower performance compared to P-TiO_2, implying the absence in synergetic effect for N-P-codoped catalyst.[271] The N-P-Mo-TiO_2 showed efficient activity for MB and sulfosalicyclic acid degradation under visible light than Mo-TiO_2 and P-N-codoped TiO_2 and the activity is attributed to efficient reduction in bandgap.[273] The phosphorous and nitrogen dopants introduce acceptor levels above VB and Mo donor levels are found below the CB edge. The XRD results showed MoO_3 phase formation at higher Mo (0.72) content, which was beneficial for improving photoactivity of N-P-Mo-TiO_2.[273]

5.0 N-TiO_2 coupled with other semiconductors

The coupling of two semiconductors with suitable band edge potentials lead to the construction of heterojunction interface between the semiconductors with electric-field-assisted charge carrier transport from one semiconductor to the other via interfaces.[274-275] The geometry of particles, surface texture, and particle size play a significant role in interparticle electron transfer.[276-277] Appropriate placement of the individual semiconductor and optimal thickness of the covering semiconductor are crucial for efficient charge separation. In addition abundant charge carriers

will be available at the surface/interface of two semiconductors for redox reactions and also extends the energy range of photoexcitation.[278-279]

The N-TiO_2 obtained by direct amination of DP25 and triethanol amine as nitrogen source showed visible light activity for MO degradation.[280] The XPS and wavelength dispersive spectroscopy spectra (WDS) spectra proved that nitrogen atoms substituted titanium (y = 27) and oxygen (x = 0.36) lattice sites with 21% nitrogen dopant concentration as Ti-O-N-O linkage (nitrogen substituted for titanium) and Ti-N-Ti-O / Ti-N-Ti-N linkage (nitrogen substituted for oxygen). In addition, Ti-O-N-N linkages also originate from nitrogen substitution for both titanium and oxygen.[281] Thus, formation of new heterostructure $(TiO_2)_m/(Ti_{1-y-m}O_{2-x-2m}N_{x+y})$ having both wide and narrow bandgap improved the visible light absorption and charge carrier separation as a result of vectorial transfer of electron and hole from narrow band $(TiO_2)_m$-$(Ti_{1-y-m}O_{2-x-2m}N_{x+y})$ to wide bandgap TiO_2.[280] The 1D N-TiO_2 nanorods with anatase-brookite heterostructure (82.4 % anatase and 17.6% brookite) showed high activity for MO and 4-CP degradation compared to TiO_2 nanoparticle without one dimensional structure under UV/visible light.[282-283] This architecture was designed by one pot solvothermal method (200-220˚ C, 48 h) using hydrazine hydrate and TiO_2 colloids as starting materials. During alkaline thermal process, titania nanoparticles are dissolved in solution and recrystallized to TiO_2 embryos. When the $N_2H_4.H_2O/TiO_2$ colloids concentration ratio is 16.8, N-TiO_2 had smaller nanorod content, since the growth of TiO_2 embryos was retarded by increase in number of N_2H_4 molecules per unit volume concentration of TiO_2 colloids. At the same time, if $N_2H_4.H_2O/TiO_2$ colloids ratio is below 2.8, ellipsoidal nano particles were observed. Under visible light, electrons from localized N 2p states in both anatase and brookite are excited to individual CB leaving holes on localized states. Meanwhile, band edge positions of anatase and brookite facilitates interfacial migration of

electrons from brookite to anatase. The energy barrier between anatase and brookite suppresses back electron transfer which functions like one way valve inhibiting recombination rate.[284-288] A same scenario occurs under UV light except that electrons in VB are excited to CB (Fig. 16).[282] N-P25TiO_2/amorphous Al_2O_3 composites fabricated via one step solution combustion method exhibited enhanced activity for MO and MB degradation mediated by hydroxyl and superoxide radicals.[289] This was ascribed to cooperative effects of amorphous $A1_2O_3$ and nitrogen doping in TiO_2 and large surface area.[289] When visible light was irradiated, electron is either transferred from nitrogen impurity state to CB of Al 3d level or from direct excitation from VB to Al 3d level (Fig. 17). The distance between aluminium and oxygen atoms in combustion synthesized amorphous Al_2O_3 samples becomes shorter and energy bandgap becomes smaller favoring electron transitions.[290] The amorphous Al_2O_3 has high electron transfer ability from P25 as it contains more defect sites than crystalline $A1_2O_3$.[289]

The pore wall structure and surface properties of mesoporous N-TiO_2/ZrO_2 resulted in fast ethylene decomposition in air under visible light.[291] The introduction of ZrO_2 stabilized its porous structure rendering large surface to volume ratio and inhibited anatase to rutile transition and it further stabilizes nitrogen in N-Ti-O structure. The preservation of interconnected porous nano networks facilitates the transport of small molecules through interior space and favored visible light harvesting through multiple scattering within solid framework.[292] The performance of N-TiO_2/V_2O_5 (0.5 wt% V_2O_5) was appreciable for gaseous toluene degradation under visible light compared to N-TiO_2, SiO_2/V_2O_5 and V_2O_5.[293] Since the band edge potential of V_2O_5 (E^0_{CB} = 0.48eV) was lower than N-TiO_2 (E^0_{CB} = -0.19eV) CB level, electron transfer from N-TiO_2 to V_2O_5 was thermodynamically favorable, facilitating partial reduction of V^{5+} to V^{4+}, the electron is then detrapped to adsorbed oxygen to promote charge separation.[294-297]

$$V^{5+}(V_2O_5) + e^- \rightarrow V^{4+} \quad (51)$$

$$V^{4+} + O_2 \rightarrow V^{5+}(V_2O_5) + O_2^{-\bullet} \quad (52)$$

The mesoporous SiOC/20wt% N-TiO_2 (65 wt% anatase and 35 wt% rutile) ceramic composites prepared by incorporation of N-TiO_2 powders into vinyl-functionalized polysiloxane polymer followed by pyrolysis (700˚ C, 2 h in argon atmosphere) enhanced the MB degradation rate under UV-vis illumination.[298] This was attributed to changes in electronic structure, synergistic effects of higher surface area and high mesoporosity that promoted the pollutant adsorption on catalyst surface. The XRD results show that pyrolysis temperature strongly influenced the phase stability as pure TiO_2 which was stable till 800˚ C and the aggregation of dopants in TiO_2 retarded the phase transformation from anatase to rutile at this temperature. On increasing pyrolysis temperature to 900˚ C, anatase phase completely disappeared with formation of new Ti_4O_7 phase and small amount of rutile. Above 900˚ C, rutile peaks completely vanished and Ti_4O_7 and Ti_2O_3 phases started to dominate. In addition, microporous pure SiOC gets is transformed to mesoporous composite due to structural rearrangement of polymer chains on the addition of N-TiO_2. The intensity of UV-visible absorption spectra was high for SiOC/20 wt% N-TiO_2 owing to the presence of amorphous SiOC matrix incorporation to crystalline oxide powders which increased the electric charge of the oxide resulting in modification of electron hole formation process.[299] The hollow N-Co-TiO_2/SiO_2 microspheres showed enhanced RhB degradation under visible light irradiation compared to N-TiO_2/SiO_2, TiO_2/SiO_2, Co-TiO_2/SiO_2.[300] Cobalt served to broaden the visible light absorption.

The N-TiO_2/ZnO nanotube arrays composite with well aligned surface structure showed gaseous NO_x decomposition under UV/visible light being superior to ZnO nanorods, ZnO

nanotube, N-TiO_2, commercial TiO_2 and ZnO nanorod arrays/N-TiO_2 composite.[301] The heterojunction structure promoted vectorial charge transfer from one semiconductor to another with thermodynamically favorable band edge position leading to increased interfacial charge transfer and catalytic efficiency (Fig. 18). The peculiar tubular nanostructure provided more interfaces for NO_x adsorption and photons were perfectly trapped and reduplicatively absorbed both inside and outside the tubes.[301] The N-TiO_2/$Bi_{20}TiO_{32}$ (10% Bi) increased the 2,4-DCP degradation under visible light due to the combined effects of visible light absorption, low charge carrier recombination and improved crystallinity accompanied by reduction of intrinsic surface defects.[302-303] The XRD and XPS results showed the presence of $Bi_{20}TiO_{32}$ on titania surface ascribed to abundant bismuth ions and interaction between surface titanium and bismuth ions during calcination. Apparently $Bi_{20}TiO_{32}$ has small bandgap of 2.09 eV, where VB is composed of hybridized largely dispersed Bi 6s and O 2p orbitals which increased the charge carrier mobility. [304-305] The ability of Bi-O bond to donate electrons helps in transferring electron to surface adsorbed species eliminates the recombination pathways. The excited electrons from nitrogen impurity band are transferred to titania and $Bi_{20}TiO_{32}$ CB under visible light. The excited electrons can also be captured by doped Bi^{4+}/ Bi^{3+} energy level below titania CB subsequently transferring electrons to adsorbed oxygen producing superoxide radicals and VB holes directly oxidizes hydroxyl anion. Finally, $Bi_{20}TiO_{32}$ also absorbs visible light generating charge carriers for further redox reactions.[302]

The high adsorption of SMZ on N-P25-TiO_2/activated carbon (AC) resulted in faster degradation under solar light.[306] This composite had anatase-rutile mixture that increased the efficiency of charge-carrier separation by transferring electrons from anatase to rutile CB[307-308] and also from rutile CB to anatase trapping sites (Fig. 19).[309] In addition, AC support reduced

the agglomeration of supported N-TiO_2 nanoparticles and doped nitrogen created localized states within the bandgap which served as trap sites for holes.[310-311] The effect of ultrasonication disruption on physical stability revealed that N-P25-TiO_2(20+15)/AC exhibited greater resistance to titania dislodgement due to stronger chemical bonding between N-P25 and N-TiO_2 (sol).[306] The N-TiO_2/AC exhibited high adsorption capacity and degradation rates for BPA over a range of excitation source and demonstrated high potential for reuse compared to unsupported photocatalyst and binary mixture of titania and AC.[312] Furthermore calcination of the composite under air ambiance removed organic residues permitting greater exposure of titania surface to receive incident light. The creation of interfacial energy between surface AC and N-TiO_2 resulted in anti calcination effect significantly restraining rutile growth.[313] The carbon coated N-TiO_2 mesostructure prepared by one step solvothermal method with chitosan as carbon and nitrogen source showed high efficiency in visible light degradation of MB compared to only carbon coated TiO_2, attributed to bandgap narrowing and the heterojunction formed between the carbon and N-TiO_2.[314] The nitrogen doping level above the VB shifts the absorption to visible light region[315] and converts some Ti^{4+} to Ti^{3+} that forms a donor energy level below the CB, additionally contributing to light absorption. The carbon species act as surface sensitizers and transports the electrons to TiO_2 CB, besides enhancing the MB adsorption on the catalyst surface due to existence of acidic surface groups.[314] The N-TiO_2 nanoparticles decorated on graphene sheets [N-TiO_2/GB] was active for MO degradation under visible light (Fig. 20).[316] The graphene in composite extends visible light absorption as a result of chemical binding via Ti-O-C bond between TiO_2 and graphene. The excellent conductivity and two dimensional planar structures facilitated rapid transport and separation of charge carriers.[317-318] The N-S-TiO_2/graphene oxide (5% GO) composite showed enhanced activity for MO degradation under UV light irradiation.[319]

The high activity was accounted to large surface area, oxygen containing functional groups and large aromatic domains that were inclined to be bound by conjugated MO molecules via π-π stacking. In the composite, excited electrons are transferred from CB to GO via percolation mechanism that accelerates the interfacial electron transfer process.[320] In addition, the dopants increased the number of electrons and holes to form reactive species and oxygen vacancy induced for charge compensation was reduced by codoping.[319] The N-TiO_2/ 8 % wt graphite-like carbon nitride (g-C_3N_4) showed significantly enhanced activity for RhB decomposition under fluorescence light irradiation due to dye adsorption and sensitizing role of g-C_3N_4.[321] SPS revealed small SPS signal for N-TiO_2/g-C_3N_4 (8% wt) implying minimum band bending difference and accumulation of static electrons on the surface.

A dual phase material (DP 160) comprising hydrated titanates ($H_2Ti_3O_7$. xH_2O) and anatase TiO_2 showed phenol degradation under visible light attributed to excitation via inter band states, surface sensitization, improved adsorptive properties of aromatic compounds due to the presence of N-carbonaceous species layer containing Ti-N bonds (eg. -O-Ti-NH^+-R-NH^+-Ti-O-) and heterojunction like structure promoted directional interfacial charge transfer.[322]

A lepidocrocite type titanate $K_{0.81}Ti_{1.73}Li_{0.27}O_4$ coupled with N-TiO_2 composite showed excellent photocatalytic activity for decomposition of NO_x gas under UV/ visible light.[323] This activity was attributed to bridging structure formed between nano and plate like particles together with increased specific surface area which provided better accessibility for the target molecules. Meanwhile, sandwich like structure increases the dispersion of N-TiO_2 inhibiting their agglomeration. The recombination of charge carriers was effectively depressed due to different bandgap structures of $K_{0.81}Ti_{1.73}Li_{0.27}O_4$ and N-TiO_2. [323] The N-TiO_2/$CaAl_2O_4$: (Eu, Nd) luminescent composite prepared by a soft planetary ball milling at 200 rpm for 20 min exhibited

potential activity for gaseous NO degradation under UV light irradiation and the persistent activity continued even after turning off the light till 3 h attributed to depression of agglomerated N-TiO_2 nanoparticles and visible light absorption by N-TiO_2 via long afterglow emitted by $CaAl_2O_4$: (Eu, Nd) even in the dark.[324] On irradiation of $CaAl_2O_4$: (Eu, Nd) electron and holes are produced in Eu^{2+} ions and Nd^{3+} ions capture some free holes moving in the VB. When the excitation source was cut off, some holes which are captured by the Nd^{3+} ions acting as traps were thermally released to the excited state of Eu^{2+}, accompanied by emission of light. This emission is a symmetrical band at 440 nm, a strong blue emission, which is attributed to the typical $4f^6\ 5d^1$ - $4f^7$ transition of Eu^{2+}.[325] The N-TiO_2 with nitrogen impurity band above VB induces a second bandgap about 2.34 eV which is lower than emitted blue luminescent energy.[45] Hence N-TiO_2 gets excited once the light is turned off. When the composite sample was prepared by planetary ball milling at 200 rpm, the extent of degradation of deNO_x increased with an increase in the ball-milling speed due to the positive effect of homogeneous mixing. While, the deNO_x degradation decreased at ball-milling speed >200 rpm due to increase in lattice strain and defect which promoted recombination of charge carrier. The optimum loading was found to be 40% N-TiO_2 which leads to better dispersion of N-TiO_2 on $CaAl_2O_4$: (Eu, Nd) surface, which is a phosphor material.[324] Similarly, N-TiO_2/$Sr_4Al_{14}O_{25}$: (Eu, Dy) was active for acetaldehyde removal under dark, compared to N-TiO_2 /$CaAl_2O_4$: (Eu, Nd).[324]

6.0 Metal deposition on N-TiO_2 (M/N-TiO_2)

The deposition of various metals like Pt, Ag, Au, Pd, Ni, Rh and Cu on semiconductor surface enhances photocatalytic activity via modifying semiconductor surface properties, discharging photogenerated electrons across the interface and provides a redox pathway with low overpotential inhibiting the recombination of charge carriers.[326-330] The formation of a space-

charge layer at the semiconductor-metal interface facilitates charge separation under band gap excitation. It is known that the surface plasmons created by the noble metal deposits on the catalyst surface couples with the electric fields of the incident radiation enhancing the separation of photogenerated charge carriers and also assists in the charge carrier transfer process across the catalyst/liquid interface.[331-332]

The photoactivity of various catalysts towards MO and MB degradation under visible light shows the following order: Ag/N-TiO_2 hollow spheres>Ag-hollow spheres>Ag-N/P25>Ag-P25> N/hollow sphere>N/P25.[333] This was ascribed to the bandgap narrowing by nitrogen doping and presence of silver clusters which serves as electron sink and thereby improves charge separation.[334] The embedded silver nanoparticles between N-TiO_2 pillars degraded RhB under visible light. The induced localized surface plasmon absorption edge of silver particles in the visible region and its role as electron sink favored efficient photocatalysis.[335] The N-TiO_2 pillar was synthesized by reactive dc sputtering to produce TiN porous film, followed by a simple oxidation process at elevated temperature in oxygen or air, while the silver nanoparticles were embedded between N-TiO_2 pillars by photoreduction of Ag^+ ions in aqueous solution under visible light. The bandgap of N-TiO_2 was tuned by controlling oxidation temperature, oxygen concentration and oxidation time. In air at 900˚ C, maximum oxidation is achieved in 5h, corresponding to blue shift from 530 (for 1h oxidation) to 500 nm (after 5h). In contrast, in pure oxygen at 900˚ C the blue shift to 500 nm is completed within 1h and no further change takes place on increasing duration (up to 10h) suggesting that replacement of nitrogen by oxygen is a gradual process and saturation level is achieved after 5h.[335] The Ag/N-TiO_2 prepared via hydrothermal process in silver-ammonia solutions showed better visible light activity for RhB degradation.[336] The XPS results suggested that Ag loading on TiO_2 surface significantly

restrained the removal of nitrogen dopant from the bulk lattice during the hydrothermal treatment (130˚ C, 3h) and its probable removal gradually decreased with increase in Ag content (Fig. 21). This stabilization of nitrogen dopant was attributed to electron transfer from Ag 5s to N 2p orbital. Since the energy of N 2p (N^{2-}) is lower than Ag 5s orbital, the electrons transfers from Ag 5s to N 2p orbital to make it completely filled (N^{3-}) electronic configuration. The fluorescence spectra revealed that the activity increases gradually with increasing Ag content initially and decreases after reaching optimal Ag/Ti molar ratio of 0.92 mol % suggesting that optimum content of Ag serves as electron traps, while superfluous Ag would be detrimental.[336] The Ag/N-TiO_2 hollow nanorod arrays synthesized on glass substrate by one pot liquid phase deposition method using ZnO nanorod arrays as template exhibited highest photocatalytic activity for MB degradation under UV and visible light illumination with 0.03 and 0.07 M $AgNO_3$ concentrations respectively.[337] This enhanced activity was attributed to synergistic effects of Ag loading, nitrogen doping and multiphase structure of anatase/rutile.[337] The Raman results suggested that $AgNO_3$ additive in the precursor solution promoted anatase to rutile phase transition. The XPS studies show Ag 3d peak around 367.8 eV with a negative shift compared to bulk Ag (368.2 eV) owing to electron transfer from TiO_2 to metallic Ag deposit.[338-340] Under visible light, electrons are excited from VB and nitrogen impurity energy levels to TiO_2 CB which is trapped by Ag deposits favoring interfacial charge transfer process.[341] The Ag/N-C-TiO_2 shows enhanced activity for DCP degradation under visible light and it also inhibited luminescent activity of *Vibrio fisheri* owing to TiO_2 induced oxidative stress which led to genotoxcity and cytotoxcity in microbial organism.[342-343]

The Pt/N-TiO_2 exhibits enhanced oxidation kinetics for acetic acid, toluene and acetaldehyde. Cu and Fe loaded N-TiO_2 showed high rates for acetic acid and formic acid

photoxidation respectively compared to N-TiO_2.[344] The extremely high rate for formic acid oxidation over Pt/N-TiO_2 is due to the combined effect of photocatalysis and thermal catalysis (in dark without illumination) at room temperature facilitated by the presence of nanosized Pt (1-2 nm) on the surface. The ESR studies confirmed the presence of O^- and O_3^- stabilized on the catalyst surface was responsible for this dark thermal catalysis. The Fenton like reactions were found to be operative with Fe and Cu loaded N-TiO_2 leading to high degradation rates.[344] The Fe/N-TiO_2 and Pt/N-TiO_2 improved the visible light induced activity for decomposition of de NO_x, wherein Pt/N-TiO_2 exhibited several times higher activity than that of N-TiO_2.[345] The activity was related to chemiluminescence intensity generated by singlet ($^1O_2$). The rate of degradation of de NO_x decreased with an increase in chemiluminescence emission intensity indicating that singlet oxygen generation was detrimental for de NO_x degradation. The photoexcitation of titania leads to the formation of superoxide radicals which is a doublet with one unpaired electron (-41.4kJ/mol). The holes may trap one electron from superoxide radical to produce singlet oxygen or triplet oxygen. The singlet oxygen has a pair of electrons in one orbital and a second empty equal-energy orbital. Metastable singlet oxygen possessed more energy (94.7 kJ/mol) than ground-state triplet oxygen (0 kJ/mol).[346] From the energy level, it is observed that superoxide radical is produced easily and quickly, while singlet oxygen formed slowly and required extended energy (Fig. 22). The formation of singlet oxygen competes with the formation of superoxide and hydroxyl radicals;[345]

$$^{\bullet}O_2^- + h^+_{VB} \rightarrow {}^1O_2 \qquad (53)$$

$$^{\bullet}O_2^- + h^+_{VB} \rightarrow {}^3O_2 \qquad (54)$$

The simultaneous surface and bulk modification achieved through Pt or Au deposition and N-F-codoping was favorable for downhill reaction (formic acid oxidation) and uphill reaction (H_2 production).[347] The NH_4F doping guarantees most active TiO_2 phase stabilized up to high calcination temperature ensuring high crystallinity and good photoinduced charge carrier production whereas Pt or Au deposition on the catalyst surface increased the charge carrier separation. But Pt was better co catalyst than Au for photocatalytic activity which was related to their work function i.e. energy required to promote an electron from the Fermi level to vacuum. Greater the difference between the metal work function and the semiconductor, higher will be the height of Schottky barrier generated by the band alignment at metal semiconductor heterojunction.[348] The efficiency of photogenerated electron trapping by the metal and subsequent transfer to oxygen molecules adsorbed on the catalyst is consequently increased.[347] The high photoactivity of Pd/N-TiO_2 (0.6% Pd) for Eosin Yellow decomposition under visible light arise from synergistic effects of palladium deposition and nitrogen doping.[349] The palladium on TiO_2 surface creates Scottky junction between metal and semiconductor which acts as a sink for photogenerated electrons.[349] The noble metal loading (Pt, Au and Ag) on mesoporous N-TiO_2 improved the CO_2 photoreduction by water to methane under visible light. The XPS results indicated that the dopant nitrogen exist as molecularly chemisorbed nitrogen species (N_2) or nitroxide species (eg NO and NO_2) which induced visible light activity.[350] The efficiency of the cocatalyst followed the order: Pt>Au>Ag with optimum loading of 0.2 wt%, 0.02 wt% and 0.1 wt% respectively. This optimum metal island traps more number of electrons whereas excess amount would serve as recombination centers and reduce the light absorption capability of the catalyst. The Pt has higher work function of 5.65 eV than Au (5.1 eV) and Ag (4.26eV).[351] Thus electrons can transfer more efficiently to Pt. Simultaneously the adsorbed

water molecules reacts with holes to form H^+ which in turn reacts with electrons detrapped by Pt to produce $H^{\cdot}$ radicals subsequently reducing CO_2 to hydrocarbons.[352-354] The optimum nitridation temperature to achieve best activity was 525˚C and optimum amount of nitrogen was 0.84% on the basis of lattice oxygen atoms. The larger amount of nitrogen would result in defect sites and non stoichoimetry in the material. The blank test performed with 0.2 wt % Pt/TiO_2 in presence of water vapor and in absence of CO_2 under UV illumination in N_2 atmosphere revealed that methane could be produced from the catalyst associated carbon residues.[350] The N-TiO_2 (B) nanofibers decorated with Pt nanoparticles showed highest hydrogen generation rates of 700 μmol/h and 2250 μmol/h under UV-A (365 nm) and UV-B (312 nm) light irradiation compared to Pd decorated N-TiO_2 nanofibers attributed to direct electron transition from p-states to empty states of Pt nano particle which are more energetically favored, compared to the conventional transition involving from VB or impurity level to CB followed by a subsequent transfer to the metal.[355] The better activity under UV-B exposure was due to large number of high energy photons enough to induce the generation of electron-hole pair. The N-TiO_2 (A) nanofibers was synthesized by the calcination of $H_{2-x}Na_xTi_yO_{2y-1}$ nanofibers at 600˚C in ammonia gas flow for 15 h, while N-TiO_2(B) was synthesized also from $H_{2-x}Na_xTi_yO_{2y-1}$ calcined in air at 600˚C for 12 h to form TiO_2 anatase nanofibers, followed by second calcinations step in ammonia gas at same temperature for 3 h.[355] In Pt/N-TiO_2, Pt has smaller particle size and high dispersion value on catalyst surface compared to palladium.[355] The amine functionalized, silicate sol gel supported, gold deposited N-P25 (APS/Au-N-P25) showed enhanced photocatalytic oxidation for CO and reduction of Hg(II) ions under visible light attributed to the synergistic effects of gold nanoparticles (with sub 5 nm size) deposited on N-P25.[356-360] When Au and NP25 are connected electrically, electron migration from TiO_2 to Au occurs until the two Fermi levels are aligned.

Hence the metal surface acquires excess negative charge and semiconductor becomes positively charged. The Au acts as an electron sink increasing interfacial charge transfer process and minimizes the recombination rates. The presence of $–NH_2$ group in amine functionalized silicate solgel with nitrogen having non bonding electrons allows interaction of Hg(II) ions on the APS/Au-N-P25surface.[361-362] This results in the increased adsorption and preconcentration of Hg(II) ions on the surface. The Au instantaneously transfers electrons to reduce Hg(II) to Hg and holes in VB oxidize sacrificial electron donor (oxalic acid). The optimization of Au was found to be 2 and 4 wt % for reduction of Hg(II) ions and CO oxidation respectively. The excess Au loading decreased the activity due to; (i) absorption and scattering of incident light by excess of Au;[363-364] (ii) shielding of incident photon at N-P25 by Au; (iii) negative effect on photoreduction due to oxidation of Au by holes or surface hydroxyl radicals.[356]

The mesosporous Cu/N-TiO_2 showed good degrading ability for gaseous xylene under UV/visible light ascribed to mesosporous structure.[365-366] The catalytic activity decreased for Cu loadings higher than 0.6 mol % as the active sites on the catalyst were covered with excess Cu, with simultaneous increase of recombination kinetics.[367] The bottles coated with Cu/N-TiO_2 films and annealed at 600˚ C degraded MB more rapidly than uncoated bottles in field trials, while N-TiO_2 coating did not show any change as the hole produced by visible light irradiation in mid gap level (induced by doping) did not have sufficient redox potential to oxidize MB.[368] The Cu doped TiO_2 showed *E. coli* and *Enterococcus faecalis* inactivation due to increased visible light absorption and anti-microbial properties of copper atoms at exposed surfaces. However, doping with nitrogen atoms (Cu/N-TiO_2) reduced the performances as nitrogen atom in lattice acts as recombination centers. The Cu/N-TiO_2 accelerated bacterial inactivation when coated on glass beads, but not when coated on internal surface of glass bottles, indicating that

reactive species produced at Cu-N-TiO_2 surface are short lived and can only diffuse short distances (in the order of μm) and that bacterial inactivation by such reactive species may thus be transport limited. The H_2O_2 and superoxide radical are important reactive species that might plausibly have a mean diffusion distances on this length scale.[369] Bacterial cells may also adhere to catalytic surface, thereby magnifying the effects of short lived radical species.[370] The formation of singlet oxygen, a less oxidative reactive oxidation species was reported to be responsible for bacterial decontamination.[371] The loading of copper (0.5 wt %) on N-TiO_2 was found to be beneficial for gaseous acetaldehyde and bactericidal activity under visible light, while loading with Pt, Zn and La did not exhibit any effect, suggesting that Cu serves as electron trap sites and extend the carrier lifetime.[367,372]

7.0 Hydrogen evolution using N-TiO_2

Solar energy is enormous in nature ($3x10^{24}$ J/year) i.e. 10000 times higher than present energy need.[373] This provides wide scope for photocatalytic reduction of water to generate clean and green fuel "hydrogen" H_2 as an energy carrier with a high calorific value 122 kJ g^{-1} (2.75 times greater than hydrocarbon fuels) is clean and renewable.[374] The recent findings reveal that N-TiO_2 could be better photocatalyst for H_2 production.

N-TiO_2 prepared by heating urea and TiO_2 at 350-700˚C in air favored hydrogen evolution under UV/visible light in presence of Na_2SO_3 as a positive hole scavenger.[373] The XPS studies showed both molecularly chemisorbed N_2 and substituted nitrogen contributing to visible light response. The calcination temperature of the catalyst removed chemisorbed nitrogen which however had least influence on photoactivity. The high activity of the sample calcined at 600˚ C resulted from phase transformation and it is based on the CB edge position. The flat band potential of rutile coincides exactly with NHE potential (H^+-H_2 level), whereas anatase is shifted

cathodically by ~200mV suggesting that driving force for water reduction is very small for rutile.[375] It is also evidenced that anatase-rutile mixture enhances electron-hole separation due to the operation of surface charge layer and space charge layer between anatase and thin rutile layer. This combined space-charge layer acts cooperatively towards the migration of holes from anatase to rutile and to the surface.[373] The platinized N-B-TiO_2 (B =1.5at %) calcined at 350˚ C showed remarkable photocatalytic activity for hydrogen production under visible light compared to N-TiO_2 attributed to synergistic effects of nitrogen and boron doping.[376] The nitrogen doping extends the visible light absorption via N-Ti-O bond while boron plays multiple roles; (i) B^{3+} substitutes Ti^{4+} lattice sites and serves as shallow traps for carriers;[377] (ii) boron eliminates oxygen vacancies induced by nitrogen doping and enhances surface hydroxyl groups on its surface;[378] (iii) boron distributed on the catalyst surface forms space charge layer to separate electron hole pairs[379] The N-Ce-TiO_2 (0.6% molar ratio) calcined at 500˚C exhibited highest hydrogen evolution under visible light irradiation ascribed to synergistic effects of codoping.[380] The XRD results indicated that as the ionic radius of Ce^{3+} and Ce^{4+} is larger than Ti^{4+} leading to lattice distortion and expansion where some strain energy is accumulated in the crystal reducing the phase transition from anatase to rutile.[380]

The hydrogen evolution with Pd cocatalyst and methanol as sacrificial reagent for various photocatalyst followed the order: N-In-TiO_2 > In-TiO_2 > N-TiO_2 > TiO_2.[381] The indium doping at cationic site decreased the bandgap by mixing of 5s and 5p orbital with Ti 3d orbital without generating any trap sites, making the electrons available at CB for reduction of protons to hydrogen.[382] In addition, impregnated Pd facilitated interfacial electrons transfer and reduced the over potential for hydrogen evolution by accumulating the electrons on Pd deposits.[383-385] The cocatalyst NiO supported on N-TiO_2 showed high hydrogen generation from aqueous methanol

solution under sunlight type irradiation, ascribed to electron trapping nature of NiO.[386] These trapped electrons in NiO initiates H^+ reduction formed by water splitting liberating hydrogen.[387] The nitrogen doping decreased the bandgap and increased the number of electrons in presence of NiO. During hydrogen evolution reaction, oxygen and nitrogen were not liberated suggesting that titanium oxynitride synthesized by trioctyl amine treatment of TiO_2 was stable under reaction conditions.[386] In another study, Pd served as better cocatalyst compared to NiO on reduced N-TiO_2 for hydrogen evolution under visible light.[388] The induced Ti^{3+} state produces anion vacancies in the lattice which introduces additional level below CB. These levels overlap with TiO_2 CB decreasing the bandgap with increase in its concentration.[388] The Pt (1 wt %) loaded N-S-TiO_2/V_2O_5 exhibited highest activity for hydrogen evolution (296.6μ mol h^{-1}) under visible light irradiation, as CB electron is trapped by Pt to reduce H^+ ions and holes oxidize methanol to form CO_2 and H_2.[389-392]

$$\text{Pt loaded } V_2O_5 \text{ /N- S-TiO}_2 \xrightarrow{h\nu} h^+ + e^- \quad (55)$$

$$2H_2O \rightarrow 2H^+ + 2OH^- \quad (56)$$

$$2e^-_{CB} + 2H^+ \rightarrow H_2 \quad (57)$$

$$CH_3OH \xrightarrow{h\nu / \text{catalyst}} HCHO + H_2 \quad (58)$$

$$HCHO + H_2O \xrightarrow{h\nu / \text{catalyst}} HCO_2H + H_2 \quad (59)$$

$$HCO_2H \xrightarrow{h\nu / \text{catalyst}} CO_2 + H_2 \quad (60)$$

The CB and VB of N-S-TiO_2 lie above energy band of V_2O_5. Thus electron accumulates in N-S-TiO_2 CB and hole in V_2O_5VB efficiently separating charge carriers at the interface.[393-396] However, Pt deposited N-TiO_2 thin film showed poor hydrogen gas evolution under visible light

than UV light due to the presence of oxygen defects which trapped the electrons necessary to initiate hydrogen production.[50] The nano composite of graphene oxide with N-TiO_2 exhibited enhanced photocatalytic efficiency for hydrogen evolution under UV/visible light attributed to nitrogen doping and incorporation of graphene oxide.[397] The nitrogen doping and formation of Ti-C, Ti-O-C bond along with the existence of Ti^{3+} red shifted the bandgap of TiO_2. The Fermi level in graphene is -4.42eV[398] close to CB energy (-4.21eV) of TiO_2. Therefore, the CB electrons are injected to Fermi level orbital in graphene while the holes are trapped by N-TiO_2. At the same time, graphene can withdraw and shuttle electrons as electron transporting bridges and electron sinks because of its ultra high electron mobility (>1000$cm^2V^{-1}s^{-1}$) and the plate like monolayer textural nature with a large specific surface area affords quick electron transfer resulting in charge carrier separation. The electrons from graphene are transferred to H^+ in aqueous methanol affording hydrogen generation and the holes irreversibly oxidize the sacrificial reagents instead of water.[397]

8.0 Reactivity of N-TiO_2 with exposed facets

Engineering the TiO_2 material with exposed crystal facets is currently a hot area in extending the photocatalytic reactions. Both theoretical and experimental studies have revealed that {001} surface of anatase TiO_2 nanosheets is much reactive than thermodynamically stable {101} surface.[399] Based on thermodynamics {101} facet with low surface energy remains most stable accompanied by diminishing of {001} and {110} facets during crystallization. The average surface energy of {001}, {100} and {101} facets are 0.90, 0.53 and 0.44 J/m^2 respectively.[400] Owing to the low atomic coordination numbers of exposed atoms and the wide bond angle of Ti-O-Ti, the anatase TiO_2 {001} facet is theoretically considered to be more reactive than the {101} facet in heterogeneous reactions.

Doping with nonmetals is reported to shift the bandgap response of {001} facets of anatase titania toward the visible region. N-TiO_2 with an exposed {001} facet (~ 67%) synthesized by solvothermal synthesis of TiN in a HNO_3-HF ethanolic solution exhibited higher activity for hydrogen evolution compared to N-TiO_2 microcrystallite with exposed {001} facet due to the larger surface area of the former compared to the latter. In addition ethanol used in the synthesis process served as a capping agent, which hindered the growth of the single crystal anatase TiO_2 because of its specific bonding with the TiO_2 surface via the Ti-O-C bond.[400 b] The solvothermal treatment of TiN in acidic $NaBF_4$ resulted in N-TiO_2 with dominant {001} facet, which exhibited high activity for MB degradation and excellent photoelectrochemical properties under visible light. The presence of weak Ti-B-F surface structure facilitated easy dissociation and exchange of surface hydroxyl groups to form hydrogen peroxide and peroxide radicals.[401-402] The photocurrent ($400\mu Acm^{-2}$) response of N-TiO_2 with dominant {001} facet is 3.3 times higher than N-P25 indicating efficient charge separation and transportation of electrons from TiO_2 surface to counter electrode via external circuit under visible light illumination.[401a] Hydrogenated N-H-F-TiO_2 with {001} facet exhibited high activity for RhB degradation under visible light due to the formation of energy belts and disorder structures.[403] The differently coordinated Ti^{3+} and oxygen vacancies like O_{vac} (F_e), O_{vac} (N_e) and Ti^{3+} (F_e), Ti^{3+} (N_e), Ti^{3+} (H), and Ti^{3+} (H') (e refers to escape for example O_{vac} (F_e) refers to oxygen vacancy induced by escape of F^- ions) narrowed the bandgap and significantly enhance the light absorption to facilitate charge carrier migration (Fig. 23).[403] The N-Mo-TiO_2 sheets with dominant {001} facets obtained by a hydrothermal process using TiN, MoO_3, HF and HNO_3 showed activity for MB and Methyl violet degradation under visible light.[189] The XPS spectra confirms the nitrogen at interstitial site or O-Ti-N structure and Mo^{6+} substitution in TiO_2. The Mo doping elevated the CB edge and expands the

TiO_2 bandgap elevating the reduction potential energy and improved the H^+ reduction ability. The surface fluorine removal from catalyst reduced the activity despite adsorption of the pollutant was enhanced.[189] The N-Ni-TiO_2 with expose {001} facets prepared by two step hydrothermal reaction using $H_2Ti_3O_7$ and HF (shape controlling agent) showed enhanced activity for MB degradation under UV/visible light attributed to its suitable bandgap (2.0 eV) and band edge positions which matched with redox potential of water.[404] The dopants nitrogen and nickle shifted up VB edge significantly leaving CB unchanged. The n-type (Ni) and p-type (N) with unequal charge states decreased the density of recombination centers and increased the migration efficiency of charge carriers. In the synthesis process, $H_2Ti_3O_7$ nanotubes were obtained by treating TiO_2 with NaOH. At this stage, few Ti-O-Ti bonds were broken followed by the formation of Ti-O-Na bonds, which on washing with acid and water generated new Ti-O-H bonds to produce metastable $H_2Ti_3O_7$, further transforming into TiO_2 nanotubes as shown below.[404]

$$TiO_2 + NaOH \rightarrow Na_2Ti_3O_7 \quad (61)$$

$$Na_2Ti_3O_7 + HCl \rightarrow H_2Ti_3O_7 \quad (62)$$

$$H_2Ti_3O_7 \rightarrow 3TiO_2 + H_2O \quad (63)$$

The hierarchical N-TiO_2 hollow sphere-in sphere microstructure comprised of nanothorns with exposed anatase {101} facets exhibited potential activity for MB and orange II degradation under visible light. This was ascribed to synergistic effects of large surface area, hierarchical structure, crystalline {101} facets on the surface and inner sphere allow multiple reflection of light with effective usage of incident photons.[405] The water was found to play a major role for hollowing process which promoted crystallization and dissolution process. When the molar ratio

of H_2O/Ti is 0.3, formation of nanothorns on the surface of spheres occurs while heavily aggregated TiO_2 solid microspheres with nanoflakes are formed without water. The hollow structure improves the specific surface area dispersion ability and light harvesting ability of photocatalyst. However, hollow spheres containing {101} facets without sphere-in sphere structures exhibited low activity.[405-408]

The MB degradation was achieved at faster rate under visible light on the surface of N-C-TiO_2 nanosheets with exposed {001} facet, compared to their microsheets and nanoparticles counterparts.[409] The fluorine ions preferentially adsorb on {001} facets hindering crystal growth along {001} axis facilitating crystalline growth in both {100} and {101} directions with lower surface energy.[410] Meanwhile, the ethanol served as capping agent by adsorbing on TiO_2 which hindered the aggregation of nanoparticles and promoted nanocrystals formation.[411-412] The carbon and nitrogen codoping intensified the absorption in the visible region and facilitated the exposure of large amount of reactive facets.[409] The N-F-TiO_2 platelets with dominant {001} facets prepared via solid state phase pathway i.e by nitriding $TiOF_2$ precursor in NH_3 gas flow demonstrated excellent performance for water oxidation under visible light.[413] The presence of fluorine dopant facilitates nitrogen doping into crystal by maintaining charge balance and stabilizing the structure.[414] When $TiOF_2$ was treated with NH_3 gas flow, the later facilitated the collapse of TiO_2 boxes into platelets and simultaneously incorporation of nitrogen atoms into TiO_2 lattice. The negligible amount of O_2 was detected with N-TiO_2 because water oxidation reaction requires removal of four protons and four electrons and the formation of oxygen-oxygen double bond.[413] The N-S-TiO_2 nanosheets with exposed {001} facets prepared by a simple mixing-calcination method using the hydrothermally prepared TiO_2 nanosheets showed enhanced degradation of 4-CP under visible light irradiation attributed to the synergetic effects

as follows;[415] (i) the red-shift of absorption edges and intense absorption in the visible-light region (ii) the exposure of highly reactive {001} facets of nanosheets. The former implies more photogenerated electrons and holes participation in the photocatalytic reactions. The latter is due to 2D nanosheets with exposed {001} facets which better adsorbs pollutant molecules due to their higher reactivity. Under visible-light irradiation, electrons can transfer from VB to impurity states easily and the electrons in the impurity states move to CB after secondary excitation. The intermediate states offer ‘‘extra steps’’ for the absorption of low energy photons via excitation of electrons at the top of VB to the intermediate bands, where they can be excited again above to the CB bottom level, resulting in effective photoresponse. The photocatalytic experiments indicated that pure TiO_2 nanosheets show visible light activity for 4-CP degradation on irradiation. The substrate-surface complexation takes place formed by a phenolate linkage reaction between the ligand and Ti (IV) site on the TiO_2 surface as shown below.

$$RTi-OH + OH-Ph \rightarrow RTi-O-Ph + H_2O \qquad (64)$$

This complexation extends the absorption of titania to visible light region through ligand to titanium charge transfer.[415] The N-S-TiO_2 nanocrystals with high percentage of {001} facets synthesized via solvent thermal process followed by calcination with thiourea at 300˚ C demonstrated superior MB degradation and photocatalytic inactivation of *E .coli* bacteria under visible light.[416] This superior activity is ascribed to reduced crystal size with {001} facets which largely increased their specific surface area (70 m^2/g) and the contact efficiency with contaminants.[416] The N-F-Cr-TiO_2 microspheres was prepared by hydrothermal method by the treatment of the thermally sprayed TiN/Ti coating with HF aqueous solution and chromium powder at 180˚C for 5~24 h.[417] In the absence of chromium powders the interaction of TiN/Ti with HF resulted in interconnected truncated bypyramids, while high energy {001} facets are

formed in the presence of chromium microspheres. The increase of surface vacancy due to chromium doping increases the surface energy contributing to the selective erosion of the truncated bipyramids to a drum like morphology. In addition incorporation of nitrogen, fluorine and chromium led to a significantly enhanced solar absorption and remarkably reduced the bandgap.[417]

9.0 Application of N-TiO_2 in organic reactions and organic synthesis

Since various intermediates are formed during titania photocatalysis, degradation reaction can be tuned at specific intervals so as to get required organic compounds, which otherwise demands harsh conditions or multiple steps for its preparation in organic protocol. Thus most of the organic compounds can be obtained in a single step under laboratory conditions.[418-419] The N-TiO_2 displayed reductive cleavage of azoxybenzene into their corresponding amines or 2-phenylindazoles with methanol in the presence of N_2 atmosphere under UV/solar light illumination.[420] The amines (aniline) were obtained in pure methanol, while 2-phenyl indazoles was formed in aqueous methanol (20% water+80% methanol). The product yield decreased with increase in carbon chain length of alcohol, highlighting the importance of solvents in tuning the reaction rate and corresponding yields. On illumination electron hole pairs are generated on TiO_2 in which CB electron is captured by oxygen retarding amine formation via reduction in aqueous methanol system. The hole oxidizes methanol generating hydroxymethyl radical and hydrogen radical that reacts with azobenzene to form hydroxymethyl adduct, which later dehydrates and cyclizes to imdazole or can be cleaved by protons to form amines (Fig. 24).[421] The as prepared tubular TiO_2 immersed in 1 M acetic acid was effective in ring opening reaction of an epoxide and Friedal Crafts reaction.[422] The protonation of oxygen atom in styrene oxide from Bronsted acidic site followed by the attack of nucleophilic part of methanol onto this carbon center leading

to ring opening reaction (Fig. 25). Friedel-Crafts reaction is initiated by activation of CO group in methyl vinyl ketone through protonation followed by an attack of π electrons in indole upon vinyl group suggesting that the catalyst exhibited a prominent acid nature.[422]

The activity of various catalyst towards one pot synthesis of quinaldines from nitrobenzene in ethanol under both UV and visible light followed the order; N-TiO_2>Pt-TiO_2>Au-TiO_2>Ag-TiO_2>bareTiO_2.[423] The photoirradiation of alcohol solution of different nitroarenes with N-TiO_2 showed that electron releasing group at the para position inhibits the condensation of amino group with aldehyde. In case of 3,5-dimethylnitrobenzene, cyclization reaction was hindered due to steric effect and decreased the product yield (66%) when compared to 3-nitrobenzene (80%). The photoinduced dehalogenation resulted in lower yields in case of 4-chloro and 4-fluronitrobenzenes (Table 5). Contrarily, addition of KI and NaI increased the product yield due to hole scavenging effect of iodide ion.[423] In another study, N-TiO_2 promoted rapid and selective quinaldine production from ethanolic solution of aniline and with other substituted anilines under UV/ visible light.[424] The initial step involved the oxidation of alcohol to aldehyde via VB holes from N-TiO_2. The oxidized product of ethanol condensed with aniline to produce an imine (Schiff base) which on further condensation and cyclization yields corresponding quinaldine. There was no significant effect with other substituent on the product yields except for halo anilines. In case of 4-chloro and 4-fluoroanilines, the yield of halo substituted quinaldines was very low due to photoinduced dehalogenation before the reaction. The N-TiO_2 with poor crystallinity prepared at low temperature by using NH_4Cl as nitrogen source showed enhanced partial oxidative transformation of 4-methoxybenzyl alcohol to p-anisaldehyde under simulated solar light.[425] The high reactivity was due to the synergistic effect of presence of anatase-rutile phases[426] which reduced the recombination rate. In addition, the

nitrogen in bulk improved the reaction rate and its presence on the catalyst surface reduced mineralization sites increasing the selectivity. Though the thermal treatments yield an improvement in crystallinity and activity (in terms of initial disappearance rate) but are highly detrimental, for selectivity and exploitation of UV light. This is due to a primary influence of particles sintering and higher crystallinity leading to high activity and low selectivity.[425] These types of photoinduced chemical transformations leading to the formation of industrially important compounds give a room to explore applications of TiO_2 in organic synthesis.[424]

10.0 Conclusion

The superiority of N-TiO_2 is demonstrated from its low cost and simple controllable synthesis, high surface hydrophillicity and photoinduced charge carrier transfer from bulk to surface under visible light. The nitrogen has similar ionic size and posses low ionization energy compared to oxygen, which effectively controls both chemical and electronic state along with the surface structure of TiO_2. Because of comparable ionic size, induced lattice distortion will not be significant and hence large number of recombination centers is not generated. In addition, nitrogen as a dopant does not segregate or lead to the formation of impure products like dopant oxide. Interaction of nitrogen dopant within titania matrix and its homogeneous distribution within the host lattice draws the attention of several researchers.

The following general conclusions can be drawn based on the literature available:

(i) The doping of nitrogen ion at substitutional or interstitial lattice position shifts the bandgap of titania to visible region, making it to operate under solar light.

(ii) Na_2EDTA, gaseous NH_3, NH_4OH, NH_4Cl, NH_4NO_3, $(NH_4)_2CO_3$, NH_2CONH_2, $C_2H_5NH_2$, $N(C_4H_9)_4$-OH, guanidine, HMT and 1,3 diaminopropane are the most used nitrogen precursors.

(iii) The annealing ambience (oxidizing/reducing/inert) changes the dopant diffusion properties into the bulk of TiO_2 lattice affecting the relative chemical stability.

(iv) Depending on the experimental conditions the possible nitrogen states in TiO_2 lattice are O-Ti-N, Ti-O-N, Ti-N-O, N-Ti-O, N-Ti-N, -(NO), -(NO2), N_b.

(v) Nitrogen doping is always accompanied by the creation of defects like Ti^{3+} ion or oxygen vacancies which can either suppress or enhance recombination pathways, depending on their distribution in the lattice.

(vi) N-TiO_2 with diverse morphologies like nanotube, nanoflowers, hollow sphere, nanosheets, fibrous, nano octahedral, rice grain, V-shape were more beneficial than regular nanoparticles due to their unique structures.

(vii) Various modifications like co-doping with metal/non metal ions, coupling with other semiconductors or surface metal deposition influences the electronic band structure and induce exceptional stability to N-TiO_2. These modifications impart multiple charge transfer pathways to hinder recombination process.

(ix) The stabilization of {001} facets by the nitrogen dopant is remarkable since such situation is hard to achieve with other metal ions.

(ix) The applications of N-TiO_2 for hydrogen evolution and in organic synthesis are still at the initial stages and much more research work is this area is needed to correlate material properties with probe reactions.

Acknowledgements

The authors acknowledge University Grants Commission (UGC) and Department of Science and Technology (DST-IDP & DST-SERC), Government of India for their financial supports.

References

(1) X. Lang, X. Chen and J. Zhao, *Chem. Soc. Rev.,* 2014, **43**, 473-486.

(2) J. B. Joo, M. Dahl, N. Li, F. Zaera and Y. D. Yin, *Energy Environ. Sci.,* 2013, **6**, 2082-2092.

(3) L. Q. Jing, W. Zhou, G. H. Tian and H. G. Fu, *Chem. Soc. Rev.,* 2013, **42**, 9509-9549.

(4) Y. J. Wang, Q. S. Wang, X. Y. Zhan, F. M. Wang, M. Safdar and J. He, *Nanoscale,* 2013, **5**, 8326-8329.

(5) X. Y. Pan, M. Q. Yang, X. Z. Fu, N. Zhang and Y. J. Xu, *Nanoscale,* 2013, **5**, 3601-3614.

(6) M. A. Lazar and W. A. Daoud, *RSC Adv.,* 2013, **3**, 4130-4140.

(7) S. Nishimoto and B. Bhushan, *RSC Adv.,* 2013, **3**, 671-690.

(8) (a)Y. Q. Qu and X. F. Duan, *Chem. Soc. Rev.,* 2013, **42**, 2568-2680. (b) Q. Xiang, J. Yu and M. Jaroniec, *Chem. Soc. Rev.,* 2012, **41**, 782-796.

(9) T. Froeschl, U. Hoermann, P. Kubiak, G. Kucerova, M. Pfanzelt, C. K. Weiss, R. J. Behm, N. Husing, U. Kaiser, K. Lansfester and M. W. Mehrens, *Chem. Soc. Rev.,* 2012, **41**, 5313-5360.

(10) N. Serpone, A. V Emeline, S. Horikoshi, V. N. Kuznetsov and V. K. Ryabchuk, *Photochem. Photobiol. Sci.,* 2012, **11**, 1121-1150.

(11) (a) L. G. Devi and R. Kavitha, *Appl. Catal. B: Environ.,* 2013, **140-141**, 559-587. (b) L. G. Devi and R. Kavitha, *Mater. Chem. Phys.,* 2014, **143,** 1300-1308. (c) R. Kavitha and L. G. Devi *J. Environ. Chem. Eng.,* 2014, **2** 857-867.

(12) (a) S. G. Kumar and L. G. Devi, *J. Phys. Chem. A*, 2011, **115,** 13211-13241. (b) L. G. Devi and S. G. Kumar, *Cent. Eur. J. Chem.,* 2011, **9,** 959-961.

(13) (a) J. Zhang, Y. Wu, M. Xing, S.A.K. Leghari, S. Sajjad, *Energy Environ. Sci.*, 2010, **3,** 715-726. (b) M.V. Dozzi, E. Selli, *J. Photochem. Photobiol. C: Photochem. Rev.,* 2013, **14,** 13-28 (c) (c) M. Pelaez, N. T. Nolan, S. C. Pillai, M.K. Serry, P. Falaras, A. G. Kontos, P. S. M.

Dunlop, J. W. J. Hamilton, J. A. Byrne, K.O. Shea, M. H. Entezari, D. D. Dionysiou, *Appl. Catal. B: Environ.* 2012, **125,** 331-349.

(14) N. Zhang, S. Q. Liu and Y. J. Xu, *Nanoscale,* 2012, **4**, 2227-2238.

(15) Z. Y. Zhou, N. Tian, J. T. Li, I. Broadwell and S. G. Sun, *Chem. Soc. Rev.,* 2011, **40**, 4167-4185.

(16) H. Tada, M. Fujishima and H. Kobayashi, *Chem. Soc. Rev.,* 2011, **40**, 4232-4243.

(17) D. Ravelli, D. Dondi, M. Fagnoni and A. Albini, *Chem. Soc. Rev.,* 2009, **38**, 1999-2011.

(18) R, Beranek and H. Kisch, *Photochem. Photobiol. Sci.,* 2008, **7**, 40-48.

(19) C. Aprile, A. Corma and H. Garcia, *Phys. Chem. Chem. Phys.,* 2008, **10**, 769-783.

(20) A. S. Weber, A. M. Grady and R. T. Koodali, *Catal. Sci. Technol.,* 2012, **2**, 683-693.

(21) S. Fukuzumi and K. Ohkubo, *Chem. Sci.,* 2013, **4**, 561-574.

(22) G. Liu, J. C. Yu, G. Q. Lu and H. M. Cheng, *Chem. Commun.,* 2011, **47**, 6763-6783.

(23) G. Liu, L. Wang, H. G. Yang, H. M. Cheng and G. Q. Lu, *J. Mater. Chem.,* 2010, **20**, 831-843.

(24) A. Kudo and Y. Miseki, *Chem. Soc. Rev.,* 2009, **38**, 253-278.

(25) S. Bingham and W. A. Daoud, *J. Mater. Chem.,* 2011, **21**, 2041-2050.

(26) C. Z. Wen, H. B. Jiang, S. Z. Qiao, H. G. Yang and G. Q. Lu, *J. Mater. Chem.,* 2011, **21**, 7052-7061.

(27) A. A. Ismail and D. W. Bahenmann, *J. Mater. Chem.,* 2011, **21**, 11686-11707.

(28) K. Lv, B. Cheng, J. Yu and G. Liu, *Phys. Chem. Chem. Phys.,* 2012, **14**, 5349-5362.

(29) L. Li, P. A. Salvador and G. S. Rohrer, *Nanoscale,* 2014, **6**, 24-42.

(30) C. W. Dunnill and I. P. Parkin, *Daltons Trans.,* 2011, **40**, 1635-1640.

(31) S. Hu, F. Li and Z. Fan, *Appl. Surf. Sci.,* 2011, **258,** 1249-1255.

(32) M. R. Hoffmann, S. T. Martin, W. Choi and D. W. Bahnemann, *Chem. Rev.,* 1995, **95,** 69-96.

(33) A. Fujishima, T.N. Rao and D.A. Tryk, *J. Photochem. Photobiol. C: Photochem. Rev.,* 2000, **1,** 1-21.

(34) X. F. Chen, X.C. Wang, Y. D. Hou, J. H. Huang, L. Wu and X. Z. Fu, *J. Catal.,* 2008, **255,** 59-67.

(35) H. Irie, Y. Wantanabe and K. Hasimoto, *J. Phys. Chem. B.,* 2003, **107,** 5483-5486.

(36) I. Nakamuru, N. Negishi, S. Kutsuna, T. Ihara, S. Sugihara and K. Takeuchi, *J. Mol. Catal. A: Chem.,* 2000, **161,** 205- 212.

(37) E. Elgniji, M. Ksibi and E. Elaloui, *J. Ind. Eng. Chem.,* 2012, **18,** 178-182.

(38) Y. Zhao, X. Qiu and C. Burda, *Chem. Mater.,* 2008, **20,** 2629-2636.

(39) J. Fang, F.Wang, K. Qian, H. Bao, Z. Jiang and W. Huang, *J. Phys. Chem. C,* 2008, **112,** 18150-18156.

(40) M. Bellardita, M. Addamo, A. D. Paola, L. Palmisano and A. M. Venezia, *Phys. Chem. Chem. Phys.,* 2009, **11,** 4084-4093.

(41) S. Hotchandani and P. V. Kamat, *J. Phys. Chem.,* 1992, **96,** 6834-6839.

(42) N. Serpone, P. Maruthamuthu, P. Pichat, E. Pelizzetti and H. Hidaka, *J. Photochem. Photobiol. A: Chem.,* 1995, **85,** 247- 255.

(43) A. D. Paola, L. Palmisano, M. Derrigo and V. Augugliaro, *J. Phys. Chem. B,* 1997, **101,** 876-883.

(44) M. Yan, F. Chen, J. Zhang and M. Anpo, *J. Phys. Chem. B,* 2005, **109,** 8673-8678.

(45) R. Asahi, T. Morikawa, T. Ohwaki, K. Aoki and Y. Taga, *Science,* 2001, **293,** 269-271.

(46) C. Di Valentin, G. Pacchioni and A. Selloni, *Phys. Rev. B,* 2004, **70,** 085116.

(47) N. Serpone, *J. Phys. Chem. B,* 2006, **110,** 24287-24293.

(48) N. T. Nolan, D. W. Synnott, M. K. Seery, S. J. Hinder, A.V. Wassenhoven, and S. C. Pillai, *J. Hazard. Mater.,* 2012, **211-212,** 88-94.

(49) V. Etacheri, M. K. Seery, S. J. Hinder and S. C. Pillai, *Chem. Mater.,* 2010, **22,** 3843-3853.

(50) S. Somekawa, Y. Kusumoto, M. Ikeda, B. Ahmmad and Y. Horie, *Catal. Commun.,* 2008, **9,** 437-440.

(51) S. Maret, E. A. Bergin and C. J. Lada, *Nature,* 2006, **442,** 425-427.

(52) C. Chen, H. Bai and C. Chang, *Phys. Chem. C,* 2007, **111,** 15228-15235.

(53) A. Kafizas, C. Crick and I. P. Parkin, *J. Photochem. Photobiol. A: Chem.,* 2010, **216,** 156-166.

(54) M. Miyauchi, A. Ikezawa, H. Tobimatsu, H. Irie and K. Hashimoto, *Phys. Chem. Chem. Phys.,* 2004, **6,** 865-870.

(55) J. Qian, G. Cui, M. Jing, Y. Wang, M. Zhang and J. Yang, *Int. J. Photoenergy,* 2012, 198497.

(56) Y. Wang, C. X. Feng, M. Zhang, J. J. Yang and Z. J. Zhang, *Appl. Catal. B: Environ.*, 2011, **104,** 268-274.

(57) Y. Wang, C. Feng, M. Zhang, J. Yang and Z. Zhang, *Appl. Catal. B: Environ.*, 2010, **100,** 80-94

(58) S. Zhang, W. Li, Z. Jin , J. Yang, J. Zhang, Z. Du and Z. Zhang, *J. Solid State Chem.,* 2004, **177,** 1365-1371.

(59) Y. Nosaka, M. Matsushita, J. Nishino and A. Y. Nosaka, *Sci. Technol. Adv. Mater.,* 2005, **6,** 143-148.

(60) D. Wu, M. Long, W. Cai, C. Chen and Y. Wu, *J. Alloys Compounds,* 2010, **502,** 289-294.

(61) A. Kachina, E. Puzenat, S. Chikh, C. Geantet, P. Delichere and P. Afanasiev, *Chem. Mater.,* 2012, **24,** 636-642.

(62) V. M. Khomenka, K. Langer, H. Rager and A. Fett, *Phys. Chem. Miner.,* 1998, **25,** 338-346.

(63) (a)Y. X. Zhang, G. H. Li, Y. X. Jin, Y. Zhang, J. Zhang and L. D. Zhang, *Chem. Phys. Lett.,* 2002, **365,** 300-304. (b) J. Yu, W. Liu and H. Yu, *Cryst. Growth Des.,* 2008, **8,** 930-934. (c) J. Yu, G. Dai and B. Cheng, *J. Phys. Chem. C,* 2010, **114**, 19378-19385.

(64) (a) P. D. Cozzoli, A. Kornowski and H. Weller, *J. Am. Chem. Soc.,* 2003, **125,** 14539-14548. (b) K. Lv, J. Yu, J. Fan and M. Jaroniec, *Cryst. Growth Des.,* 2011, **13,** 7044-7148.

(65) (a) W. Zhou, X. Liu, J. Cui, D. Liu, J. Li, H. Jiang, J. Wang and H. Liu, *CrystEngComm,* 2011, **13,** 4557-4563. (b) J. Yu and J. Zhang, *Dalton Trans.,* 2010, 39, 5860-5897.

(66) C. C. Hu, T. C. Hsu and L. H. Kao, *Int. J. Photoenergy,* 2012, 391958.

(67) J. Wang, W. Zhu, Y. Zhang and S. Liu, *J. Phys. Chem. C,* 2007, **111,** 1010-1014.

(68) Z. Zhao, J. Fan, J. Wang and R. Li, *Catal. Commun.,* 2012, **21,** 32-37.

(69) Y. Wang and D. J. Doren, *Solid State Commun.,* 2005, **136,** 186-189.

(70) J.Y. Lee, J. Park and J. H. Cho, *Appl. Phys. Lett.,* 2005, **87,** 011904.

(71) S. In, P. C. K. Vesborg, B. L. Abrams, Y. Hou and I. Chorkendorff, *J. Photochem. Photobiol. A: Chem.,* 2011, **222,** 258-262.

(72) Z. Jiang, F. Yang, N. Luo, B. T. T. Chu, D. Sun, H. Shi, T. Xiao and P. P. Edwards, *Chem. Commun.,* 2008, 6372-6374.

(73) Q. Wang, X. Yang, X. Wang, M. Huang and J. Hou, *Electrochim. Acta,* 2012, **62,** 158-162.

(74) Y. Lai, J. Huang, H. Zhang, V. Subramaniam, Y. Tang, D. Gong, L. Sundar, L. Sun, Z. Chen and C. Lin. *J. Hazard. Mater.,* 2010, **184,** 855-863.

(75) M. Sathish, B. Viswanathan and R.P. Viswanath, *Appl. Catal. B: Environ.,* 2007, **74,** 307-312.

(76) Y. N. Huo, Y. Jin, J. Zhu and H. X. Li, *Appl. Catal. B: Environ.,* 2009, **89,** 543-550.

(77) H. Z. Zhang and J. F. Banfield, *J. Mater. Res.,* 2000, **15,** 437-448.

(78) T. Osaki, K. Nagashima, K. Watari and K. Tajiri, *J. Non-Cryst. Solids,* 2007, **353,** 2436-2442.

(79) D. P. Subagio, M. Srinivasan, M. Lim and T. T. Lim, *Appl. Catal. B: Environ.,* 2010, **95,** 414-422.

(80) H. J. Cho, P. G. Hwang and D. Jung, *J. Phys. Chem. Solids,* 2011, **72,** 1462-1466.

(81) G. Liu, L. Wang, C. Sun, Z. Chen, X. Yan, L. Cheng, H. M. Cheng and G. Q. M. Lu, *Chem. Commun.,* 2009, 1383-1385.

(82) T. Sasaki, M. Watanabe, H. Hashizume, H. Yamada, H. Nakazawa, *J. Am. Chem. Soc.,* 1996, **118,** 8329-8335.

(83) G. Liu, L. Wang, C. Sun, X. Yan, X. Wang, Z. Chen, S. C. Smith, H. M. Cheng and G. Q. Lu, *Chem. Mater.,* 2009, **21,** 1266-1274.

(84) J. Fu, Y. Tian, B. Chang, F. Xi and X. Dong, *Chem. Eng. J.,* 2013, **219,** 155-161.

(85) Y. Cheng, Y. Huang, P.D. Kanhere, V.P. Subramaniam, D. Gong and S. Zhang, *Chem. Eur. J.*, 2011, **17,** 2575-2578.

(86) Z. Xiong and X. Zhao, *J. Am. Chem. Soc.,* 2012, **134,** 5754-5757.

(87) H. Tong, S. Ouyany, Y. Bi, N. Umezawa, M. Oshikiri, and J. Ye, *Adv. Mater.,* 2012, **24,** 229-251.

(88) Z. Lin, A. Orlov, R. M. Lambert and M. C. Payne, *J. Phys. Chem. B,* 2005, **109,** 20948-20952.

(89) K. M. Parida, S. Pany and B. Naik, *Int. J. Hydrogen Energy,* 2013, **38,** 3545-3553.

(90) X. Wang, J. C. Yu, C. Ho, Y. Hou and X. Fu, *Langmuir,* 2005, **21,** 2552-2559.

(91) J. Du, G. Zhao, Y. Shi, H. Yang, Y. Li, G. Zhu, Y. Mao, R. Sa and W. Wang, *Appl. Surf. Sci.,* 2013, **273,** 278-286.

(92) V. J. Babu, M. K. Kumar. A. S. Nair, T. L. Kheng, S. I. Allakhverdiev and S. Ramakrishna, *Int. J. Hydrogen Energy,* 2012, **37,** 8897-8904.

(93) S. Wang, J. Xu, H. Ding, S. Pan, Y. Zhang and G. Li, *CrystEngComm,* 2012, **14,** 7672-7679.

(94) E. Hosono, S. Fujihara, K. Kakiuchi and H. Imai, *J. Am. Chem. Soc.,* 2004, **126,** 7790-7791.

(95) F. P. Rotzinger and M. Gratzel, *Inorg. Chem.,* 1987, **26,** 3704-3708.

(96) L. Kavan, B. O'Regan, A. Kay and M. Gratzel, *J. Electroanal. Chem.,* 1993, **346,** 291-307.

(97) T. Guillet, R. Grousson, V. Voliotis, X. L. Wang and M. Ogura, *Phys. Rev. B: Condens. Matter,* 2003, **68,** 045319.

(98) J. M. Wu and B. Qi, *J. Phys. Chem. C*, 2007, **111,** 666-673.

(99) S. Yin and T. Sato, *J. Mater. Chem.*, 2005, **15,** 4584-4587.

(100) J. Wu, B. Haung, M. Wang and A. Osaka, *J. Am. Ceram Soc.*, 2006, **89,** 2660-2663.

(101) (a) A. G. Kontos, M. Pelaez, V. Likodimos, N. Vaenas, D. D. Dionysiou and P. Falaras, *Photochem. Photobiol. Sci.,* 2011, **10,** 350-354. (b) P. Zhou, J. Yu and Y. Wang, *Appl. Catal. B: Environ.,* 2013, **142-143,** 45-53. (c) X. Wang, K. Wang, K. Feng, F. Chen, H. Yu and J. Yu, *J. Mol. Catal. A: Chem.,* 2014, **391,** 92-98. (d) J. Yu, M. Zhou, B. Cheng and X. Zhao, *J. Mol. Catal. A: Chem.,* 2006, **246,** 179-184. (e) M. Zhou and J. Yu, *J. Hazard. Mater.,* 2008, **152,** 1229-1236.

(102) K. Shankar, K. C. Tep, G. K. Mor and C. A. Grimes, *J. Phys. D: Appl. Phys.,* 2006, **39,** 2361.

(103) Y. C. Nah, I. Paramasivam and P. Schmuki, *ChemPhyChem,* 2010, **11,** 2698-2713.

(104) A. E. R. Mohamed and S. Rohani, *Energy Environ. Sci.,* 2011, **4,** 1065-1086.

(105) J. Yuan, E. Wang, Y. Chen, W. Yang, J. Yao and Y. Cao, *Appl. Surf. Sci.,* 2011, **257,** 7335-7342.

(106) E. Finazzi, C. D. Valentin and Pacchioni, *J. Phys. Chem. C,* 2009, **113,** 220-228.

(107) D. Chen, D. Yang, Q. Wang and Z.Y. Jiang, *Ind. Eng. Chem. Res.,* 2006, **45,** 4110-4116.

(108) H. Geng, S. Yin, X. Yang, Z. Shuai and B. Liu, *J. Phys.: Condens. Matter,* 2006, **18,** 87-96.

(109) Y. Huang, W. Ho, Z. Ai, X. Song, L. Zhang and S. Lee, *Appl. Catal. B: Environ.,* 2009, **89,** 398-405.

(110) A. M. Czoska, S. Livraghi, M. C. Paganini, E. Giamello, C. D. Valentin and Pacchioni, *Phys. Chem. Chem. Phys.,* 2011, **13,** 136-143.

(111) S. C. Moon, H. Mametsuka, S. Tabata and E. Suzuki, *Catal. Today,* 2000, **58,** 125-132.

(112) S. In, A. Orlov, R. Berg, F. Garcia, S. P. Jimenez, M. S. Tikhov, D. S. Wright and R. M. Lambert, *J. Am. Chem. Soc.,* 2007, **129,** 13790-13791.

(113) B. Gao, Y. Ma, Y. Cao, W. Yang and J. Yao, *J. Phys. Chem. B,* 2006, **110,** 14391-14397.

(114) O. Carp, C.L. Huisman and A. Reller, *Prog. Solid State Chem.,* 2004, **32,** 33-177.

(115) G. Liu, L. Yin, J. Wang, P. Niu, C. Zhen, Y. Xie and H. Cheng, *Energy Environ. Sci.,* 2012, **5,** 9603-9610.

(116) X. B. Chen, L. Liu, P. Y. Yu and S. S. Mao, *Science,* 2011, **331,** 746-750.

(117) D. Chen, Z. Jiang, J. Geng, Q. Wang, and D. Yang, *Ind. Eng. Chem. Res.*, 2007, **46,** 2741-2746.

(118) Y. L. Pang and A. Z. Abdullah, *Chem. Eng. J.,* 2013, **214,** 129-138.

(119) R. Vinu and G. Madras, *Environ. Sci. Technol.,* 2009, **43,** 473-479.

(120) F. Dong, W. Zhao and Z. Wu, *Nanotechnol.,* 2008, **19,** 1-10.

(121) X. Yang, C. Cao, L. Erickson, K. Hohn, R. Maghirang and K. Klabunde, *J. Catal.*, 2008, **260,** 128-133.

(122) J. Yang, H. Bai, X. Tan and J. Lian, *Appl. Surf. Sci.*, 2006, **253,** 1988-1994.

(123) K. Suriye, P. Praserthdam and B. Jongsomjit, *Appl. Surf. Sci.*, 2007, **253,** 3849-3855.

(124) M. Antonopoulou, A. Giannakas and I. Konstantinou, *Int. J. Photoenergy,* 2012, 520123.

(125) Y. Wu, M. Xing, B. Tian, J. Zhang and F. Chen, *Chem. Eng. J.,* 2010, **162,** 710-717.

(126) C. Minero, G. Mariella, V. Maurino, D. Vione and E. Pelizzetti, *Langmuir,* 2000, **16,** 8964-8972.

(127) C. Minero, G. Mariella, V. Maurino, D. Vione and E. Pelizzetti, *Langmuir,* 2000, **16,** 2632-2641.

(128) Z. He, W. Que, J. Chen, X. Yin, Y. He and J. Ren, *ACS Appl. Mater. Interfaces,* 2012, **4,** 6816-6826.

(129) J. Wang, D. N. Tafen, J. P. Lewis, Z. L. Hong, A. Manivannan, M. J. Zhi, M. Li and N. O. Wu, *J. Am. Chem. Soc.,* 2009, **131,** 12290-12297.

(130) W. Chen, Z. L. Fan, B. Zhang, G. J. Ma, K. Takanabe, X. X. Zhang and Z. P. Lai, *J. Am. Chem. Soc.,* 2011, **133,** 14896-14899.

(131) C. X. Wang, L. W. Yin, L. Y. Zhang, N. N. Liu, N. Lun and Y. X. Qi, *ACS Appl. Mater. Interfaces,* 2010, **2,** 3373-3377.

(132) L. F. Zhang, R. Chandrasekar, J. Y. Howe, M. K. West, N. E. Hedin, W. J. Arbegast and H. Fong, *ACS Appl. Mater. Interfaces,* 2009, **1,** 987-991.

(133) P. G. Hu, G. J. Du, W. J. Zhou, J. J. Cui, J. J. Lin, H. Liu, D. Liu, J. Y. Wang and S. W. Chen, *ACS Appl. Mater. Interfaces,* 2010, **2,** 3263-3269.

(134) Z. Ai, Z. Gao, K. Su, W. Ho and L. Zhang, *Catal. Commun.,* 2012, **29,** 189-193.

(135) S. Guo, S. Han, H. Mao, C. Wu, L. Jia, B. Chi, J. Pu and L. Jian, *J. Alloys. Compounds,* 2012, **544,** 50-54.

(136) Y. Sohn, *Appl. Surf. Sci.,* 2010, **257,** 1692-1697.

(137) Q. Xiao, L. Ouyang, L. Gao and C. Yao, *Appl. Surf. Sci.,* 2011, **257,** 3652-3656.

(138) V. Etacheri, M. K. Seery, S. J. Hinder and S. C. Pillai, *Inorg. Chem.,* 2012, **51,** 7164-7173.

(139) X. Tianhua, S. Chen-lu, L. Yong and H. J. Gao-rong, *Zhejiang Univ. Sci. B*, 2006, **7,** 299-303.

(140) M. D. Segall, P. J. D. Lindan, M. J. Probert, C. J. Pickard, P. J. Hasnip, S. J. Clark and M. C. Payne, *J. Phys.: Condens. Matter.,* 2002, **14,** 2717.

(141) L. Kavan, M. Gratzel, S. E. Gilbert, C. Klemenz and H. J. Scheel, *J. Am. Chem. Soc.,* 1996, **118,** 6716-6723.

(142) G. Zhang, X. Ding, F. He, X. Yu, J. Zhou, Y. Hu and J. Xie, *J. Phys. Chem. Solids,* 2008, **69,** 1102-1106.

(143) H.X. Li, J.X. Li and Y.N. Huo, *J. Phys. Chem. B*, 2006, **110,** 1559–1565.

(144) A. E. Giannakas, M. Antonopoulou, Y. Deligiannakis and I. Konstantinou, *Appl. Catal. B: Environ.,* 2013, **140-141,** 636-645.

(145) L. Pan, J. J. Zou, S. Wang, Z. F. Haung, X. Zhang and L. Wang, *Appl. Surf. Sci.,* 2013, **268,** 252-258.

(146) G. Liu, X. Li, J. Zhao, H. Hidaka, N. Serpone and Serpone, *Environ. Sci. Technol.,* 2000, **34,** 3982-3990.

(147) L. Pan, J. J. Zou, S. Wang, X. Y. Liu, X. Zhang and L. Wang, *ACS Appl. Mater. Interfaces* 2012, **4,** 1650-1655

(148) Y. Cong, B. Z. Tian and J. L. Zhang, *Appl. Catal. B: Environ.,* 2011, **101,** 376-381.

(149) V. M. Flores, D.W. Bahnemann and T. Ohno, *Appl. Catal. B:Environ.,* 2011, **103,** 99-108.

(150) P. L. Zhang, S. Yin and T. Sato, *Appl. Catal. B: Environ.* 2011, **103,** 462-469.

(151) R. Jaiswal, N. Patel, D.C. Kothari and A. Miotello, *Appl. Catal. B: Environ.,* 2012, **126,** 47-54.

(152) Y. Cong, J. L. Zhang, F. Chen and M. Anpo, *J. Phys. Chem. C,* 2007, **111,** 6976-6982.

(153) S. Liu, T. Xie, Z. Chan and J. Wu, *Appl. Surf. Sci.,* 2009, **255,** 8587-8592.

(154) R. Dholam, N. Patel and A. Miotello, *Int. J. Hydrogen Energy,* 2011, **36,** 6519-6528.

(155) Y. Hu, X. Zhang and C. Wei, *Res. Chem. Intermed.*, 2010, **36,** 95-101.

(156) A. W. Xu, Y. Gao and H. Q. Liu, *J. Catal.,* 2002, **207,** 151-157.

(157) R. Arroyo, G. Corboda, J. Padilla and V. H. Lara, *Mater. Lett.,* 2002, **54,** 397-402.

(158) I. Othman, R. M. Mohamed and F. M. Ibrahem, *J. Photochem. Photobiol. A: Chem.,* 2007, **189,** 80-85.

(159) L. G. Devi, N. Kottam and S. G. Kumar, *J. Phys. Chem. C* 2009, **113,** 15593-15601

(160) L. G. Devi, N. Kottam S. G. Kumar and K. S. A. Raju. *Catal. Lett.,* 2009, **131,** 612-617.

(161) L. G. Devi, S. G. Kumar, B. N. Murthy and N. Kottam, *Catal. Commun.,* 2009, **10** 794-798.

(162) L. G. Devi, N. Kottam, B. N. Murthy and S. G. Kumar, *J. Mol. Catal. A: Chem.,* 2010, **328,** 44-52.

(163) B. Naik and K. M. Parida, *Ind. Eng. Chem. Res.,* 2010, **49,** 8339-8346.

(164) X. Shen, J. Guo, Z. Liu and S. Xie, *Appl. Surf. Sci.,* 2008, **254,** 4726-4731

(165)Y. Sakatani, D. Grosso, L. N. C. Boissiere, G. J. de A. A. Soler-Illia and C. Sanchez, *J. Mater. Chem.,* 2006, **16,** 77-82.

(166) Z. Bian, J. Zhu, S. Wang, Y. Cao, X. Qian, H. Li, *J. Phys. Chem. C,* 2008, **112,** 6258-6262.

(167) H. Zhang, Y. Liang, X.Wu and H. Zheng, *Mater. Res. Bull.,* 2012, **47,** 2188-2192.

(168) C. D. Valentin, G. Pacchioni, H. Onishi and A. Kudo *Chem. Phys. Lett.,* 2009, **469,** 166-171.

(169) S. A. Bilmes, P. Mandelbaum, F. Alvarez and N. M. Victoria, *J. Phys. Chem. B,* 2000, **104,** 9851-9858

(170) W. Gopel, G. Rocker and R. Feierabend, *Phys. Rev. B,* 1983, **28,** 3427-3438.

(171) H. Zhang, G. Mia, X. Ma, B. Wang and H. Zheng, *Mater. Res. Bull.,* 2014, **55,** 26-32.

(172) H. Zhang, K. Tan, H. Zheng, Y. Gu and W. F. Zhang, *Mater. Chem. Phys.,* 2011, **125,** 156-160.

(173) R. A. Lucky and P. A. Charpentier, *Appl. Catal. B: Environ.,* 2010, **96,** 516-523.

(174) K.M.N. Parida and B. Naik, *J. Colloid Interface Sci.,* 2009, **333,** 269-276.

(175) J. Zhu, J. Ren, Y. Huo, Z. Bian and H. Li, *J. Phys. Chem. C,* 2007, **111,** 18965-18969.

(176) F. K. Han, V.S.R. Kambala, M. Srinivasan, D. Rajarathnam and R. Naidu, *Appl. Catal. A: Gen.*, 2009, **359,** 25-40.

(177) M. M. Joshi, N.K. Labhsetwar, P. A. Mangrulkar, S.N. Tijare, S. P. Kamble and S. S. Rayalu, *Appl. Catal. A: Gen.,* 2009, **357,** 26-33.

(178) B. Gao, X. Luo, H. Fu, B. Lin, Y. Chen and Z. Gu, *Mater. Res. Bull.*, 2013, **48,** 587-594.

(179) T. M. Breault and B. M. Bartlett, *J. Phys. Chem. C,* 2013, **117,** 8611-8618.

(180) M. A. Rauf and S. S. Ashraf, *Chem. Eng. J.,* 2009, **151,** 10-18.

(181) X. T. Pian, B. Z. Lin, Y. L. Chen, J. D. Kaung, K. Z. Zhang and L. M. Fu, *J. Phys. Chem. C,* 2011, **115,** 6531-6539.

(182) X. Chen and S. S. Mao, *Chem. Rev.,* 2007, **107,** 2891-2959.

(183) J. F. Baumard and E. Tani *J. Chem. Phys.,* 1977, **67,** 857-860.

(184) T. Cottineau, N. Bealu, P. A. Gross, S. N. Pronkin, N. Keller, E. R. Savinova and V. Keller, *J. Mater. Chem. A,* 2013, **1,** 2151-2160.

(185) R. Long and N. J. English, *Chem. Phys. Lett.,* 2009, **478,** 175-179.

(186) R. Long and N. J. English, *Appl. Phys. Lett.,* 2009, **94,** 132102.

(187) M. Li, J. Zhang and Y. Zhang, *Catal. Commun.,* 2012, **29,** 175-179.

(188) X. G. Ma, Y. Wu, Y. H. Lu, Y. J. Wang, and Y. F. Zhu. *J. Phys. Chem. C,* 2011, **115,** 16963-19969.

(189) J. Zhang, J. H. Xi and Z. G. Ji, *J. Mater. Chem.,* 2012, **22,** 17700-17708.

(190) X. Cheng, X. Yu and Z. Xing, *J. Colloid. Interface Sci.,* 2012, **372,** 1-5.

(191)H. Gao, B. Lu, F. Liu and Y. Liu and X. Zhao, *Int. J. Photoenergy,* 2012, 453018.

(192) E. Wang, T. He, L. Zhao, Y. Chen and Y. Cao, *J. Mater. Chem.,* 2011, **21,** 144-150.

(193) Y. A. Cao, W. S. Yang, W. F. Zhang, G. Z. Liu and P. Yue, *New J. Chem.,* 2004, **28,** 218-222.

(194) Q. Kang, B.Yuan, J. Xu and M. Fu., *Catal Lett.,* 2011, **141,**1371-1377.

(195) D. E. Gu, B. C. Yang and Y. D. Hu, *Catal Commun.,* 2008, **9,** 1472-1476.

(196) E. Wang, P. Zhang, Y. Chen, Z. Liu. T. He and Y. Cao, *J. Mater. Chem.,* 2012, **22,** 14443-14449.

(197) S. S. Thind, G. Wu and A. Chen, *Appl. Catal. B: Environ.,* 2012, **111-112,** 38-45.

(198) A. Kubacka, G. Colon and M. Garcia, *Appl. Catal. B: Environ.,* 2010, **95,** 238-244.

(199) A. Kubacka, M. Garcia and G. Colon, *J. Catal.,* 2008, **254,** 272-284.

(200) J. Li, J. Xu, W. Dai, H. Li and K. Fan, *Appl. Catal. B: Environ.,* 2008, **82,** 233-243.

(201) Y. Wang, B. Wu and Q. Xu, *Appl. Catal. B: Environ.,* 2005, **59,** 139-146.

(202) M.T. Tsai, *J. Non-Cryst. Solids,* 2002, **298,** 116-130.

(203) Y. Shen, T. Xiong, T. Li and K.Yang, *Appl. Catal. B: Environ.,* 2008, **83,** 177-185.

(204) A. M. Marquez, J. J. Plata, Y. Ortega, J. F. Sanz, G. Colon, A. Kubacka and M. F. Garcia, *J. Phys. Chem. C,* 2012, **116,** 18759-18767.

(205) J. Gong, W. Pu, C. Yang and J. Zhang, *Chem. Eng. J.,* 2012, **209,** 94-101.

(206) H. G. Yu, H. Irie, Y. Shimodajra, Y. Hosogi, Y. Kuroda, M. Miyauchi and K. Hashimoto, *J. Phys. Chem. C,* 2010, **114,** 16481-16487.

(207) J. J. Xu, Y. H. Ao, D. G. Fu and C. W. Yuan, *Colloids Surf. A: Physicochem. Eng. Aspects* 2009, **334,** 107-111.

(208) K.T. Ranjit, I. Willner, S. H. Bossmann and A. M. Braun, *J. Catal.,* 2001, **204,** 305-313.

(209) K.T. Ranjit, I. Willner, S.H. Bossmann and A. M. Braun, *Environ. Sci. Technol.,* 2001, **35,** 1544-1549.

(210) B. M. Reddy, P. M. Sreekanth, E. P. Reddy, Y. Yamada, Q. Xu, H. Sakurai and T. Kobayashi, *J. Phys. Chem. B,* 2002, **106,** 5695-5700.

(211) C. Liu, X. Tang, C. Mo and Z. Qiang, *J. Solid State Chem.,* 2008, **181,** 913-919.

(212) C. Wang, Y. Ao, P. Wang, J. Hou and J.Qian, *Powder Technol.,* 2011, **210,** 203-207.

(213) P. F. Ji, J. L. Zhang, F. Chen and M. Anpo, *Appl. Catal. B:Environ.*, 2009, **85,** 148-154.

(214) P. F. Ji, J. L. Zhang, F. Chen and M. Anpo, *J. Phys. Chem. C,* 2008, **112,** 17809-17813.

(215) P. F. Ji, L. Z. Wang, F. Chen and J. L. Zhang, *ChemCatChem,* 2010, **2**, 1552-1554.

(216) B. M. Reddy, A. Khan, Y. Yamada, T. Kobayashi, S. Loridant and J. Volta, *J. Phys. Chem. B.*, 2003, **107,** 5162-5167.

(217) J. Lin and J.C. Yu, *J. Photochem. Photobiol. A*: *Chem.,* 1998, **116,** 63-67.

(218) J. Fang, X. Bi, D. Si, Z. Jiang and W. Huang, *Appl. Surf. Sci.*, 2007, **253,** 8952-8961.

(219) Z. Liu, B. Guo, L. Hong and H. Jiang, *J. Phys. Chem. Solids,* 2005, **66,** 161-167.

(220) J. Yang, J, Dai and J. Li, *Appl. Surf. Sci.,* 2011, **257,** 8965-8973.

(221) J. Arbiol, J. Cerda, G. Dezanneau, A. Cirera, F. Peiro, A. Cornet and J.R. Morante, *J. Appl. Phys.*, 2002, **92,** 853-861.

(222) R. Kralchevska, M. Milanova, D. Hristov, A. Pintar and D. Todorovsky, *Mater. Res. Bull.* 2012, **47,** 2165-2177.

(223) Y. Ma, J. Zhang, B. Tian, F. Chen and L. Wang, *J. Hazard. Mater.,* 2010, **182,** 386-393.

(224) A.W. Xu, Y. Gao and H.Q. Liu, *J. Catal.,* 2002, **207,** 151-157.

(225) L. G. Devi, B. N. Murthy and S. G. Kumar, *Chemosphere*, 2009, **76,** 1163-1166.

(226) L. G. Devi, N. Kottam, S. G. Kumar and K. E. Rajashekhar, *Cent. Eur. J. Chem.*, 2010, **8,** 142-148.

(227) L. G. Devi and S. G. Kumar, *Appl. Surf. Sci.*, 2011, **257,** 2779-2790.

(228) Y. Pleskov, *Soviet Electrochem.,* 1981, **17,** 1-25.

(229) L. G. Devi and S. G. Kumar, *Appl. Surf. Sci.,* 2012, **261,** 137-146.

(230) J. Xu, Y. Ao, D. Fu and C. Yuan, *J. Colloid Interface Sci.,* 2008, **328,** 447-451.

(231) E. Borgarello, J. Kiwi, M. Gratzel, E. Pelizzetti and M. Visca, *J. Am. Chem. Soc.* 1982, **104,** 2996-3002.

(232) F. B. Li, X. Z. Li, M. F. Hou, K.W. Cheah and W.C.H. Choy, *Appl. Catal. A*: *Gen.,* 2005, **285,** 181-189.

(233) J. Shi, H. Cui, X. Zong, S. Chen, J. Chen, B. Xu, W. Yang, L. Wang and M. Fu, *Appl. Catal. A: Gen.,* 2012, **435-436,** 86-92.

(234) Y. Cui, L. Liu, B. Li, X. Zhou and N. Xu, *J. Phys. Chem. C,* 2010, **114,** 2434-2439.

(235) H.G. Yang and H.C. Zeng, *J. Phys. Chem. B,* 2004, **108,** 3492-3495.

(236) X.W. Lou, C.L. Yuan and L.A. Archer, *Small,* 2007, **3,** 261-265.

(237) J. Li and H. C. Zeng, *J. Am. Chem. Soc.,* 2007, **129,** 15839-15847.

(238) Y. Xie and C. Yuan, *Mater. Res. Bull.,* 2004, **39,** 533-543.

(239) F. B. Li, X. Z. Li, M. F. Hou, K.W. Cheah and W.C. H. Choy, *Appl. Catal. A: Gen.,* 2005, **285,** 181-189.

(240) J.W. Shi, X. Yan, H. J. Cui, X. Zong, M. L. Fu, S. Chen and L. Wang, *J. Mol. Catal. A: Chem.*, 2012, **356,** 53-60.

(241) H. Liu, G. Liu, G. Xie, M. Zhang, Z. Hou and Z. He, *Appl. Surf. Sci.,* 2011, **257,** 3728-3732.

(242) Z. B. Zhang, C. C. Wang, R. Zakaria and J. Y. Ying, *J. Phys. Chem. B,* 1998, **102,** 10871-

(243) B. Singhal, A. Porwal, A. Sharma, R. Ameta and S. C. Ameta, *J. Photochem. Photobiol. A: Chem.,* 1997, **108,** 85-88.

(244) K. L. Lv, J. Hu, X. Li and M. Li, *J. Mol. Catal. A: Chem.,* 2012, **356,** 78-84.

(245) K. L. Lv, J. G. Yu, K. J. Deng, X. H. Li and M. Li, *J. Phys. Chem. Solids,* 2010, **71,** 519-522.

(246) Y. M. Xu, K. L. Lv, Z. G. Xiong, W. H. Leng, W. P. Du, D. Liu and X. J. Xue, *J. Phys. Chem. C,* 2007, **111,** 19024-19032.

(247) K. L. Lv, X. F. Li, K. J. Deng, J. Sun, X. H. Li and M. Li, *Appl. Catal. B: Environ.,* 2010, **95,** 383-392.

(248) Y. Wang, Y. Huang, W. Ho, L. Zhang, Z. Zou and S. Lee, *J. Hazard. Mater.,* 2009, **169,** 77-87.

(249) A. Scafani and J. M. Hermann, *J. Phys. Chem.*, 1996, **100,** 13655-13661.

(250) M. Andersson, L. Osterlund, S. Ljungstrom and A. Palmqvist, *J. Phys. Chem. B,* 2002, **106,** 10674-10679.

(251) Y. Cong, J. L. Zhang, F. Chen, M. Anpo and D. N. He, *J. Phys. Chem. C*, 2007, **111,** 10618-10623.

(252) X. Cheng, X.Yu and Z. Xing *Appl. Surf. Sci.,* 2012, **258,** 7644-7650.

(253) J. Liqiang, F. Honggang, W. Baiqi, W. Dejun, X. Baifu, L. Sudan and S. Jiazhang, *Appl. Catal. B*: *Environ.,* 2006, **62,** 282-291.

(254) J. Liqiang, S. Xiaojun, S. Jing, C. Weimin, X. Zili, D. Yaoguo and F. Honggang, *Solar Energy Mater. Solar Cells,* 2003, **79,** 133-151.

(255) Q. Xu, D. V. Wellia M. Alam Sk, K. H. Lim, J. S. C. Loo, D. W. Lia, R. Amal, and T. T. Y. Tan, *J. Photochem. Photobiol. A: Chem.,* 2010, **210,** 181-187.

(256) X. Yang, C. Cao, L. Erickson. K. Hohn, R. Maghirang and K. Klabunde, *J. Catal.,* 2008, **260,** 128-133.

(257) D. G. Haung, S. J. Liao, J. M. Liu, Z. Dang and L. Petrik, *J. Photochem. Photobiol. A: Chem.,* 2006, **184,** 282-288.

(258) E. Allain, S. Besson, C. Durand, M. Moreau, T. Gacoin and J. P. Boilot, *Adv. Funct. Mater.,* 2007, **17,** 549-554.

(259) W. Y. Gan, S. W. Lam, K. Chiang, R. Amal, H. Zhao and M. P. Brungs, *J. Mater. Chem.,* 2007, **17,** 952-954.

(260) X. Cheng, X.Yu and Z. Xing, *Mater. Res. Bull.,* 2012, **47,** 3804-3809.

(261) X. Shi, H. Qin, X. Yang and Q. Zhang, *Mater. Res. Bull.,* 2012, **47,** 4347-4352.

(262) Y. Yang, H.Y. Wang, X. Li and C. Wang, *Mater. Lett.*, 2009, **63,** 331-333.

(263) D. N. Ke, H. J. Liu, T.Y. Peng, X. Liu and K. Dai, *Mater. Lett.,* 2008, **62,** 447-450.

(264) A. Charanpahari, S.S. Umare, S.P. Gokhale, V. Sudarsan, B. Sreedhar and R. Sasikala *Appl. Catal. A: Gen.*, 2012, **443-444,** 96-102.

(265) J. Xu, Y. Ao, D. Fu and C. Yuan, *J. Hazard. Mater.,* 2009, **164,** 762-768.

(266) Y. Xie and C. Yuan, *Appl. Catal. B: Environ.*, 2003, **46,** 251-259.

(267) F. Dong, W. Zhao and Z. Wu, *Nanotechnol.,* 2008, **19,** 365607-365617.

(268) W. Wang, C. Lu, Y. Ni, M. Su, W. Huang and Z. Xu, *Appl. Surf. Sci.,* 2012, **258,** 8696-8703.

(269) K. Obata, H. Irie, and K. Hashimoto, *Chem. Phys.,* 2007, **339,** 124-132.

(270) X. P. Cao, D. Li, W. H. Jing, W. H. Xing and Y. Q. Fan, *J. Mater. Chem.,* 2012, **22,** 15309-15315.

(271) H. Jiang, P. Yan. Q. Wang, S. Zang, J. Li and Q. Wang, *Chem. Eng. J.,* 2013, **215-216,** 348-357.

(272) S. H. Wang and S. Q. Zhou, *J. Hazard. Mater.,* 2011, **185,** 77-85.

(273) Y. Shen, T. Xiong, H. Du, H. Jin, J. Shang and K.Yang, *J. Sol-Gel Sci. Technol.,* 2009, **50,** 98-102.

(274) (a) N. Serpone, E. Borgarello and M. J. Gratzel, *Chem. Soc. Chem. Commun.,* 1984, 342-344. (b) J. Yu, S. Wang, J. Low and W. Xiao, *Phys. Chem. Chem. Phys.* 2013, **15,** 16883-16890. (c) M. Zhou, J. Yu, S. Liu, P. Zhai and L. Jiang, *J. Hazard. Mater.,* 2008, **157,** 1141-1148. (d) T. Giannakopoulou, N. Todorova, M. Giannoui, J. Yu and C. Trapalis, *Catal. Today,* 2014, **230,**

174-180. (e) G. Dai, J. Yu and G. Liu, *J. Phys. Chem. C* 2011, **115,** 7339-7346. (f) X. Wang, S. Li, Y. Ma, H. Yu and J. Yu, *J. Phys. Chem. C,* 2011, **115,** 14648-14655.

(275) (a) N. Serpone, P. Maruthamuthu, P. Pichat, E. Pelizzetti and H. J. Hidaka, *Photochem. Photobiol. A: Chem.*, 1995, **85,** 247-255. (b) S. G. Kumar and K. S. R. Koteswara Rao, *Energy Environ. Sci.*, 2014, **7,** 45-102.

(276) K.Vinodgopal and P.V. Kamat, *Environ. Sci. Technol.*, 1995, **29,** 841-845.

(277) Y. Cao, X. Zhang, W. Yang, H. Du, Y. Bai, T. Li and Yao, *J. Chem. Mater.*, 2000, **12,** 3445-3448.

(278) W. Ho, J. C. Yu, J. Lin, J. Yu and P. Li, *Langmuir,* 2004, **20,** 5865-5869.

(279) H. Park, W. Choi and M. R. Hoffmann, *J. Mater. Chem.,* 2008, **18,** 2379-2385.

(280) F. Peng, L. Cai, L. Huang, H. Yu and H. Wang, *J. Phys. Chem. Solids*, 2008, **69,** 1657-1664.

(281) M. Sathish, B. Viswanathan, R. P. Viswanath and C. S. Gopinath, *Chem. Mater.,* 2005, **17,** 6349-6353.

(282) L. Gai, X. Duan, H. Jiang, Q. Mei, G. Zhou, Y. Tian and H. Li, *CrystEngComm,* 2012, **14,** 7662-7671.

(283) N. Wu, J. Wang, D. Nyago Tafen, H. Wang, J. Zheng, J. P. Lewis, X. Liu, S. S. Leonard and A. Manivannan, *J. Am. Chem. Soc.,* 2010, **132,** 6679-6685.

(284) T. A. Kandiel, A. Feldhoff, L. Robben, R. Dillert and D. W. Bahnemann, *Chem. Mater.,* 2010, **22,** 2050-2060.

(285) T. A. Kandiel, L. Robben, A. Alkaim and D. Bahnemann, *Photochem. Photobiol. Sci.,* 2013, **12,** 602-609.

(286) J. C. Yu, L. Zhang and J. Yu, *Chem. Mater.,* 2002, **14,** 4647-4653.

(287) G. Tian, H. Fu, L. Jing, B. Xin and K. Pan, *J. Phys. Chem. C,* 2008, **112,** 3083-3089.

(288) H. U. Lee, S. C. Lee, J. H. Seo, W. G. Hong, H. Kim, H. J. Yun, H. J. Kim and J. Lee, *Chem. Eng. J.,* 2013, **223,** 209-215.

(289) F. Li, Y. Zhao, Y. Hao, X. Wang, R. Liu, D. Zhao and D. Chen *J. Hazard. Mater.,* 2012, **239-240,** 118-127.

(290) M. Ishimaru, Y. Hirotsu, I.V. Afanasyev-Charkin and K. E. Sickafus, *J. Phys.: Condens. Mater.,* 2002, **14,** 1237-1247.

(291) X. Wang, J. C. Yu, Y, Chen, L. Wu and X. Fu, *Environ Sci. Technol.,* 2006, **40**, 2369-2374.

(292) A. Hagfeldt and M. Gratzel, *Acc. Chem. Res.,* 2000, **33,** 269-277.

(293) F. Dong, Y. Sun and M. Fu, *Int. J. Photoenergy,* 2012, 569716.

(294) Z. Wu, F. Dong, Y. Liu and H. Wang, *Catal. Commun.,* 2009, **11,** 82-86.

(295) J. Yu and J. Ran, *Energy, Environ. Sci.,* 2011, **4,** 1364-1371.

(296) H. Jiang, M. Nagai and K. Kobayashi, *J. Alloys Compd.*, 2009, **479,** 821-827.

(297) X. Yong and M. A. A. Schoonen, *Am. Mineral*., 2000, **85,** 543-556.

(298) M. Hojamberdiev, R. Prasad, K. Morita, Y. Zhu, M. A. Schiavon, A. Gurlo and R. Riedel, *Appl. Catal. B: Environ.,* 2012, **115-116,** 303-313.

(299) T. Xu, L. Zhang, H. Cheng and Y. Zhu, *Appl. Catal. B: Environ.,* 2011, **101,** 382-387.

(300) L. Zhang, X. Li, Z. Chang and D. Li, *Mater. Sci. Semicond. Process.,* 2011, **14,** 52-57.

(301) Y. Haung, Y. Wei, J. Wu, C. Guo, M. Wang, S. Yin and T. Sato, *Appl. Catal. B: Environ.,* 2012, **123-124,** 9-17.

(302) S. Bagwasi, Y. Niu, M. Nasir, B. Tian and J. Zhang, *Appl. Surf. Sci.,* 2013, **264,** 139-147

(303) A. Testino, I.R. Bellobono, V. Buscaglia, C. Canevali, M. D'Arienzo, S. Polizzi, R. Scotti and F. Morazzoni., *J. Am. Chem. Soc.,* 2007, **129,** 3564-3575.

(304) L. Kong, H. Chen, W. Hua, S. Zhang and J. Chen, *Chem. Commun.,* 2008, 4977-4979

(305) H. Cheng, B. Huang, Y. Dai, X. Qin, X. Zhang, Z. Wang and M. Jiang, *J. Solid State Chem.,* 2009, **182,** 2274-2278.

(306) P.Yap, Y. Cheah, M. Srinivasan and T. Lim, *Appl. Catal. A: Gen.,* 2012, **427-428,** 125-136.

(307) K. M. Schindler and M. Kunst, *J. Phys. Chem.,* 1990, **94,** 8222-8226.

(308) R. I. Bickley, T. G. Carreno, J. S. Lees, L. Palmisano and R .J. D. Tilley, *J. Solid State Chem.,* 1991, **92,** 178-190.

(309) D. C. Hurum, A. G. Agrios, K. A. Gray, T. Rajh, and M. C. Thurnauer, *J. Phys. Chem. B.* 2003, **107,** 4545-4549.

(310) R. Beranek, B. Neumann, S. Sakthivel, M. Janczarek, T. Dittrich, H. Tributsch and H. Kisch, *Chem. Phys.,* 2007, **339,** 11-19.

(311) C. D. Valentin, E. Finazzi, G. Pacchioni, A. Selloni, S. Livraghi, M.C. Paganini and E. Giamello, *Chem. Phys.,* 2007, **339,** 44-56.

(312) P. Yap, T. Lima and M. Srinivasan, *Catal. Today,* 2011, **161,** 46-52.

(313) Y. Li, S. Zhang, Q. Yu andW. Yin, *Appl. Surf. Sci.,* 2007, **253,** 9254-9258.

(314) X. M. Yan, J. Kang, L. Gao, L. Xiong and P. Mei, *Appl. Surf. Sci.* 2013, **265,** 778-783.

(315) D. Mitoraj and H. Kisch, *Angew. Chem. Int. Ed.,* 2008, **47,** 9975-9978.

(316) N. R. Khalid, E. Ahmed, Z. Hong, Y. Zhang and M. Ahmad, *Curr. Appl. Phys.,* 2012, **12,** 1485-1492.

(317) N. L. Yang, J. Zhai, D. Wang, Y. S. Chen and L. Jiang, *ACS Nano*, 2010, **4,** 887-894.

(318) B. Neppolian, A. Bruno, C.L. Bianchi and M. A. Kumar, *Ultrason. Sonochem.,* 2012, **19**, 9-15.

(319) X. Shang, M. Zhang, X. Wang and Y. Yang, *J. Exp. Nanosci.,* 2012, 1-13.

(320) Y. P. Zhang and C. X. Pan, *J. Mater. Sci.,* 2011, **46,** 2622-2626.

(321) N. Yang, G. Li, W. Wang, X. Yang and W. F. Zhang, *J. Phys. Chem. Solids,* 2011, **72,** 1319-1324.

(322) Y. Cheng, V. Subramaniam, D. Gong, Y. Tang, J. Highfield, S. Pehkonen, P. Pichat, M. Schreyer and Z. Chen, *J. Solid State Chem.,* 2012, **196,** 518-527.

(323) P. Zhang, X. Liu, S. Yin and T. Sato, *Appl. Catal. B: Environ.,* 2010, **93,** 299-303.

(324) H. Li, S. Yin and T. Sato, *Appl. Catal. B: Environ.,* 2011, **106,** 586-591.

(325) S. H. Choi, N.H. Kim, Y. H. Yun and S. C. Choi, *J. Ceram. Process, Res.,* 2006, **7,** 62-65.

(326) (a) M. V. Dozzi, L. Prati, P. Canton and E. Selli, *Phys. Chem. Chem. Phys.,* 2009, **11,** 7171-7180. (b) Y. Wang, J. Yu, W. Xiao and Q. Li, *J. Mater. Chem. A,* 2014, **2,** 3847-3855. (c) J. Yu, W. Wang, B. Cheng and B. L. Su, *J. Phys. Chem. C,* 2009, **113,** 6743-6750.

(327) M. I. Litter, *Appl. Catal. B: Environ.,* 1999, **23,** 89-114.

(328) A. Primo, A. Corma and H. Garcia, *Phys. Chem. Chem. Phys.,* 2011, **13**, 886-910.

(329) (a) P. Kamat, *J. Phys. Chem. B,* 2002, **106,** 7729-7744. (b) Z. Xu, J. Yu and G. Liu, *Eelctrochem. Commun.,* 2011, 13, 1260-1263. (c) J. Yu, L. Yue, S. Liu, B. Huang and X. Zhang, *J. Colloid Interface Sci.,* 2009, **334,** 58-64. (d) J. Yu, L. Qi and M, Jaroniec, *J. Phys. Chem. C* **2010,** 114, 13118-13125.

(330) V. Brezova, A. Blazkova, L. Karpinsky, J. Groskova, B. Havlinova, V. Jorik and M. Ceppan, *J. Photochem. Photobiol., A: Chem.,* 1997, **109,** 177-183.

(331) J. Lee and W. Choi, *Environ. Sci. Technol.,* 2004, **38,** 4026-4033.

(332) P. D. Cozzoli, M. L. Curri and A. Agostiano, *Chem. Commun.,* 2005, 3186-3188.

(333) J. Lu, F. Su, Z. Haung, C. Zhang, Y. Liu, X. Ma and J. Gong, *RSC Adv.,* 2013, **3,** 720-724.

(334) E. W. McFarland and J. Tang, *Nature,* 2003, **421,** 616-618.

(335) W. Jiang, N. Ullah, G. Divitini, C. Ducati, R. V. Kumar, Y. Ding and Z. H. Barber *Langmuir,* 2012, **28,** 5427-5431.

(336) Y. Gao, P. Fang, F. Chen, Y. Liu, Z. Liu, D. Wang and Y. Dai, *Appl. Surf. Sci.,* 2013, **265,** 796-801.

(337) M. Wu, B. Yang, Y. Lv, Z. Fu, J. Xu, T. Guo and Y. Zhoa, *Appl. Surf. Sci.,* 2010, **256,** 7125-7130.

(338) J. X. Li, J. H. Xu, W. L. Dai and K. N. Fan, *J. Phys. Chem. C*, 2009, **113,** 8343-8349.

(339) E. Stathatos, P. Lianos, P. Falaras and A. Siokou, *Langmuir,* 2000, **16,** 2398-2400.

(340) Y. H. Ao, J. J. Xu, D. G. Fu and C. W. Yuan, *J. Phys. Chem. Solids,* 2008, **69,** 2660-2664.

(341) B. Z. Tian, C. Z. Li, F. Gu and H. B. Jiang, *Catal. Commun.*, 2009, **10,** 925-929.

(342) J. Virkutyte and R. S. Varma., *RSC Adv.,* 2012, **2,** 1533-1539.

(343) A. Kumar, A. K. Pandey, S. S. Singh, R. Shanker and A. Dhawan, *Free Radical Biol. Med.,* 2011, **51,** 1872-1881.

(344) (a) T. Morikawa, T. Ohwaki, K. Suzuki, S. Moribe and S. Kubota, *Appl. Catal. B: Environ.,* 2008, **83,** 56-62. (b) L. G. Devi, S. G. Kumar, K. M. Reddy and C. Munikrishnappa, *J. Hazard. Mater.,* 2009, **164,** 459-467 (c) L. G. Devi, K. E. Rajashekhar, K. S. A. Raju and S. G. Kumar, *J. Mol. Catal. A: Chem.,* 2009, **314,** 88-94. (d) L. G. Devi, K. E. Rajashekhar, K. S. A. Raju and S. G. Kumar, *Desalination*, 2011, **270,** 31-39. (e) L. G. Devi, K. S. A. Raju and S. G. Kumar, *J. Environ. Monit.,* 2009, **11,** 1397-1404, (f) L. G. Devi, S. G. Kumar and K. M. Reddy. *Cent. Eur. J. Chem.*, 2009, **7,** 468-477.

(345) S. Yin, B. Liu, P. Zhang, T. Morikawa, K. Yamanaka and T. Sato, *J. Phys. Chem. C,* 2008, **112,** 12425-12431.

(346) J. R. Kanofsky, *Chem. Biol. Interact.,* 1989, **70,** 1-28.

(347) M. V. Dozzi, A. Saccomanni, M. Altomare and E. Selli, *Photochem. Photobiol. Sci.,* 2013, **12,** 595-601.

(348) P. V. Kamat, *J. Phys. Chem. Lett.,* 2012, **3,** 663-672.

(349) A. T. Kuvarega, R. W. M. Krause and B. B. Mamba, *J. Phys. Chem. C,* 2011, **115,** 22110-22120.

(350) X. Li, Z. Zhuang, W. Li and H. Pan, *Appl. Catal. A: Gen.,* 2012, **429-430,** 31-38.

(351) N. Strataki, N. Boukos, F. Paloukis, S. G. Neophytides and P. Lianos, *Photochem. Photobiol. Sci.,* 2009, **8,** 639-643.

(352) A. H. Yahaya, M. A. Gondal and A. Hameed, *Chem. Phys. Lett.,* 2004, **400,** 206-212.

(353) K. Koci, L. Obalova, L. Matejova, D. Placha, Z. Lacny, J. Jirkovsky and O. Solcova, *Appl. Catal. B: Environ.,* 2009, **89,** 494-502.

(354) S. S. Tan, L. Zou and E. Hu, *Catal. Today*, 2008, **131,** 125-129.

(355) M. C. Wu, J. Hiltunen, A. Sapi, A. Avila, W. Larsson, H. C. Lia, M. Huuhtanen, G. Toth, A. Shchukarev, N. Laufer, A. Kukovecz, Z. Konya, J. P. Mikkola, R. Keiski, W. F. Su, Y. F. Chen, H. Jantunen, P. M. Ajayan, R. Vajtai and K. Korda, *ACS Nano,* 2011, **5,** 5025-5030.

(356) A. Pandikumar, K. Sivaranjani, C. S. Gopinath and R. Ramaraj, *RSC Adv.,* 2013, **3,** 13390-13398.

(357) A. Sanchez, S. Abbet, U. Heiz, W. D. Schneider, H. Hakkinen, R. N. Barnett and U. Landman, *J. Phys. Chem. A,* 1999, **103,** 9573-9578.

(358) S. Laursen and S. Linic, *Phys. Rev. Lett.,* 2006, **97,** 026101.

(359) S. Laursen and S. Linic, *Phys. Chem. Chem. Phys.,* 2009, **11,** 11006-11012.

(360) C. T. Campbell, *Science,* 2004, **306,** 234-235.

(361) M. S. Chen and D. W. Goodman, *Science,* 2004, **306,** 252-255.

(362) R. G. Pearson, *J. Am. Chem. Soc.,* 1963, **85,** 3533-3539.

(363) V. Subramanian, E. E. Wolf and P. V. Kamat, *J. Phys. Chem. B,* 2001, **105,** 11439-11446.

(364) K. Yu, Y. Tian and T. Tatsuma, *Phys. Chem. Chem. Phys.,* 2006, **8,** 5417-5420.

(365) C. S. Kim, J. W. Shin, Y. H. Cho, H. D. Jang, H. S. Byun and T. O. Kim, *Appl. Catal. A: Gen,* 2013, **455,** 211-218.

(366) W. N. Wang, J. H. Park and P. Biswas, *Catal. Sci. Technol.*, 2011, **1,** 593-600.

(367) T. Morikawa, Y. Irokawa, and T. Ohwaki, *Appl. Catal. A*: Gen., 2006, **314,** 123-127.

(368) M. B. Fishera, D. A. Keaneb, P. F. Ibanez, J. Colreavy, S. J. Hinderd, K. G. McGuigana, and S. C. Pillai, *Appl. Catal B: Environ.,* 2013, **130-131,** 8-13.

(369) Y. Kikuchi, K. Sunada, T. Iyoda, K. Hashimoto and A. Fujishima, *J. Photochem. Photobiol. A: Chem.*, 1997, **106,** 51-56.

(370) Y. Horie, M. Taya and S. Tone, *J. Chem. Eng. Japan*, 1998, **31,** 922-929.

(371) J. A. R. Herrera and C. Pulgarin, *Solar Energy,* 2010, 84, 37-43.

(372) S. Ikeda, N. Sugiyama, B. Pal, G. Marci, L. Palmisano, H. Noguchi, K. Uosaki, B. Ohtani, Phys. Chem. Chem. Phys. 2001, **3,** 267-273.

(373) (a) J. Yuan, M. Chen, J. Shi and W. Shangguan, *Int. J. Hydrogen Energy,* 2006, **31,** 1326-1331. (b) Q. Xiang and J. Yu, *J. Phys. Chem. Lett.,* 2013, **4,** 753-759. (c) Q. Xiang, J. Yu and M. Jaroniec, *J. Am. Chem. Soc*., 2012, **134,** 6575-6578.

(374) (a) M. M. Joshi, P. A. Mangrulkar, S. N. Tijare, P. S. Padole, D.V. Parwate, N. K. Labhsetwar and S. S. Rayalu, *Int. J. Hydrogen Energy,* 2012, **37**, 10457-10461. (b) Q. Li, H.

Meng, P. Zhou, Y. Zheng, J. Wang, J. Yu, and J. Gong, *ACS Catal.*, 2013, **3,** 882-889. (c) Q. Xiang, J.Yu and M. Jaroniec, *J. Phys. Chem. C,* 2011, **115,** 7355-7363.

(375) K. E. Karakitsou and X. E. Verykios, *J. Phys. Chem.,* 1993, **97,** 1184-1189.

(376) Y. Li, G. Ma, S. Peng, G. Lu and S. Li, *Appl. Surf. Sci.,* 2008, **254,** 6831-6836.

(377) F. Zhuge, L. Jin and G. Lu, *J. Mol. Catal., (China)* 2007, **21,** 233-238.

(378) T. Ihara, M. Miyoshi, Y. Iriyama, O. Matsumoto and S. Sugihara, *Appl. Catal. B: Environ.,* 2003, **42,** 403-409.

(379) Y.V. Pleskov, *J. Soviet Electrochem.,* 1981, **17,** 1-25.

(380) X. Sun, H. Liu, J. Dong, J. Wei and Y. Zhang *Catal. Lett.*, 2010, **135**, 219-225.

(381) R. Sasikala, A. R. Shirole, V. Sudarsan, Jagannath, C. Sudakar, R. Naik, R. Rao, and S. R. Bharadwaj, *Appl. Catal. A: Gen.,* 2010, **377,** 47-54.

(382) X. Yang, Y. Wang, L. Xu, X. Yu, Y. Guo, *J. Phys. Chem. C,* 2008, **112**,11481-11489.

(383) R. Sasikala, V. Sudarshan, C. Sudakar, R. Naik, L. Panicker and S. R. Bharadwaj, *Int. J. Hydrogen Energy,* 2009, **34**, 6105-6113.

(384) W. Sun, S. Zhang, Z. Liu, C. Wang, Z. Mao, *Int. J. Hydrogen Energy,* 2008, **33,** 1112-1117.

(385) P.V. Kamat, *J. Phys. Chem. C,* 2007, **111,** 2834-2860.

(386) O. D. Jayakumar, R. Sasikala1, C. A. Betty, A. K. Tyagi, S. R. Bharadwaj, U. K. Gautam, P. Srinivasu, and A. Vinu, *J. Nanosci. Nanotechnol.,* 2009, **9,** 4663-4667.

(387) K. Domen, S. Naito, T. Onishi, K. Tamaru and Soma, *J. Phys. Chem.,* 1982, **86,** 3657-3661.

(388) F. N. Sayed, O. D. Jayakumar, R. Sasikala, R. M. Kadam, S. R. Bharadwaj, L. Kienle, U. Schürmann, S. Kaps, R. Adelung, J. P. Mittal and A. K. Tyagi, *J. Phys. Chem. C.* 2012, **116**, 12462-12467.

(389) S. Martha, D. P. Das, N. Biswal and K. M. Parida, *J. Mater. Chem.,* 2012, **22,** 10695-10703.

(390) H. Lv, L. Ma, P. Zeng, D. Ke and T. Peng, *J. Mater. Chem.,* 2010, **20,** 3665-3672.

(391) K. M. Parida, M. Satpathy and L. Mohapatra, *J. Mater. Chem.,* 2012, **22,** 7350-7357.

(392) J. Lv, T. Kako, Z. Li, Z. Zou and J. Ye, *J. Phys. Chem. C,* 2010, **114,** 6157- 6162.

(393) Y. Wang, Y. R. Su, L. Qiao, L. X. Liu, Q. Su, C. Q. Zhu and X. Q. Liu, *Nanotechnol.,* 2011, **22,** 225702.

(394) M. Gratzel, *Nature,* 2001, **414,** 338-344.

(395) R. Souda, W. Hayami, T. Aizawa and Y. Ishizawa, *Surf. Sci.,* 1993, **285,** 265-274.

(396) A. Suli, M. I. Torok and I. Hevesi, *Thin Solid Films,* 1986, **139,** 233-246.

(397) F. Pei, Y. Liu, S. Xu, J. Lu, C.Wang and S. Cao, *Int. J. Hydrogen Energy,* 2013, **38,** 2670 - 2677.

(398) X. Wang, L. J. Zhi and K. Mullen, *Nano Lett*., 2008, **8,** 323-327.

(399) X. Q. Gong and A. Selloni, *J. Phys. Chem. B,* 2005, **109,** 19560-19562.

(400) (a) M. Lazzeri, A. Vittadini and A. Selloni, *Phys. Rev. B,* 2002, **65,** 119901. (b) L. Qi, J. Yu and M. Jaroniec, *Phys. Chem. Chem. Phys.,* 2011, **13**, 8915-8923. (c) Q. Xiang, J. Yu and M. Jaroniec, *Chem. Commun.,* 2011, **47**, 4532-4534. (d) J. Yu, J. Fan and K. Lv, *Nanoscale,* 2010, **2,** 2144-2149. (e) J. Yu, G. Dai, Q. Xiang and M. Jaroniec, *J. Mater. Chem.,* 2011, **21,** 1049-1057. (f) K. Lv, Q. Xiang and J. Yu, *Appl. Catal. B: Environ.,* 2011, **104,** 275-281.

(401) (a) X. Zhou, F. Peng, H. Wang, H. Yu and Y. Fang *Chem. Commun.,* 2012, **48**, 600-602.

(b) Q. Xiang, J. Yu, W. Wang and M. Jaroniec, *Chem. Commun.,* 2011, **47**, 6906-6908.

(402) T. Hirakawa and Y. Nosaka, *Langmuir,* 2002, **18,** 3247-3254.

(403) W.Wang, C. Lu, Y. Ni, M. Su and Z. Xu, *Appl. Catal. B: Environ.,* 2012, **127,** 28-35.

(404) Y. Zhang, C. Li and C. Pan, *J. Am. Ceram. Soc.,* 2012, **95,** 2951-2956.

(405) J. H. Pan, G. Han, R. Zhou and X. S. Zhao, *Chem. Commun.,* 2011, **47**, 6942-6944.

(406) J. H. Pan, X. Zhang, A. J. Du, D.D. Sun and J.O. Leckie, *J. Am. Chem. Soc.,* 2008, **130,** 11256-11257.

(407) J. H. Pan, H. Dou, Z. Xiong, C. Xu, J. Ma and X. S. Zhao, *J. Mater. Chem.,* 2010, **20,** 4512-4528.

(408) Z. Bian, J. Zhu, F. Cao, Y. Lu and H. Li, *Chem. Commun.,* 2009, 3789-3791.

(409) G. Dai, S. Liu, Y. Liang, H. Liu and Z. Zhong, *J. Mol. Catal. A: Chem.,* 2013, **368-369,** 38- 42.

(410) H. M. Zhang, P. Liu, F. Li, H.W. Liu, Y. Wang, S. Q. Zhang, M. X. Guo, H. M. Cheng and H. J. Zhao, *Chem. Eur. J.,* 2011, **17,** 5949-5957.

(411) Q. J. Xiang and J.G. Yu, *Chinese J. Catal.*, 2011, **32,** 525-531.

(412) M.Y. Xing, D.Y. Qi, J. L. Zhang and F. Chen, *Chem. Eur. J.*, 2011, **17,** 11432-11436.

(413) X. Zong, Z. Xing, H. Yu, Z. Chen, F. Tang, J. Zou, G. Q. Lu and L. Wang, *Chem. Commun.,* 2011, **47**, 11742-11744.

(414) K. Maeda, B. Lee, D. Lu and K. Domen, *Chem. Mater.,* 2009, **21,** 2286-2291.

(415) Q. Xiang, J. Yu, and M. Jaroniec, *Phys. Chem. Chem. Phys.,* 2011, **13**, 4853-4861.

(416) W. Shi, W. Yang, Q. Li, S. Gao. P. Shang and J. K. Shang, *Nanoscale Res. Lett.,* 2012, **7,** 590.

(417) J. M. Wu and M. L. Tang, *Nanoscale,* 2011, **3,** 3915- 3922.

(418) M. A. Fox and M.T. Dulay, *Chem. Rev.,* 1993, **93,** 341-357.

(419) N. Serpone, *J. Phys. Chem. B*, 2006, **110,** 24287-24293.

(420) K. Selvam, S. Balachandran, R. Velmurugan and M. Swaminathan, *Appl. Catal. A: Gen.,* 2012, **413-414,** 213-222.

(421) K. Shibata, T. Mimura, M. Matsui, T. Sugiura and H. Minoura, *J. Chem. Soc. Chem. Commun.*, 1988, 1318-1320.

(422)Y. Hirose, T. Mori, Y. Morishita, A. Itadani, T. Kudoh, T. Ohkubo, T. Matsuda, S. Kittaka, and Y. Kuroda, *Inorg. Chem.,* 2011, **50,** 9948-9957

(423) K. Selvam and M. Swaminathan, *RSC Advances,* 2012, **2,** 2848-2855.

(424) K. Selvam and M. Swaminathan, *Synth. React. Inorg. Met.-Org. Chem.,* 2013, **43,** 500-508.

(425) S. Yurdakal, V. Augugliaro, V. Loddo, G. Palmisano and L. Palmisano, *New. J. Chem.,* 2012, **36**, 1762-1768.

(426) T. Ohno, K. Sarukawa, K. Tokieda and M. Matsumura, *J. Catal.,* 2001, **203,** 82-86.

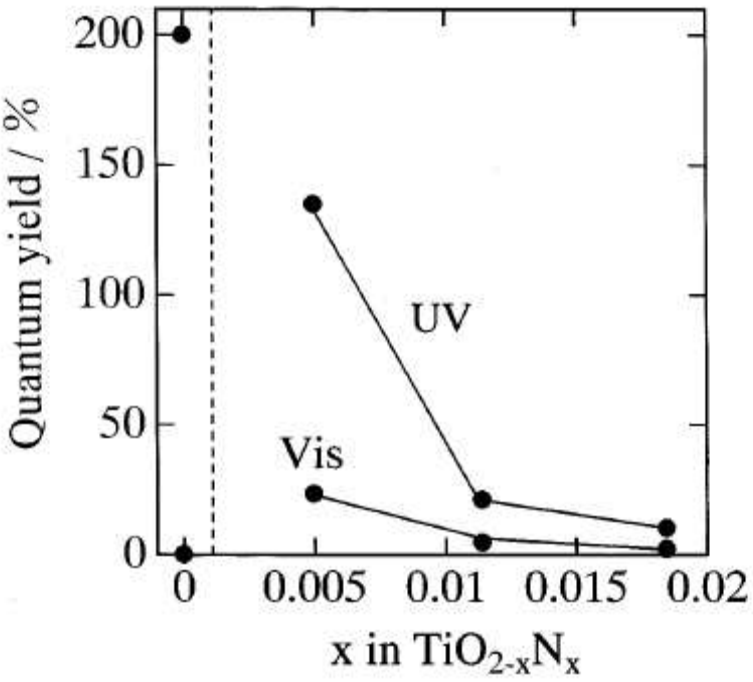

Figure1. Quantum efficiency versus nitrogen dopant content (x) in TiO_2 for the decomposition of gaseous 2-propanol under UV and visible light irradiation

Reprinted with permission from ref. 35, Copyrights (2003) American Chemical Society

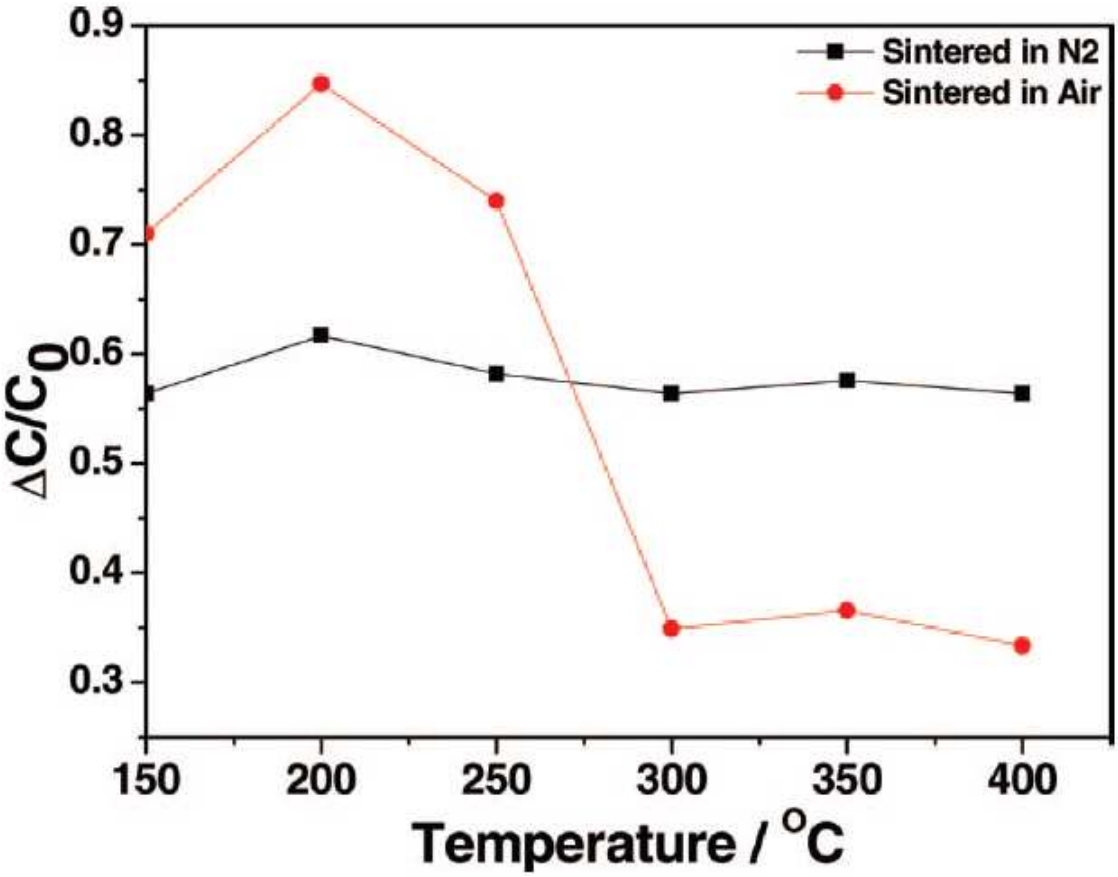

Figure 2. C/C_0 versus temperature plot for N-TiO_2 sintered at different temperatures (for 30 min) either in air or in N_2 atmospheres. Photocatalytic activity was measured after 160 min of irradiation by a Xe arc lamp with wavelength > 400 nm.

Reprinted with permission from ref. 38, Copyrights (2008) American Chemical Society

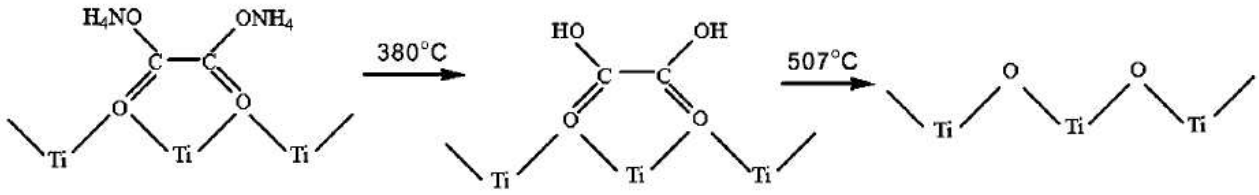

Figure. 3 Mechanism of Bronsted acid site formations on the surface of N-TiO_2 calcined at 400° C (a schematic illustration)

Reprinted with permission from ref. 39, Copyrights (2008) American Chemical Society

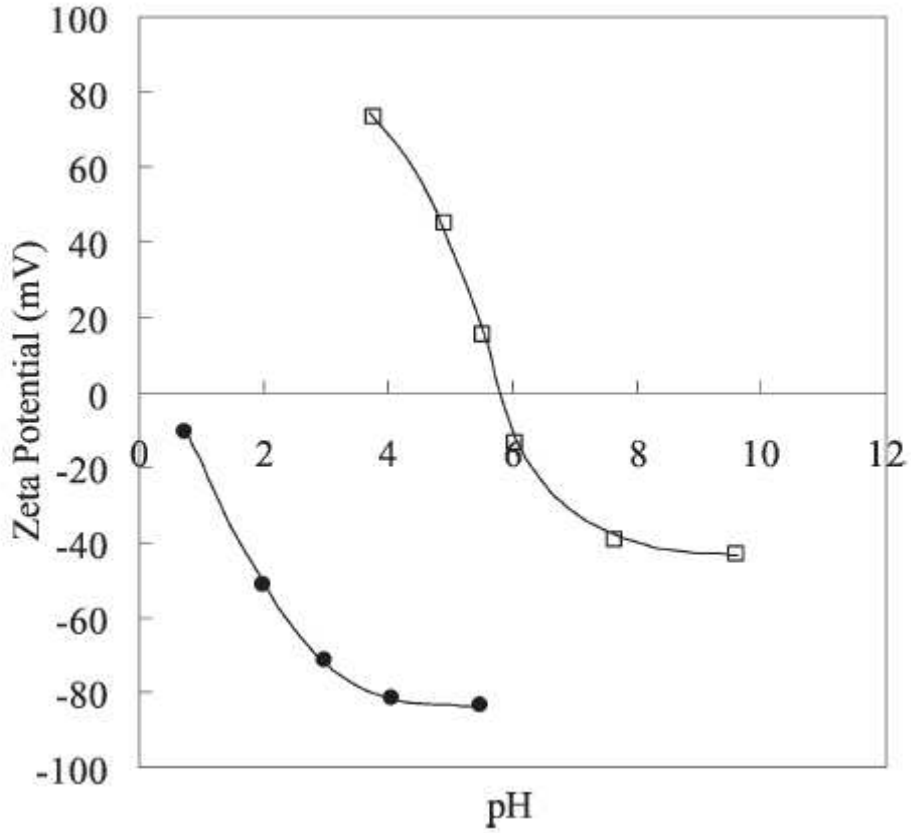

Figure 4. Zeta potential versus pH value for the thin films, open Square: pure TiO_2, closed circle: N-TiO_2 (annealed in NH_3 at 600 ^{0}C).

Reprinted with permission from ref. 54, Copyrights (2004) Royal Society of Chemistry

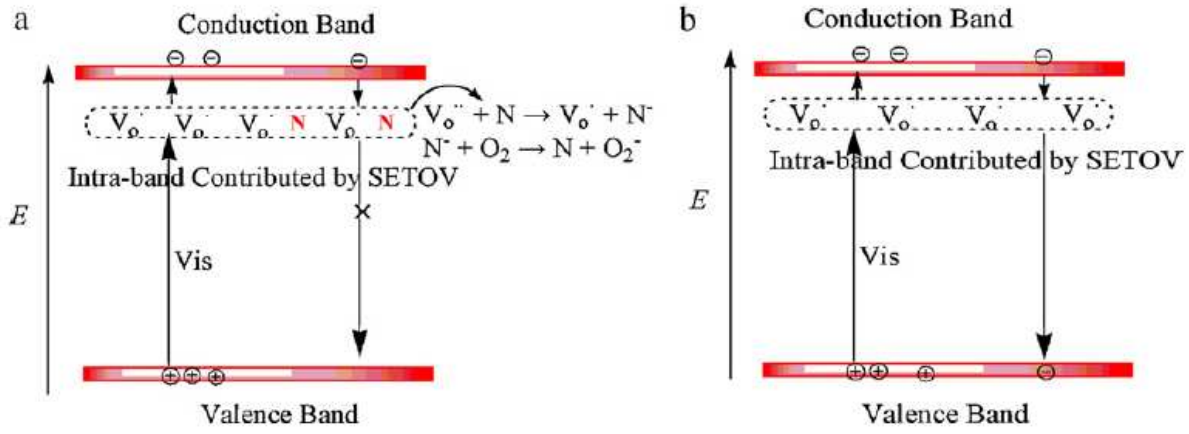

Figure. 5 Schematic illustrations of the role of nitrogen dopant in preventing photogenerated charge carrier recombination (a) for N-TiO_2 with enhanced visible light absorption and photocatalytic activity (b) for novel TiO_2 with enhanced visible light absorption but without photocatalytic activity.

Reprinted with permission from ref. 58, Copyrights (2004) Elsevier Publications

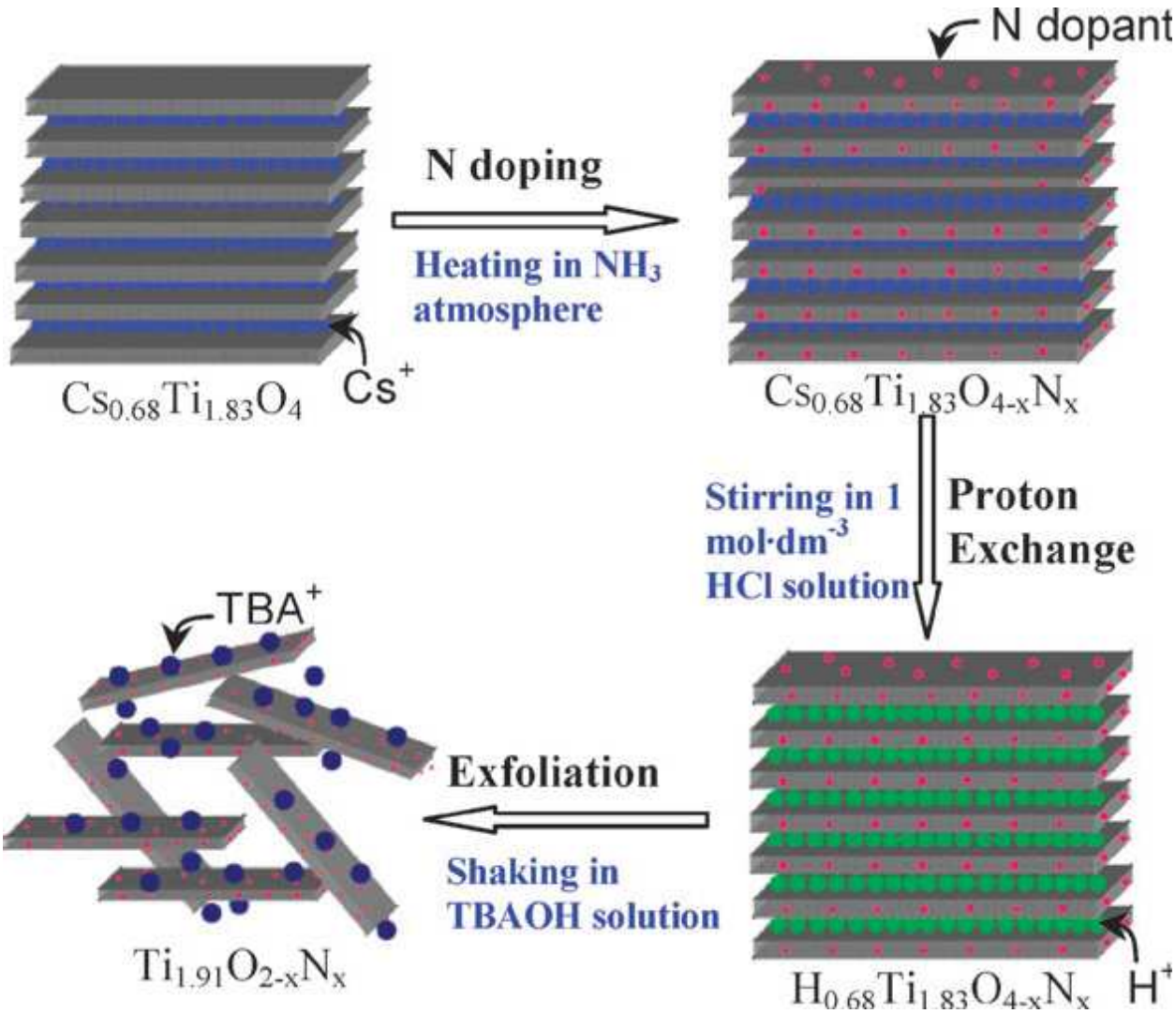

Figure 6 Schematic procedure for the preparation of nitrogen-doped $Ti_{1.91}O_{2-x}N_x$ nanosheets starting from $Cs_{0.68}Ti_{1.83}O_4$. TBA^+: tetrabutylammonium ion.

Reprinted with permission from ref. 81, Copyrights (2009) Royal Society of Chemistry

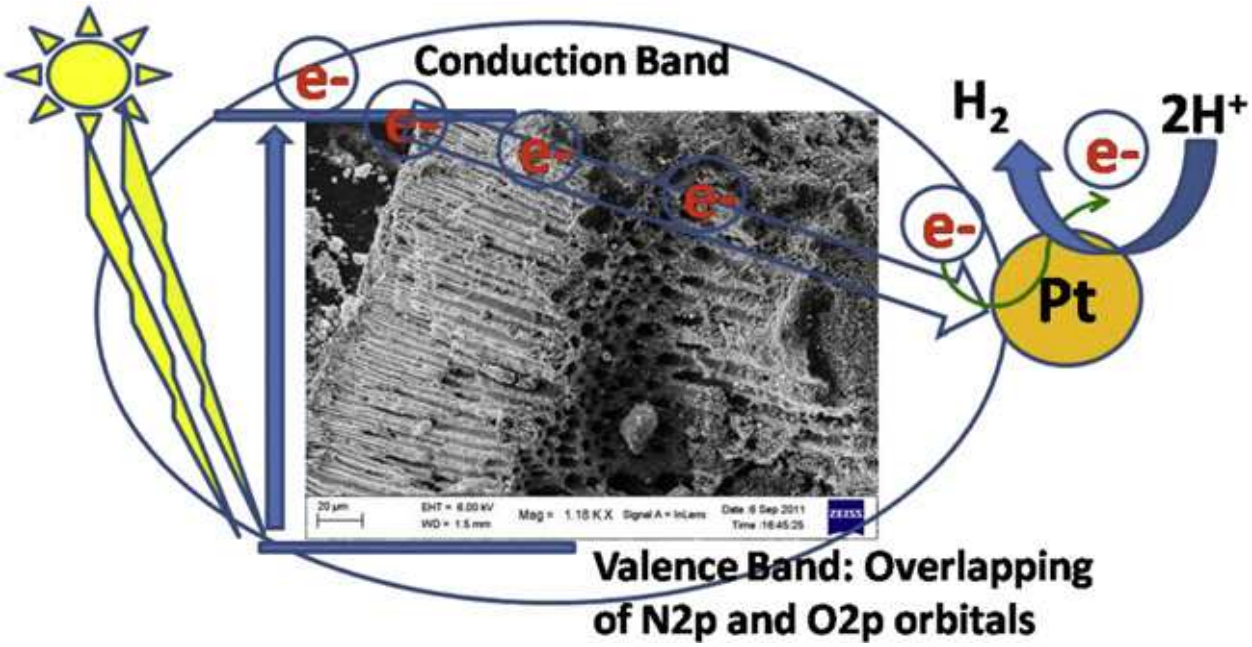

Figure 7 Illustration of the mechanism of hydrogen production from fibrous hierarchical meso-macroporous N-TiO_2 under visible light irradiation.

Reprinted with permission from ref. 89, Copyrights (2013) Elsevier Publications

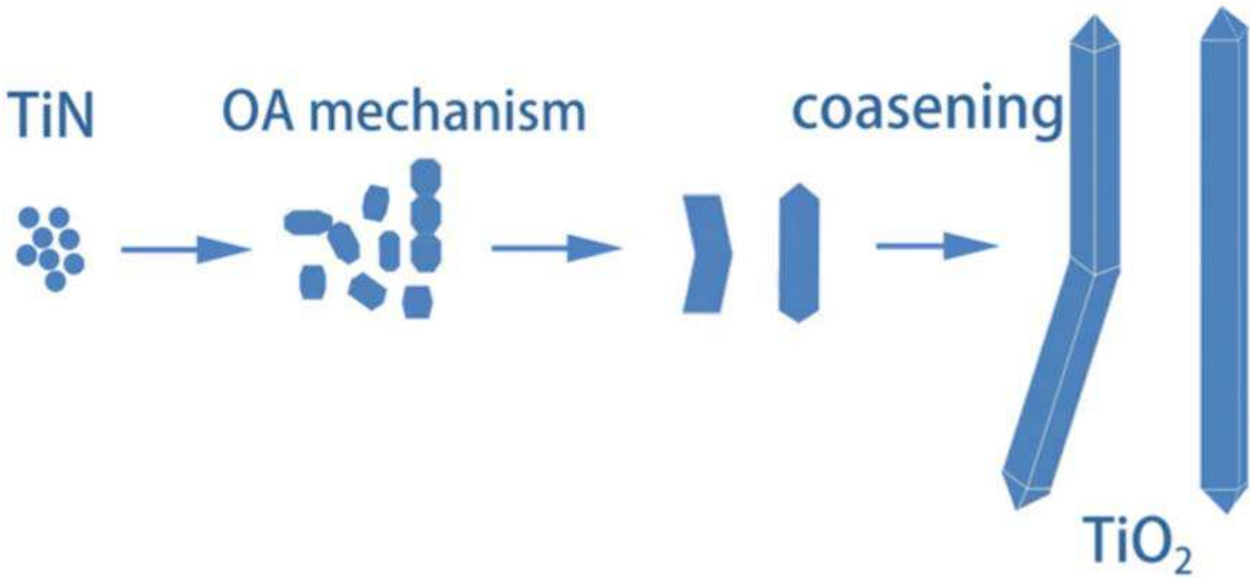

Figure 8. The mechanism of formation of straight and V-shaped N-TiO_2 nanorods starting from TiN

Reprinted with permission from ref. 93, Copyrights (2012) Royal Chemical Society

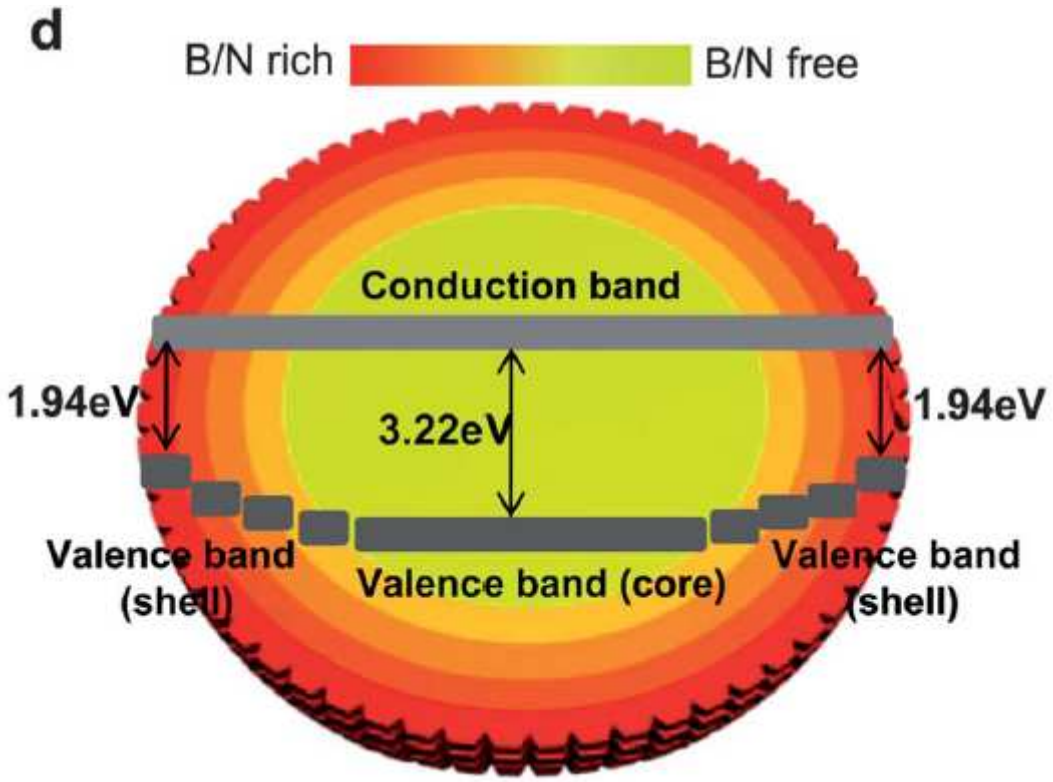

Figure 9 Schematic band structure of boron and nitrogen doped red TiO_2 depicting band gap gradient.

Reprinted with permission from ref. 115, Copyrights (2012) Royal Chemical Society

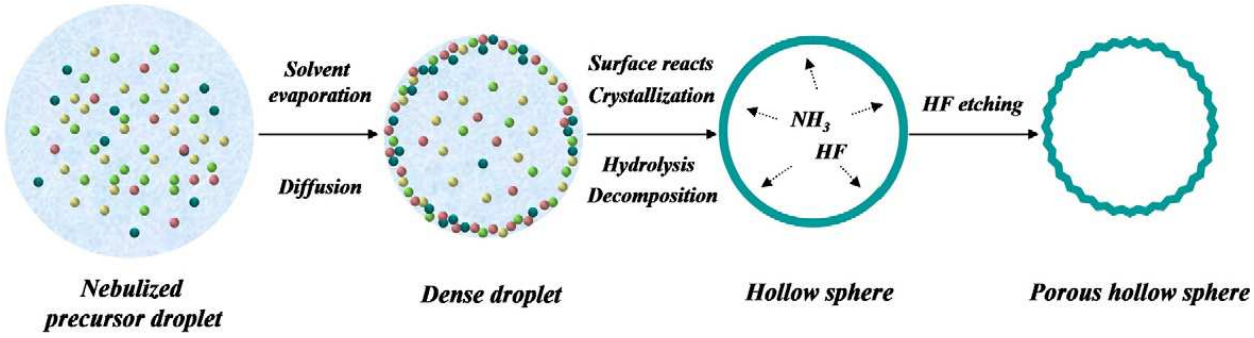

Figure 10 Illustration of various multistage process involved in the formation of N-Si-TiO_2 porous hollow microsphere.

Reprinted with permission from ref. 134, Copyrights (2012) Elsevier Publications

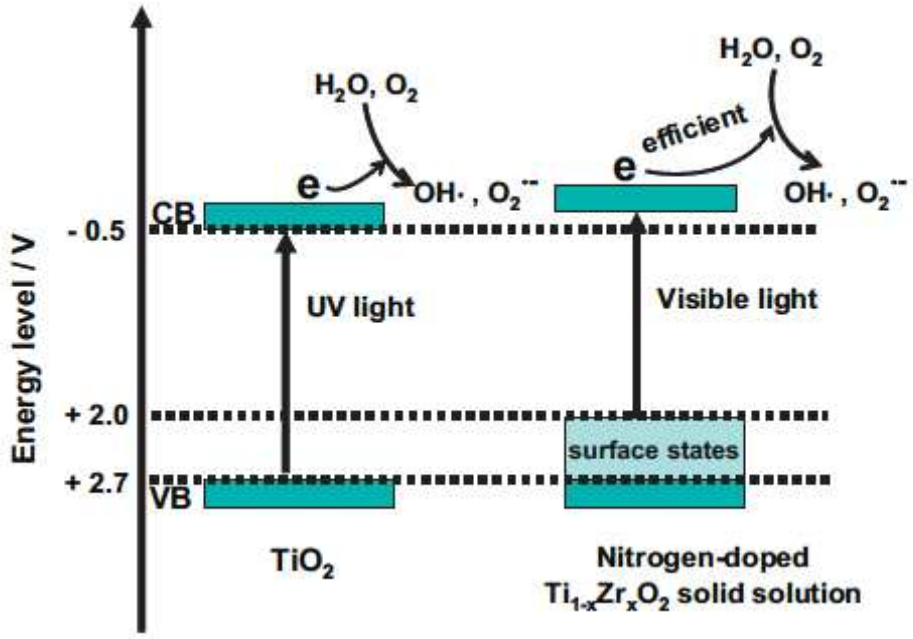

Figure 11 Schematic illustration of band structure of TiO_2 and nitrogen doped $Ti_{1-x}Zr_xO_2$ solid solution as photocatalysts for the production of various free radicals.

Reprinted with permission from ref. 178, Copyrights (2013) Elsevier Publications

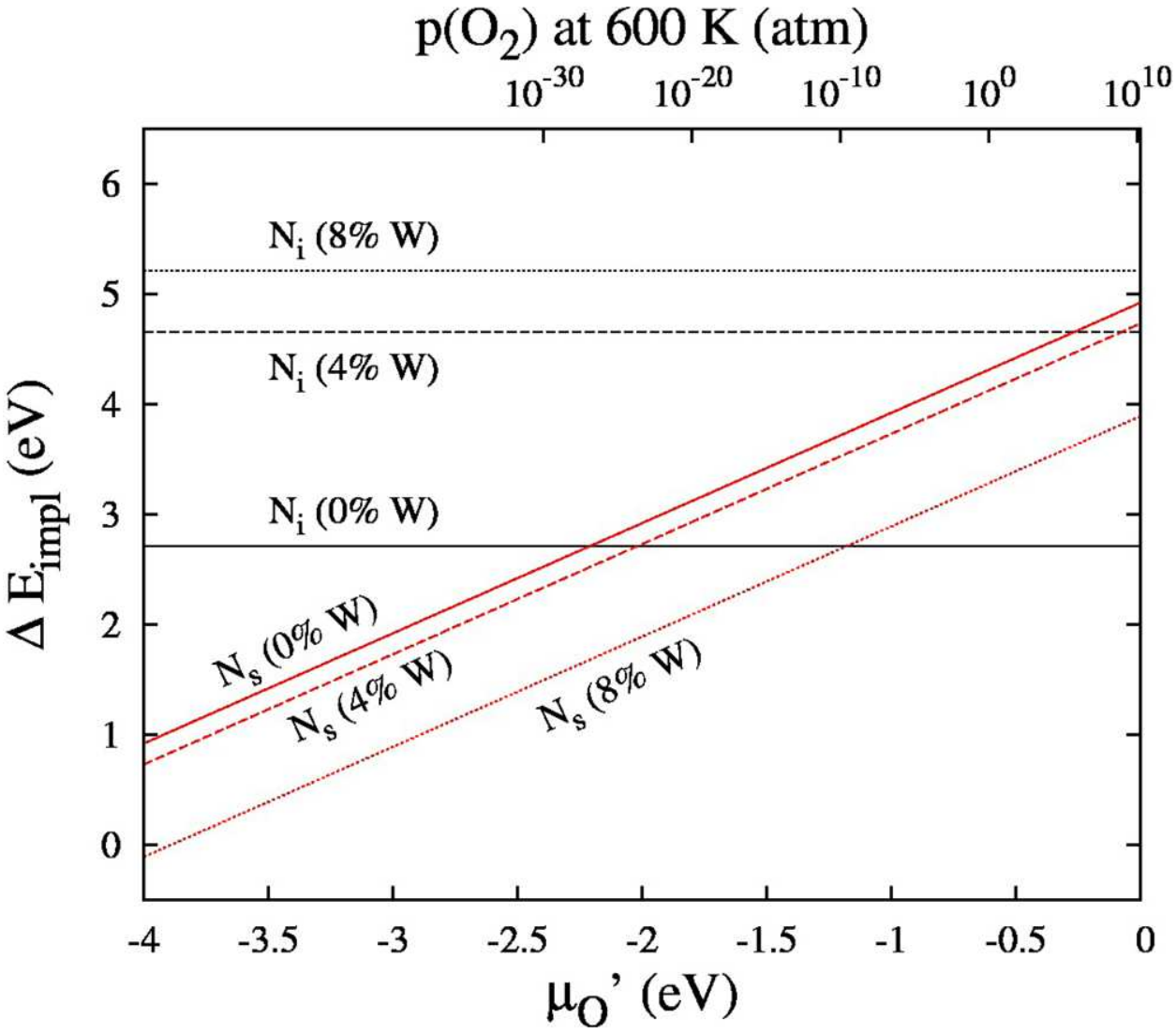

Figure 12 Implantation energies (in eV) as a function of the oxygen chemical potential μ′O (bottom axis) or O_2 partial pressure (top axis) at a fixed temperature (T = 600 °C) for interstitial and substitutional nitrogen dopant in W-doped and undoped (101) anatase surface models. Reprinted with permission from ref. 204, Copyrights (2012) American Chemical Society

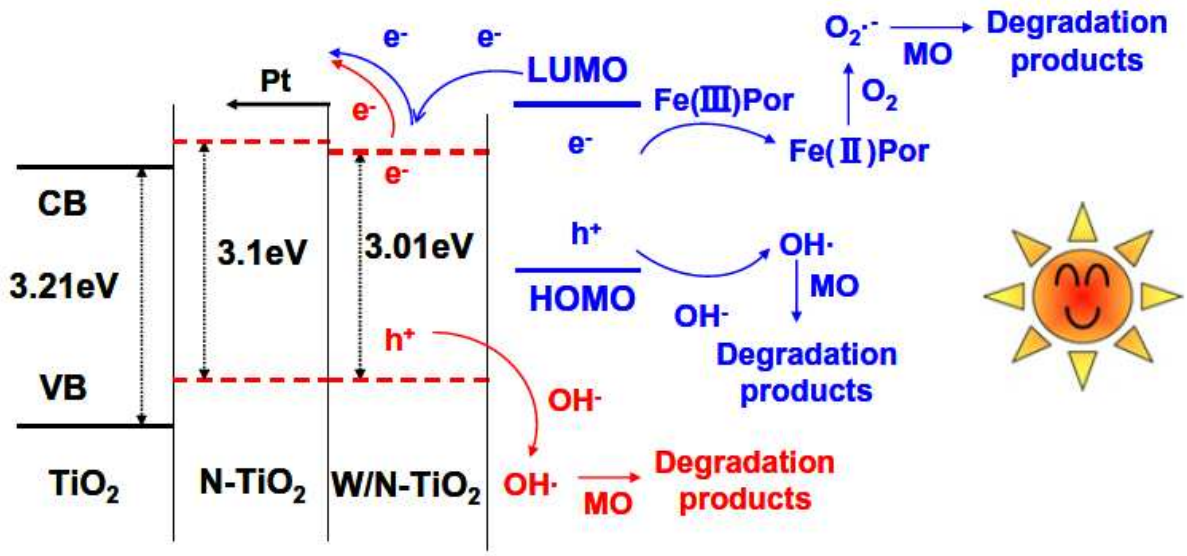

Figure 13 The illustration of the band structure of TiO_2, N-TiO_2 and N-W-TiO_2-Fe-Chl excited under visible illumination showing photosensitization by Fe^{3+}-Porphyrin

Reprinted with permission from ref. 205, Copyrights (2012) Elsevier Publications

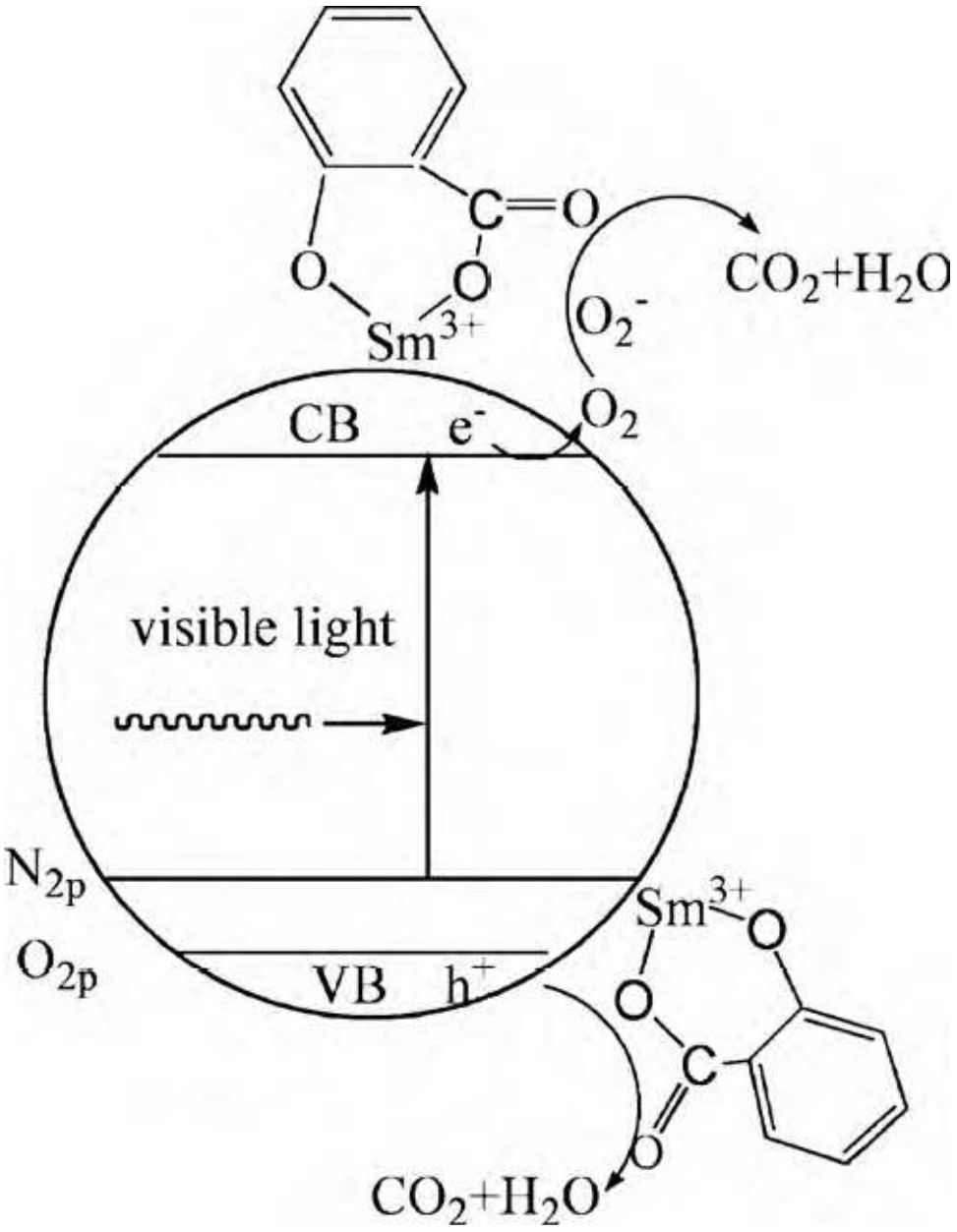

Figure 14 Formation of Lewis acid base complexes between Sm-N-TiO_2 and salicylic acid and its photocatalytic process under visible light irradiation

Reprinted with permission from ref. 223, Copyrights (2012) Elsevier Publications

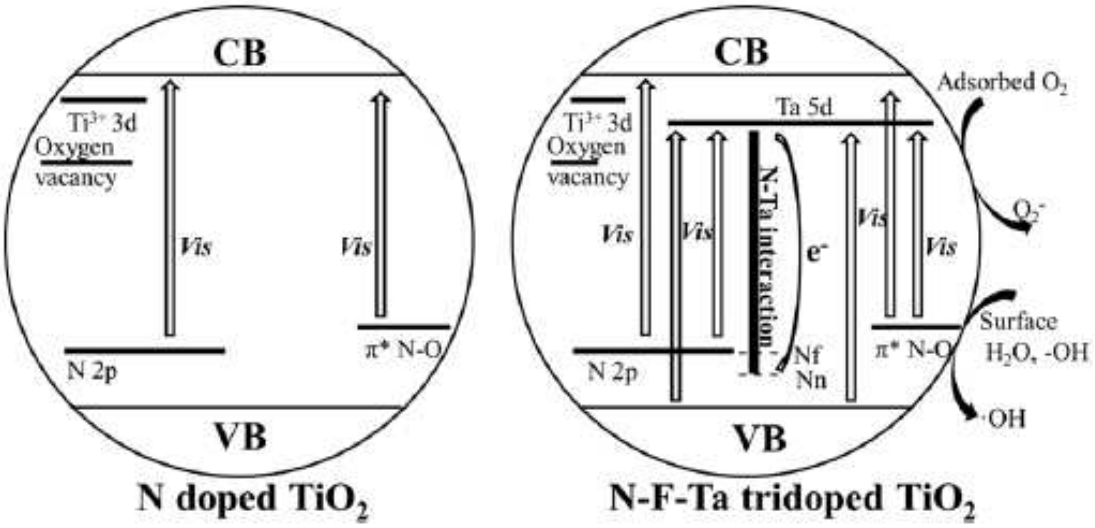

Figure 15 Comparison and modification of band structure for N-TiO_2 and tridoped N-F-Ta-TiO_2.

Reprinted with permission from ref. 268, Copyrights (2012) Elsevier Publications

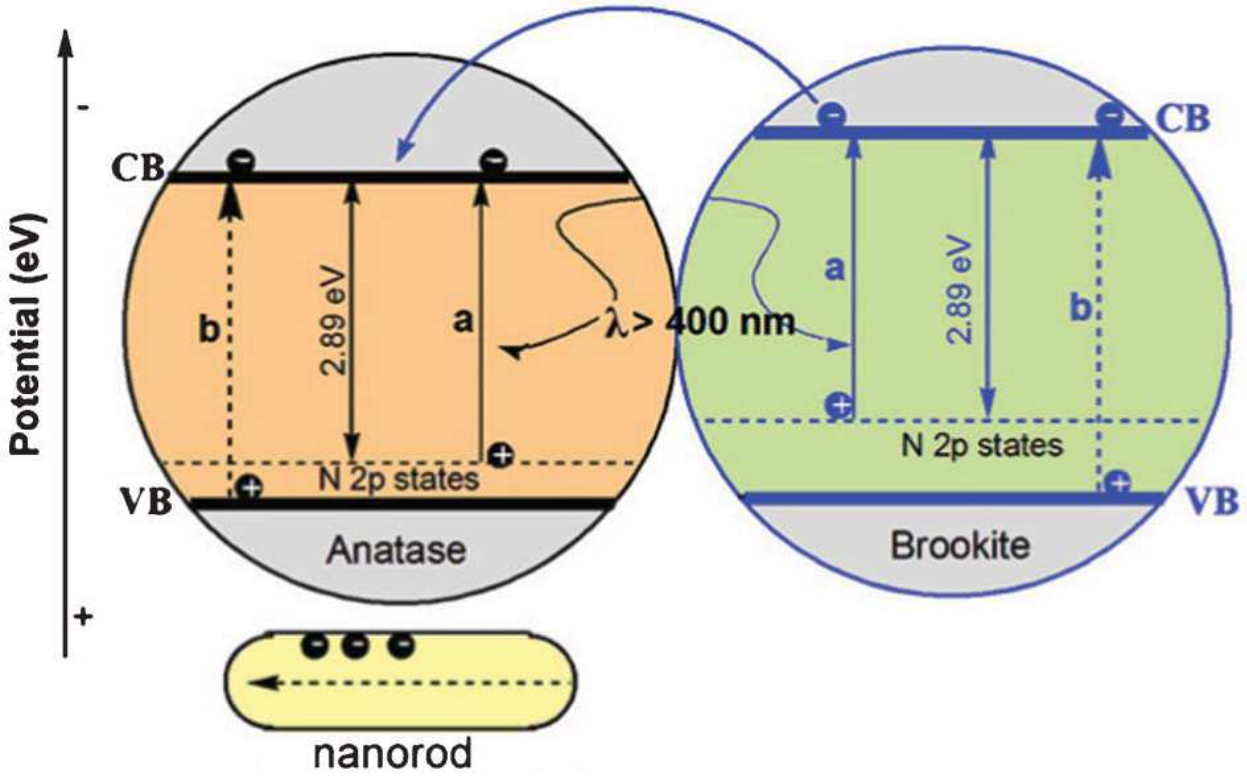

Figure.16 Electron migration process in one-dimensional nanorod along with nitrogen doped anatase and brookite structures: (path a) under visible light irradiation; (path b) under UV light illumination.

Reprinted with permission from ref. 282, Copyrights (2012) Royal Society of Chemistry

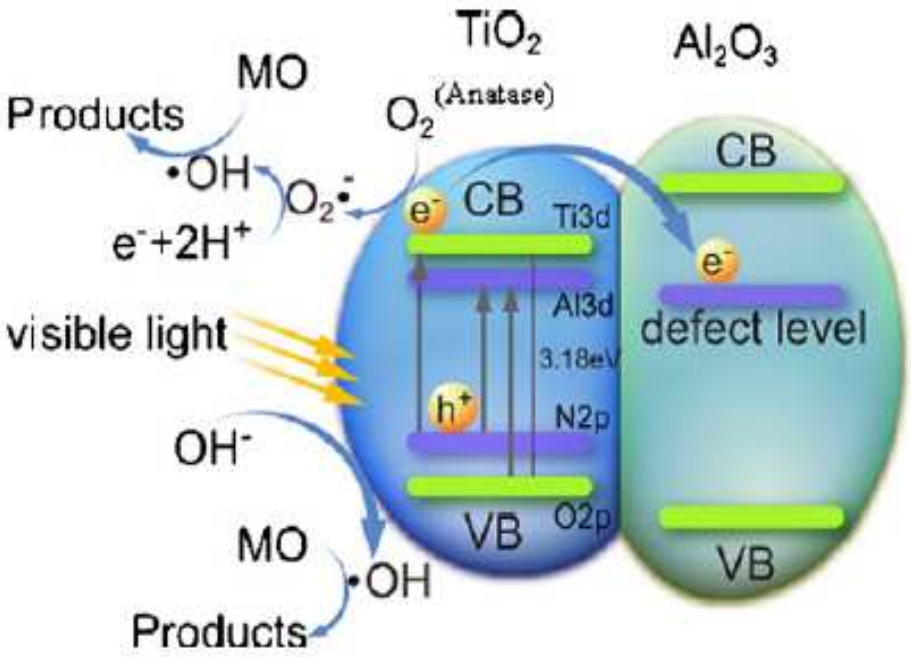

Figure 17 Pictorial representation of possible photo degradation mechanism of MO over N-TiO_2/Al_2O_3 composite under visible-light irradiation.

Reprinted with permission from ref. 289, Copyrights (2012) Elsevier Publications.

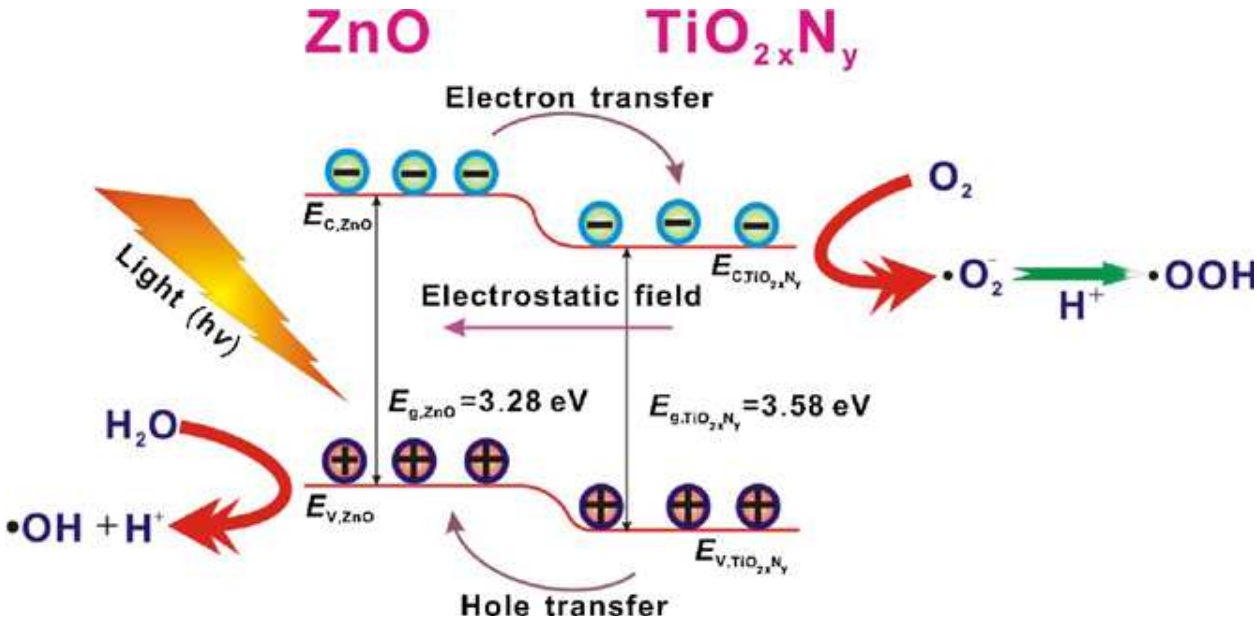

Figure 18 Schematic illustration of charge carrier separation and band structure of ZnO/N-TiO_2 semiconductor heterojunction.

Reprinted with permission from ref. 301, Copyrights (2012) Elsevier Publications

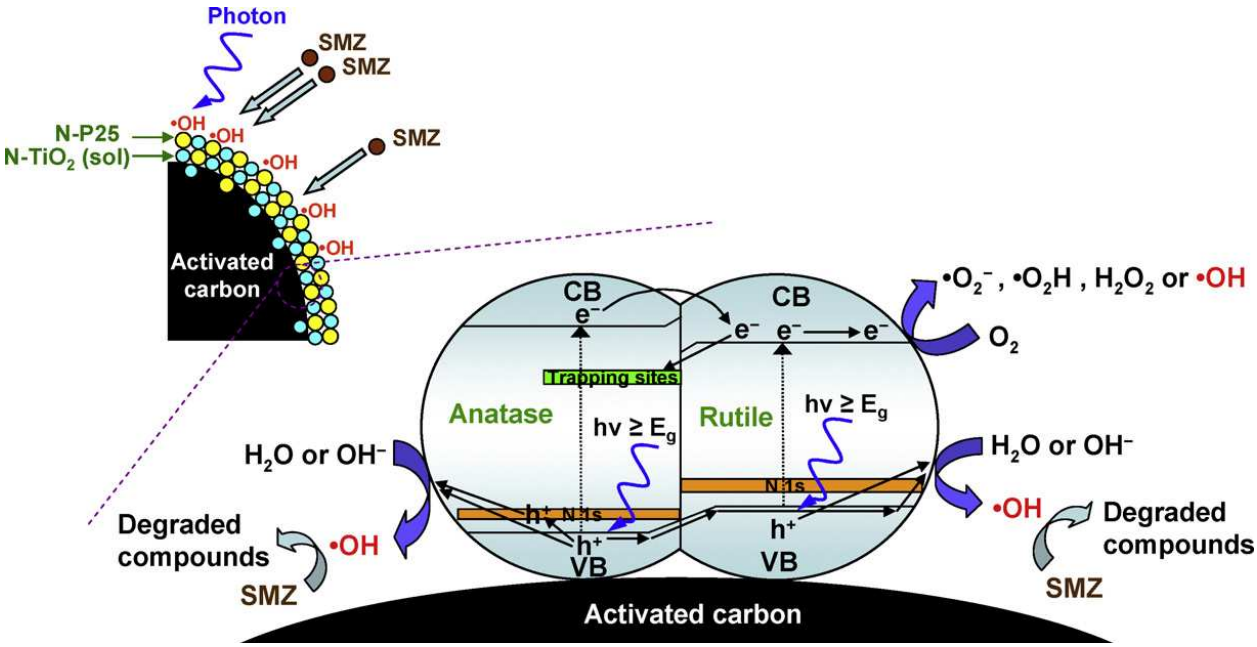

Figure 19 Schematic illustration of the proposed photocatalytic mechanisms of anatase and rutile N-TiO_2 supported on activated carbon.

Reprinted with permission from ref. 306, Copyrights (2012) Elsevier Publications

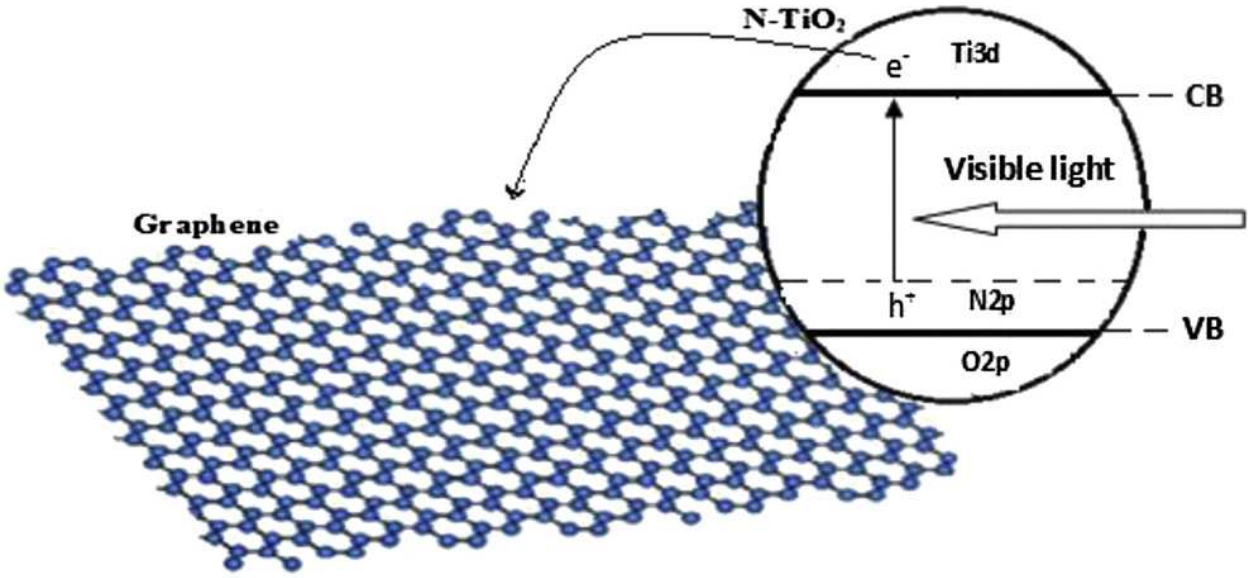

Figure 20 Proposed mechanism for the enhanced visible light photocatalytic activity of graphene/N-TiO_2 composite photocatalysts.

Reprinted with permission from ref. 316, Copyrights (2012) Elsevier Publications

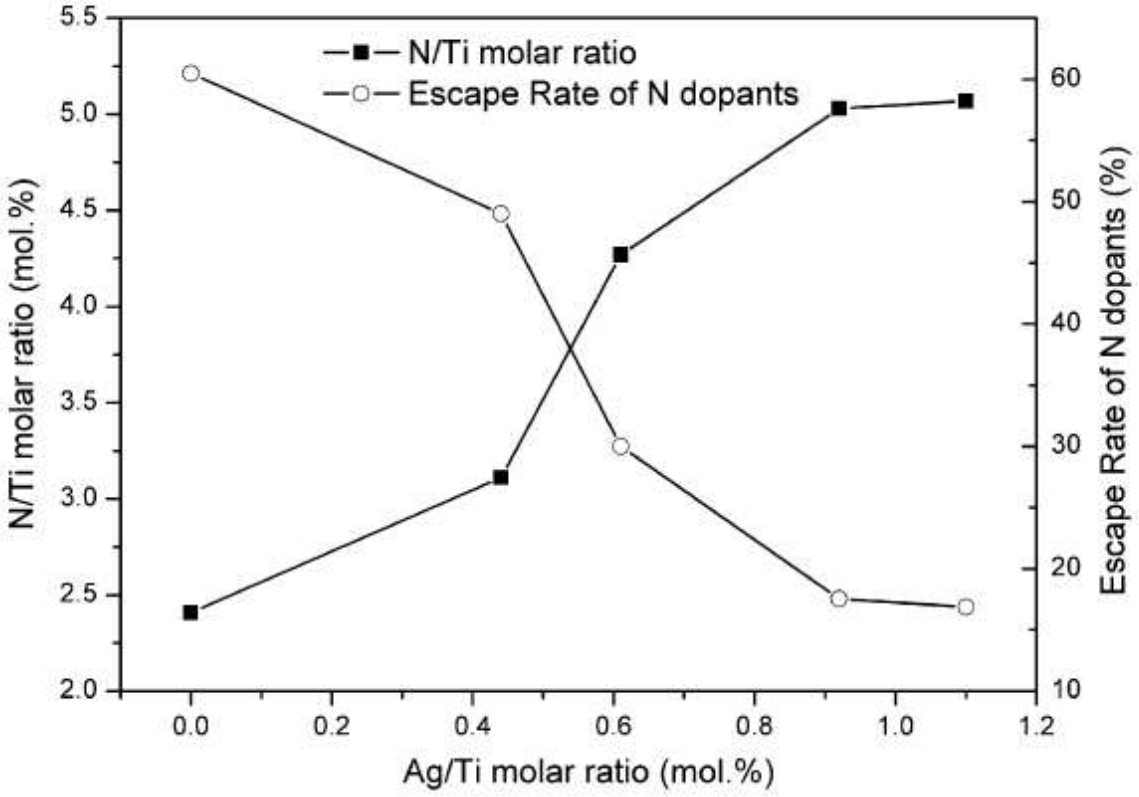

Figure 21 Effect of amount of Ag loading on the stability of implanted nitrogen in TiO_2 after hydrothermal treatment.

Reprinted with permission from ref. 336, Copyrights (2013) Elsevier publications

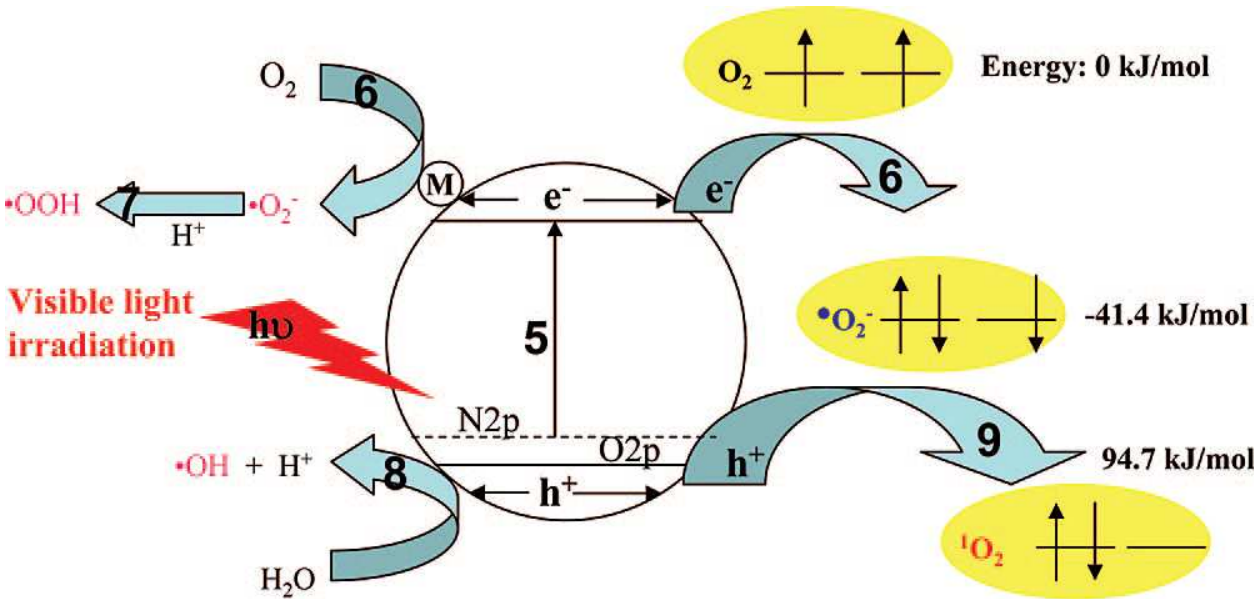

Figure 22 Schematic illustration of the photoinduced charge transformation on N-TiO_2 with metallic loading. The formation of singlet oxygen competes with the formation of superoxide and hydroxyl radicals.

Reprinted with permission from ref. 345, Copyrights (2008) American Chemical Society

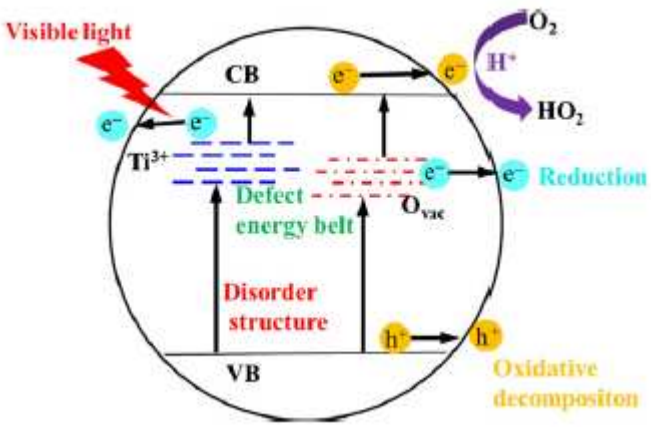

Figure 23 The schematic illustration of band structure, disorder structure and defect energy belt of N-H-F-TiO_2 and its visible light photocatalytic activity.

Reprinted with permission from ref. 403, Copyrights (2012) Elsevier publications

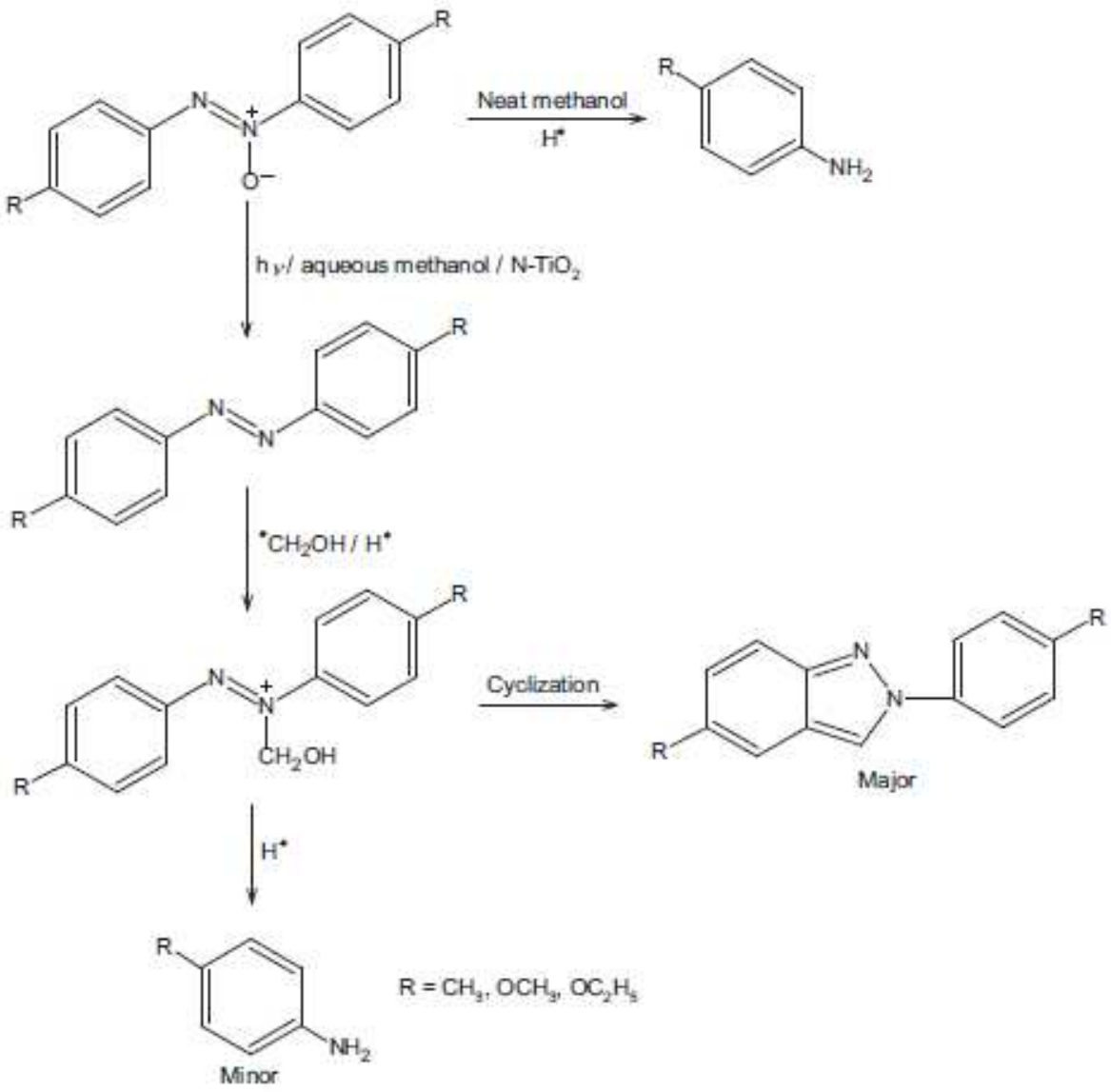

Figure 24 Possible reaction pathways for the reductive cleavage of azoxybenzene into their corresponding amines. Reprinted with permission from ref. 420, Copyrights (2012) Elsevier publications

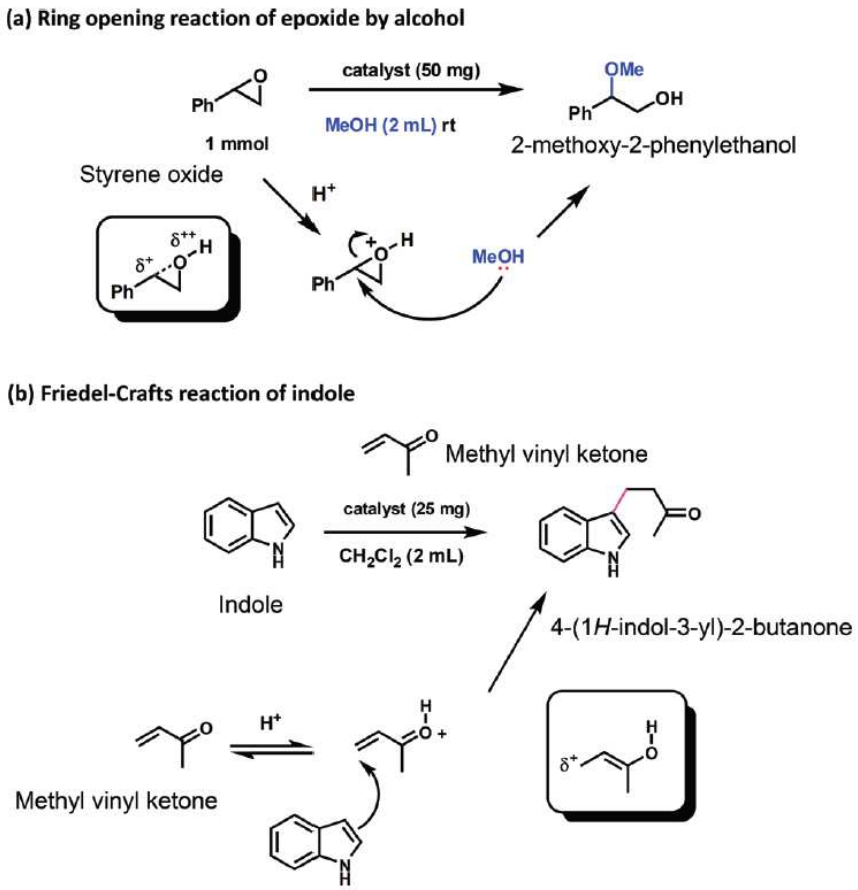

Figure 25 Schematic representation of (a) Ring opening reaction of epoxide by alcohol (b) Friedel-Crafts reaction of indole.

Reprinted with permission from ref. 422, Copyrights (2011) American Chemical Society

Table 1 Stability of lattice nitrogen in $TiOHN_x$ and $TiON_{10}$ photocatalysts for its use in three repetitive cycles and comparison of their activities.

Sample	Fresh catalyst/at%	First reuse /at%	Second reuse/at%	Third reuse/at%
$TiOHN_x$	1.4	1.28	1.26	1.26
$TiON_{10}$	0.32	0.24	0.20	0.18

Reprinted with permission from ref. 31, Copyright (2011) Elsevier Publications

Table.2 Pseudo-first-order rate constant (k') and regression coefficient (R^2) values for various photocatalysts under different light illumination sources for the photocatalytic degradation of BPA.

Sample	Blue LED		Green LED		Yellow LED	
	k′ (h^{-1})	R^2	k′ (h^{-1})	R^2	k′ (h^{-1})	R^2
TiO_2 powder (pH 6.0)	0.238	0.996	0.034	0.931	0.034	0.932
TiO_2 hollow sphere (pH 6.0)	0.353	0.977	0.048	0.981	0.040	0.978
N-TiO_2 hollow sphere (pH 6.0)	1.131[a]	0.989	0.148	0.976	0.076	0.969
N-TiO_2 hollow sphere (pH 3.0)	0.507[a]	0.971	-	-	-	-
N-TiO_2 hollow sphere (pH 10)	1.342[a]	0.971	-	-	-	-

[a] within the initial 3h of reaction.

Reprinted with permission from ref. 79, Copyrights (2010) Elsevier Publications

Table 3. Phase composition, grain size, surface area and micropore volume values of P25-TiO_2, Undoped TiO_2 and C-N-S-TiO_2 (R = 4.2) photocatalyst.

Sample	Phase composition (%)			Grain size (nm)	Surface area (m^2g^{-1})	Micropore volume (ccg^{-1})
	Anatase	Rutile	Brookite			
P25-TiO_2	82	18	0	23	58.2	-
Undoped TiO_2	85	10	5	6.94	111	0.140
C-N-S-TiO_2 (R = 4.2)	100	0	0	5.23	194	0.230

Reprinted with permission from ref. 252, Copyrights (2012) Elsevier Publications

Table 4 First order kinectic apparent rate constants and relative coefficients for the degradation of MB over various photocatalyst under visible and UV light irradiation.

Photocatalyst	K_{app} under visible light irradiation (min^{-1})	R^2	K_{app} under UV irradiation (min^{-1})	R^2
TiO_2	9.2×10^{-3}	0.995	1.06×10^{-3}	0.986
Yb-TiO_2	1.09×10^{-2}	0.990	1.44×10^{-2}	0.992
N-TiO_2	7.35×10^{-3}	0.996	5.42×10^{-4}	0.992
P-TiO_2	2.95×10^{-2}	0.992	2.90×10^{-3}	0.999
N-Yb-TiO_2	1.92×10^{-2}	0.996	1.44×10^{-3}	0.999
N-P-TiO_2	2.52×10^{-2}	0.991	2.22×10^{-3}	0.999
N-P-Yb-TiO_2 (1 wt % PO_4^{3-})	1.56×10^{-2}	0.990	1.59×10^{-3}	0.999
N-P-Yb-TiO_2 (5 wt % PO_4^{3-})	4.66×10^{-2}	0.996	4.15×10^{-3}	0.990
N-P-Yb-TiO_2 (10 wt % PO_4^{3-})	1.81×10^{-2}	0.982	2.58×10^{-3}	0.992

Reprinted with permission from ref. 271, Copyrights (2013) Elsevier Publications

Table 5. Photocatalytic synthesis of various substituted quinaldines using N-TiO_2[a]

Reactant	Product yield (%)	Byproduct	Conversion
Nitrobenzene	Quinaldine (70)	29	99
3-Nitrobenzene	2,7-Dimethylquinoline (80)	18	98
4-Nitrobenzene	2,6-Dimethylquinoline (75)	23	98
4- Methoxy-nitrobenzene	6-Methoxy-2-methylquinoline (70)	26	96
3-Methoxy-nitrobenzene	7-Methoxy-2-methylquinoline (72)	22	94
3,5-Dimethoxyl-nitrobenzene	2,5,7-Trimethylquinoline (66)	19	85
4-Chloro-nitrobenzene	6-Chloro-2-methylquinoline (36)	64	99
4-Fluro-nitrobenzene	6-Fluoro-2-methylquinoline (20)	79	99

Where [a] All reactions were performed with a 25 mM alcoholic solution of the reactant containing 50 mg of N-TiO_2 suspension, Intensity (I) =1.381 x 10^{-6} einstein $L^{-1}s^{-1}$, irradiation time = 5 h

Reprinted with permission from ref. 423, Copyrights (2012) Royal Society of Chemistry